DISSERTATION

Using A Coupled Atmospheric-Biospheric Modeling System (GEMRAMS) to Model the Effects of Land-Use/Land-Cover Changes on the Near-Surface Atmosphere

Submitted by

Adriana Beatriz Beltrán

Department of Atmospheric Science

In partial fulfillment of the requirements

For the Degree of Doctor of Philosophy

Colorado State University

Fort Collins, Colorado

Fall 2005

Reproduced with permission of the copyright owner. Further reproduction prohibited without permission.

UMI Number: 3200655

INFORMATION TO USERS

The quality of this reproduction is dependent upon the quality of the copy submitted. Broken or indistinct print, colored or poor quality illustrations and photographs, print bleed-through, substandard margins, and improper alignment can adversely affect reproduction.

In the unlikely event that the author did not send a complete manuscript and there are missing pages, these will be noted. Also, if unauthorized copyright material had to be removed, a note will indicate the deletion.

UMI®

UMI Microform 3200655

Copyright 2006 by ProQuest Information and Learning Company.

All rights reserved. This microform edition is protected against unauthorized copying under Title 17, United States Code.

ProQuest Information and Learning Company
300 North Zeeb Road
P.O. Box 1346
Ann Arbor, MI 48106-1346

Reproduced with permission of the copyright owner. Further reproduction prohibited without permission.

COLORADO STATE UNIVERSITY

August 29, 2005

WE HEREBY RECOMMEND THAT THE DISSERTATION PREPARED UNDER OUR SUPERVISION BY ADRIANA BEATRIZ BELTRÁN ENTITLED **USING A COUPLED ATMOSPHERIC-BIOSPHERIC MODELING SYSTEM (GEMRAMS) TO MODEL THE EFFECTS OF LAND-USE/LAND-COVER CHANGES ON THE NEAR-SURFACE ATMOSPHERE** BE ACCEPTED AS FULFILLING IN PART REQUIREMENTS FOR THE DEGREE OF DOCTOR OF PHILOSOPHY.

Committee on Graduate Work

Dr. William R. Cotton

Dr. A. Scott Denning

Dr. Ingrid C. Burke

Dr. Roger A. Pielke Sr., **Adviser**

Dr. Steven A. Rutledge, **Department Head**

Reproduced with permission of the copyright owner. Further reproduction prohibited without permission.

ABSTRACT OF DISSERTATION

USING A COUPLED ATMOSPHERIC-BIOSPHERIC MODELING SYSTEM (GEMRAMS) TO MODEL THE EFFECTS OF LAND-USE/LAND-COVER CHANGES ON THE NEAR-SURFACE ATMOSPHERE

A coupled atmospheric-biospheric model is a particularly valuable tool to study the potential effects of land-use/land-cover changes on near-surface atmosphere since the atmosphere and biosphere are allowed to dynamically interact through the surface and canopy energy balance. GEMRAMS is an ecophysiological process-based model, comprised of the Regional Atmospheric Modeling System (RAMS) and the General Energy and Mass Transport Model (GEMTM), and was used in this study.

At a regional and seasonal scale, several spring-early summer simulations were conducted on a southern South America domain. GEMRAMS were able to simulate the observed monthly temperature and precipitation. Sensitivity to lateral boundary conditions was explored for RAMS using NCEP and ECMWF reanalysis as atmospheric forcing. Land-cover scenarios representing current, natural, and afforestation conditions were implemented for this region and used to simulate the impacts of land-cover changes on near-surface atmosphere. Changes in near-surface fluxes and temperature depended on the type of vegetation conversion and the season. Warmer temperatures were found in the conversion from wooded grasslands or forest to agriculture. Afforestation and conversion from grass to agriculture led to a cooler and wetter near-surface atmosphere. Additional

Reproduced with permission of the copyright owner. Further reproduction prohibited without permission.

simulations with a double CO_2 concentration were also performed to assess the relative contributions of the land-cover and doubled CO_2 forcing to meteorological and biological variables. At a local and diurnal scale, GEMRAMS was used to evaluate the effects of observed vegetation changes that occurred in the northern Chihuahuan Desert, from grasslands in the mid-1800s to shrublands in the late 1900s. Simulations were performed using detailed vegetation maps for 1858 and 1998. Surface flux changes and the associated effects on near-surface temperature were spatially heterogeneous: different vegetation changes led to different effects, but albedo was the dominant parameter controlling the energy budget. Sensitivity experiments to soil moisture and mesquite cover were also conducted. Results of this study show that simulated shifts in vegetation led to complex interactions between biophysical and physiological characteristics of land and surface fluxes. These results also demonstrate that vegetation itself is a weather and climate variable as it significantly influences temperature, humidity, and surface fluxes.

Adriana Beatriz Beltrán
Department of Atmospheric Science
Colorado State University
Fort Collins, 80523
Fall 2005

Reproduced with permission of the copyright owner. Further reproduction prohibited without permission.

ACKNOWLEDGMENTS

I thank my adviser Roger A. Pielke Sr. for all his continuous guidance and support during this doctoral journey. I also greatly appreciate the support of the members of my graduate committee, Drs. Indy Burke, William R. Cotton, and Scott Denning I thank Molly Brown, from NASA, for providing the NDVI data used in this research. Also, Deb Peters, Keirith Snyder, and Al Rango from the Long Term Ecological Research Jornada Experimental Range, Las Cruces, New Mexico, provided the input data for some of the simulations performed in this study.

I am also thankful to present and past students and staff of the Pielke research group, for the cooperation, assistance, and encouragement I received during all these years. The "long-distance" support of all my family and friends in Argentina and around the world was also invaluable. My "new" family and friends in Colorado were also there, in good and bad times. I am indebted to the financial support of the Universidad de Buenos Aires, Facultad the Agronomía, Argentina that made possible my trip to Colorado and to pursue a Ph.D. at Colorado State University. I could not have accomplished this without that initial support.

Funding for this research was provided by NSF Grants DEB 9632852 and DEB 0217631. Additional support was provided by NASA Grant No. NAG5-11370. A scholarship granted by the University of Buenos Aires is also gratefully acknowledged.

Reproduced with permission of the copyright owner. Further reproduction prohibited without permission.

TABLE OF CONTENTS

Reproduced with permission of the copyright owner. Further reproduction prohibited without permission.

Reproduced with permission of the copyright owner. Further reproduction prohibited without permission.

LIST OF TABLES

Reproduced with permission of the copyright owner. Further reproduction prohibited without permission.

Reproduced with permission of the copyright owner. Further reproduction prohibited without permission.

LIST OF FIGURES

Reproduced with permission of the copyright owner. Further reproduction prohibited without permission.

Reproduced with permission of the copyright owner. Further reproduction prohibited without permission.

Reproduced with permission of the copyright owner. Further reproduction prohibited without permission.

Reproduced with permission of the copyright owner. Further reproduction prohibited without permission.

Reproduced with permission of the copyright owner. Further reproduction prohibited without permission.

Chapter 1

INTRODUCTION

1.1 Incorporating Interactive LAI on Climate Models

Observations and modeling studies show that land-surface properties can influence the near surface-atmosphere through exchanges of heat, moisture, momentum, gases, and aerosols, on timescales ranging from seconds to years, and on local to global spatial scales (Pielke et al. 1998; Pielke 2001; Pitman 2003; Foley et al. 2005).

Deforestation, afforestation, desertification, cultivation, and increasing irrigation areas are some landscape modifications that often lead to changes of surface and vegetation characteristics, like albedo, leaf area, roughness length, and root biomass distribution, can lead to changes in near-surface fluxes that may affect weather and climate. These changes can potentially feedback to the biophysical variables, enhancing or decreasing the initial perturbation (Pitman 2003). There are numerous papers that document these interactions, for example see Pielke at al. (1998) and Raddatz (2005).

Leaf Area Index (LAI) is one of the vegetation characteristics used in atmospheric models that provides information about the amount of vegetation present. LAI constitutes a very interactive part of the climate system, playing a major role in influencing the surface fluxes. Temperature and precipitation, through soil moisture, are the main atmospheric variables controlling LAI seasonal evolution. Satellite-derived data (i.e., Normalized Difference Vegetation Index - NDVI) can be used to estimate LAI (Sellers et

Reproduced with permission of the copyright owner. Further reproduction prohibited without permission.

al. 1996; Myneni et al. 1997; Los et al. 2000; Buermann et al. 2002). Recent efforts to incorporate this "observed" LAI in regional and global atmospheric models showed that climate is very sensitive to this variable. They also show an improvement in the simulation of precipitation and temperature over the use of LAI based on a fixed seasonal variation assigned to each vegetation type (Randall et al. 1996; Bounoua et al. 2000; Buermann et al. 2001; Lu and Shuttleworth 2002). When using regional climate models (RCM) as a tool to perform dynamical downscaling from a larger-scale data set or to address sensitivity to some internal or external forcing, it is possible to directly assimilate this LAI data as an "observed" boundary condition for a given time. Nevertheless, there is no two-way interaction between vegetation and atmosphere. However, when RCMs are used to assess potential effects of changes in vegetation that implied changes in LAI amount and seasonality, or when the two-way interactions between vegetation and atmosphere need to be addressed (Tsvetsinskaya et al. 2001a,b; Eastman et al. 2001a; Lu et al. 2001; Narisma et al. 2003; Narisma and Pitman 2004), explicit plant growth models need to be incorporated to the model. This LAI evolution according to modeled precipitation and temperature is also required in a fully "predictive framework" (Castro et al. 2005), when, for example, an RCM is used to perform extended range or seasonal forecasts. Arora (2002) presents a summary of most of the plant growth models used in climate simulations.

The Regional Atmospheric Modeling System (RAMS) is a state-of-the-art RCM developed at Colorado State University (Pielke et al. 1992; Cotton et al. 2003). It has been successfully coupled to two ecological models CENTURY (Lu et al. 2001) and GEMTM (Eastman et al. 2001a,b) to study the effects of intraseasonal variability, CO_2

Reproduced with permission of the copyright owner. Further reproduction prohibited without permission.

effects and landscape change over continental US. GEMRAMS (the coupled modeling system RAMS and GEMTM) has also been used over Australia to study the effects of biospheric CO_2 feedbacks and historical land-cover changes (Narisma et al. 2003; Narisma and Pitman 2004). GEMRAMS is the RCM used in this work.

One of the main features of GEMRAMS is that the atmosphere and biosphere are allowed to dynamically interact through the surface and canopy energy balance. Temperature, precipitation, humidity, and winds as well as surface fluxes, are predicted by RAMS; vegetation grows in GEMTM as a function of temperature, radiation, soil and atmosphere water status. The interactions between transpiration, photosynthesis, and root water uptake can be represented explicitly. In other words, RAMS uses the values of canopy conductance, LAI, and root distribution computed by GEMTM components to calculate transpiration and root water uptake.

The use of modeling simulations to understand South America climate have increased in recent years. Global atmospheric and regional climate models are being used to study different aspects of the climate. A recent intercomparison of six AGCM on South America for an El Niño year (1997/98) showed deficiencies in simulating observed rainfall anomalies over Uruguay and southern Brazil during that year (Zhou and Lau 2002). Several RCMs have been applied in South America, most of them with a focus on tropical regions or entire South America (Horel et al. 1994; Figueroa et al. 1995; Berbery and Collini 2000; Chou et al. 2000, 2002; Saulo et al. 2000; Misra et al. 2002a,b, 2003; Nicolini et al. 2002a,b; Qian et al. 2003; Roads et al. 2003; Rojas and Seth 2003; Seth and Rojas 2003; Seth et al. 2004; Sun et al. 2005).

Reproduced with permission of the copyright owner. Further reproduction prohibited without permission.

RAMS has been used to study precipitation over southeastern South America associated with strong low-level jet conditions (Nicolini et al. 2002b); also Weaver et al. (2002) studied the sensitivity of mesoscale circulations to model configuration in a domain centered over northwestern Brazil. A Brazilian version of RAMS (BRAMS) is being run operationally at the Department of Atmospheric Sciences at Sao Paulo University, Brazil (http://www.master.iag.usp.br/) and at the Centro de Previsao de Tempo e Estudos Climaticos (CPTEC)-INPE(http://tucupi.cptec.inpe.br/meio_ambiente).

Important land-surface changes in the southern part of South America have occurred similar to other regions of the world. Land-use/land-cover changes have affected the functioning of temperate ecosystems in South America (Paruelo et al. 2000) and may affect the hydrological cycle (Engel et al. 2005; Nosetto et al. 2005) but the impacts of those changes on the near-surface atmosphere have not been fully explored in this region.

This work differs from other studies by focusing on mid-latitude South America, and by using a regional coupled atmospheric-biospheric model to study the potential effects of LULC changes on near-surface climate in different spatial and temporal scales. A regional and seasonal scale is considered for the South America LULC changes scenarios. At a local and diurnal scale, impacts of historical vegetation changes are studied for a semiarid region in New Mexico, USA.

The first objective of this work is to evaluate the performance of RAMS and the coupled modeling system GEMRAMS on southern South America, test its sensitivity to lateral boundary conditions, and explore the effects of interannual variability on near-surface temperature, humidity, sensible and latent heat fluxes and precipitation. The

Reproduced with permission of the copyright owner. Further reproduction prohibited without permission.

second objective is to assess potential impacts of LULC changes using GEMRAMS on different time and spatial scales.

1.2 The Coupled Modeling System: Overview of the Models

GEMRAMS, comprised of the Colorado State University version of the Regional Atmospheric Modeling System 4.3 (RAMS; Pielke et al. 1992; Cotton et al. 2003) and the General Energy and Mass Transport Model (GEMTM; Chen and Coughenour 1994, 2004) was used in the simulations. GEMRAMS has been used to study the effects of land-cover and CO_2 changes on weather and climate (Eastman et al. 2001a,b; Narisma et al. 2003; Narisma and Pitman 2004; Pitman et al. 2004).

RAMS is a general-purpose, atmospheric-simulation model that includes the equations of motion, heat, moisture, and continuity in a terrain-following coordinate system. It is a fully three-dimensional and non-hydrostatic model. RAMS also includes a soil-vegetation-atmosphere transfer scheme, the Land Ecosystem-Atmosphere Feedback model version 2 (LEAF-2; Walko et al. 2000) that represents the storage and exchange of heat and moisture associated with the vegetation and canopy air and soil.

GEMTM is an ecophysiological process-based model that can be used to simulate the dynamic interactions between the atmosphere and the growing canopy (Chen and Coughenour 1994). Several of the GEMTM components were coupled to RAMS: canopy radiation transfer, plant and root growth, soil water dynamics, biomass production, and soil respiration submodels. Complete descriptions of each of the GEMTM components can be found in Chen and Coughenour (1994), and Chen et al. (1994). These components require an additional set of parameters, mostly vegetation dependent, to characterize

Reproduced with permission of the copyright owner. Further reproduction prohibited without permission.

these biological processes. They were obtained from global and local references (e.g., Woodrow and Berry 1988; Amthor 1989; Boote and Loomis 1991; Raich and Schlesinger 1992; Soriano 1991; Dickinson et al. 1993, 1998; Schulze et al. 1994; Larcher 1995; Nikolov et al. 1995; Madonni and Otegui 1996; Sellers et al. 1996; Cárcova et al. 2000; White et al. 2000; Villamil et al. 2001; Zeng 2001).

In GEMRAMS, the near-surface atmosphere and biosphere are allowed to dynamically interact through the surface and canopy energy balance. Eastman (1999) and Eastman et al. (2001a) describe in detail how the coupling between GEMTM and RAMS is performed. A schematic of the coupled system is shown in Figure 1.1.

Precipitation, canopy air and soil temperature, humidity, winds, as well as surface fluxes (e.g., latent and sensible heat) are predicted by RAMS. At each timestep, photosynthesis at the leaf-level is calculated for sunlit and shaded leaves and also separately for C_3 and C_4 species (see Chen et al. 1994, 1996 and Farquhar et al. 1980 for details) as a function of photosynthetic active radiation (PAR) and temperature. Water stress effect on assimilation rate is also considered, and estimated using empirical vegetation dependent functions (Coughenour 1984). The weighting value of these functions is 1 for a relatively wet soil, and decreases linearly to 0 for values of plant water potential low enough that it shuts off photosynthesis. Sunlit and shaded leaves stomatal conductance is computed using the semi-empirical linear Ball-Berry relationship based on net photosynthesis, relative humidity and leaf-surface CO_2 (Ball et al. 1987).

At the canopy level, photosynthesis and conductance are calculated by scaling-up from the corresponding sunlit and shaded leaves values using sunlit and shaded LAI (Chen and Coughenour 1994; de Pury and Farquhar 1997). Sunlit and shaded LAI

Reproduced with permission of the copyright owner. Further reproduction prohibited without permission.

components are calculated using light extinction coefficients form a multi-level canopy radiation model (Goudriaan 1977). Canopy transpiration is estimated in LEAF-2 using the sunlit and shaded conductances and LAI.

The available photosynthate is allocated to leaves, stems, roots, and reproductive organs with variable partition coefficients, which are functions of soil water conditions. As water stress increases, the fraction allocated to root growth increases. Maintenance and growth respiration and mortality for each of these biomass components are computed based on empirical relationships based on air and soil temperature, and soil moisture. Daily, at 0 UTM (2100 LST) in these simulations, a new total LAI value is estimated from the daily leaf biomass growth, using the vegetation-prescribed specific leaf area. Also, the root profile is updated daily through the processes of branching, extension and death (Chen and Lieth 1993).

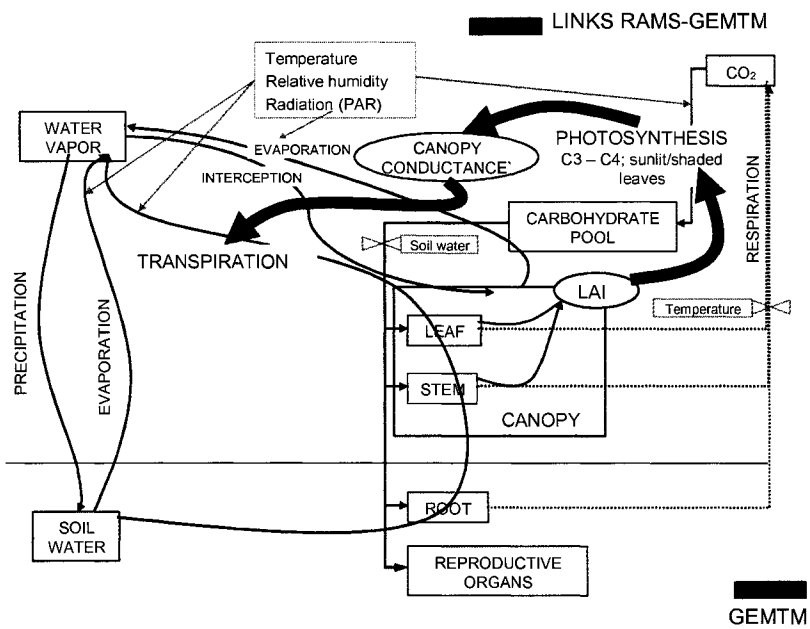

Figure 1.1. Conceptual diagram of the LEAF2-GEMTM coupling. Green lines represent the GEMTM-plant component, and the blue lines represent the water pathway. The brown arrows represent the links between RAMS-LEAF2 and GEMTM.

Reproduced with permission of the copyright owner. Further reproduction prohibited without permission.

Chapter 2

RAMS SIMULATIONS OVER SOUTHERN SOUTH AMERICA

2.1 General Climatic Aspects During Southern South America Austral Summer

The main features related to the present work will be given in this section. A more comprehensive description of the summer climate of southern South America (SSA) can be found in Nogués-Paegle (2002) and references therein.

The climate of SSA (Figure 2.1) is governed by distinctive local geographical features as well as by remote factors. Both the Atlantic and Pacific Oceans have a great influence on this region. The presence of the Cordillera de los Andes constitutes one of the major factors determining many of the climate features in this region. The high, steep and narrow Andes not only constitute a barrier to the westerly flow north of 40°S but they also deflect the tropical easterlies, channeling the tropical moisture southeastward into the eastern and central part of the region (Inzunza and Berri 1990; Paegle 1998; Saulo et al. 2000). This South American low-level jet (SALLJ) is one of the factors that determine the precipitation in the central and northeastern part of SSA (Salio et al 2002; Nicolini et al. 2002a). Incorrect representation of the steep topography in atmospheric general circulation models, and consequently a deficient LLJ, was one of the main causes of failure in simulating observed rainfall anomalies over Uruguay and southern Brazil during one El Niño year (Zhou and Lau 2002).

Reproduced with permission of the copyright owner. Further reproduction prohibited without permission.

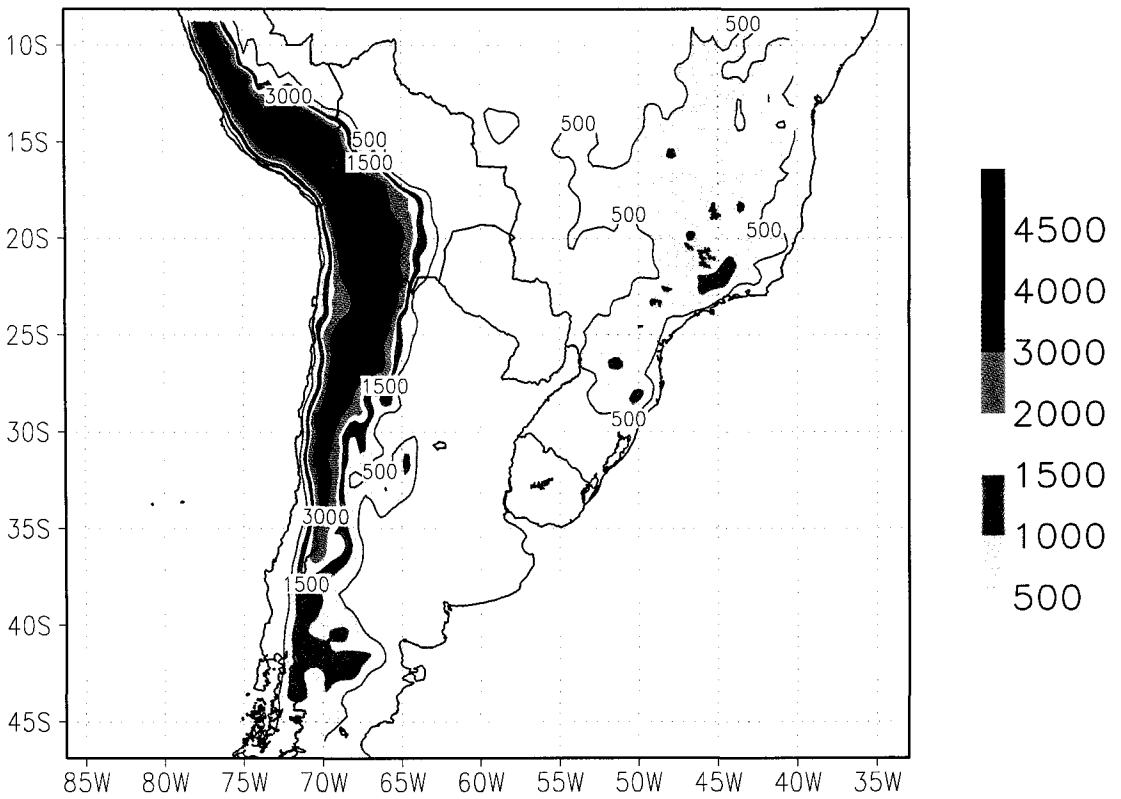

Figure 2.1. Topography (m) in the southern South America domain.

Interannual variability in rainfall has been associated with the extreme phases of the El Niño-Southern Oscillation ENSO phenomenon (Aceituno 1988; Ropelewski and Halpert 1987, 1989; Kiladis and Diaz 1989; Grimm et al. 2000; Penalba et al. 2005). The ENSO signal on precipitation in this region has a significant spatial variability, and it also depends on each event. Over southern Brazil, eastern Argentina, and Uruguay, the general pattern of the ENSO signal on precipitation corresponds to wetter than normal conditions during October to March for El Niño events, and drier than normal conditions from September to December during La Niña events. Precipitation anomalies associated with ENSO events affect crop yields in the Pampas (Podestá et al. 1999; Messina et al.

Reproduced with permission of the copyright owner. Further reproduction prohibited without permission.

1996a,b 1999). The ENSO signal in this southeastern South America region is also present in satellite-derived indices, like NDVI (Myneni et al. 1997), LAI (Buermann et al. 2002), and the NOAA/NESDIS Global Vegetation Index, GVI (Kogan 2000). They all found strong negative anomalies of the indices (e.g., indicating severe moisture and thermal stress in the case of GVI) associated with La Niña conditions and positive anomalies associated with El Niño events.

Very large decadal changes in precipitation have occurred in the central and eastern part of southern South America over the last century (Castañeda and Barros 1994; Barros et al. 2000). A relatively dry 1931-1960 period was followed by a wet one, characterized by a steady increase in annual precipitation (Hoffmann et al. 1997). Changes have occurred also in the seasonal cycle. An increase in summer (December to February) rainfall during 1961-1990 is found in the western semiarid marginal area of the Pampas region (Rusticucci and Penalba 2000; Hurtado et al. 1996). An increase in summer precipitation in that area from approximately 100 mm in 1941-1950 to approximately 200 mm in 1981-1990, has contributed to an increase of the proportion of area cultivated with summer crops (Sierra et al. 1995; Viglizzo et al. 2000).

Spatial and temporal variability is also observed in temperature in this region (Hoffman et al. 1997; Rosenblüth et al. 1997). Generalized warming is found between 20 °S and 40°S since the beginning of the 1900's (Hoffman et al. 1997). Positive anomalies in the decadal mean temperature between 1981-1990 and 1901-1910 are positive in most of that region, with negative values only found in the southern part of the Pampas and around 25°S in northwestern Argentina (Rusticucci and Penalba 2000). For the 1901-1990 period, the warmest decade was the 1943-1952 one, with anomalies up to 0.8°C.

Reproduced with permission of the copyright owner. Further reproduction prohibited without permission.

The decades 1955-1964 and 1966-1975 are the ones with large cooling, and negative anomalies of up to -0.6°C. Changes are also observed in maximum and minimum temperatures. Rusticucci and Barrucand (2004) analyzed trends in mean maximum and minimum temperature for austral winter (June-July-August) and summer (December-January-February) over the 1959-1998 period. They found a statistically significant increase in mean maximum temperature in central Argentina during the summer (December to February), with values up to -6.9°C (100 yr^{-1}). In contrast, positive trends of up 6.2°C (100 yr^{-1}) in mean minimum temperature were found throughout most of the central and eastern part of Argentina. Large spatial heterogeneity characterized all the different analyses.

The objectives of this work are:

- to evaluate the performance of RAMS and GEMRAMS on southern South America on precipitation and temperature.
- to address the sensitivity of near-surface atmosphere to large-large-scale forcing and interannual variability.
- to address the sensitivity of near-surface atmosphere to potential impacts of LULC changes and increase of carbon dioxide on southern South America.

Reproduced with permission of the copyright owner. Further reproduction prohibited without permission.

2.2 Data Sets Required for Initializing and Driving the Modeling System

Several updates for this South America domain were performed to the surface boundary datasets provided with the standard RAMS 4.3 version. Heterogeneous soil texture information was derived from the Soil and Terrain (SOTER) database for Latin America and the Caribbean (SOTER 1998). This geo-referenced soil database consists of more than 1490 mapping units, with at least one soil profile assigned to each unit. The predominant soil texture class in the profile was assigned to each of the 5 × 5 arc-minute pixels, and regridded to the GEMRAMS grid (Figure 2.2).

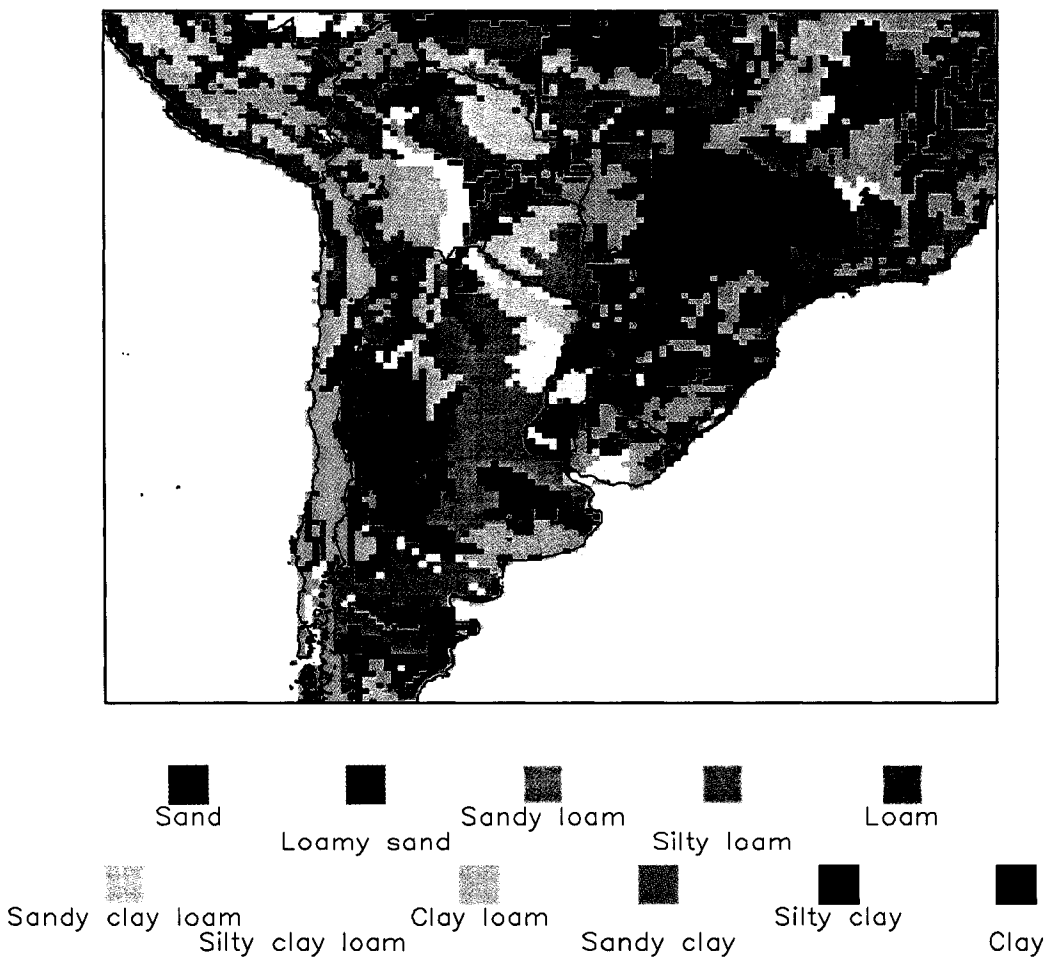

Figure 2.2. Soil types distribution for the modeling domain.

Reproduced with permission of the copyright owner. Further reproduction prohibited without permission.

This GEMRAMS version uses a combination of vegetation classes derived from the Biosphere-Atmosphere Transfer Scheme (BATS) (Dickinson et al. 1993) and the Land Data Assimilation System (LDAS). The standard source of the land-cover database to initialize the vegetation distribution is the Global Land Cover Characteristics database version 1.2 Global Ecosystems framework (Olson 1994). An updated version 2.0, obtained from the USGS website (http://edcdaac.usgs.gov/glcc/globdoc2_0.asp), is used in these simulations. The revised areas for South America in this new version are located mainly in the semiarid and subtropical regions, and give a better representation of the observed vegetation in those areas. This revised 2.0 version corrected some of the inaccuracies reported by Paruelo et al. (2001). This 1 km × 1 km dataset is reprojected onto a regular latitude-longitude grid with a 30-arc second spacing for its use in RAMS. This database consists of a total of 94 ecosystem classes. As part of RAMS pre-processing, these ecosystems classes are regrouped onto the combination of 18 BATS and 13 LDAS classes.

One caveat of the BATS/LDAS classes is that it does not discriminate between winter and summer crops, only a "Crop/mixed farming" vegetation type is considered. The simulations span a 5 month period, from September (early spring) to January (mid summer), and encompass part of the phenological cycle of those crops. Thus, several grid cells of the simulation domain were reclassified onto wheat, as the main winter crop, and corn and soybean, as the main summer crops.

In the Pampas region, the main source used to perform this reclassification was the county harvested area for each crop, obtained from the database of the Agriculture Department of Argentina. The mean distribution for 1996-2000 of the dominant crop was

Reproduced with permission of the copyright owner. Further reproduction prohibited without permission.

remapped into the RAMS grid. The Ecosystems Function Types distribution from Paruelo et al. (2001) was used to check this reclassification. For the rest of the domain, Ramankutty and Foley (1998), Still et al. (2003) and maps from USDA (USDA, 1987) were used to reassign wheat, corn, and soybean to the "Crop/mixing farming" type in the center of Chile, southern Brazil, Uruguay, and a few grid cells in Perú, Paraguay, and Bolivia.

Also, grid cells classified as "Crop/mixed farming" in the central-eastern portion of the Pampas were reclassified as tall grass (Soriano 1991). They comprise the Flooding Pampas (Soriano 1991; Hall et al. 1992; Paruelo et al. 2001), mostly covered by perennial grasslands (cultivated pastures and native grasslands). A large number of small (less than 1 km) wetlands are located throughout the central Pampas (Gomez and Toresani 2001). In addition, this region experiences frequent flooding conditions due to its very slight terrain slope and a high water table, although the extent and duration is highly variable. Small floods tend to occur almost every year, during winter to early spring (Paruelo and Sala 1990). Widespread and prolonged floods may occur approximately once every decade associated with large precipitation events (Soriano 1991). In the last 25 years, major flood events in this region occurred in 1980, 1985 to 1987, 1993, 1995, and 2000-2001 (Brakenridge et al. 2003; Herzer et al. 2004). Figure 2.3 is the final land-cover/land- use map used in the simulations.

Reproduced with permission of the copyright owner. Further reproduction prohibited without permission.

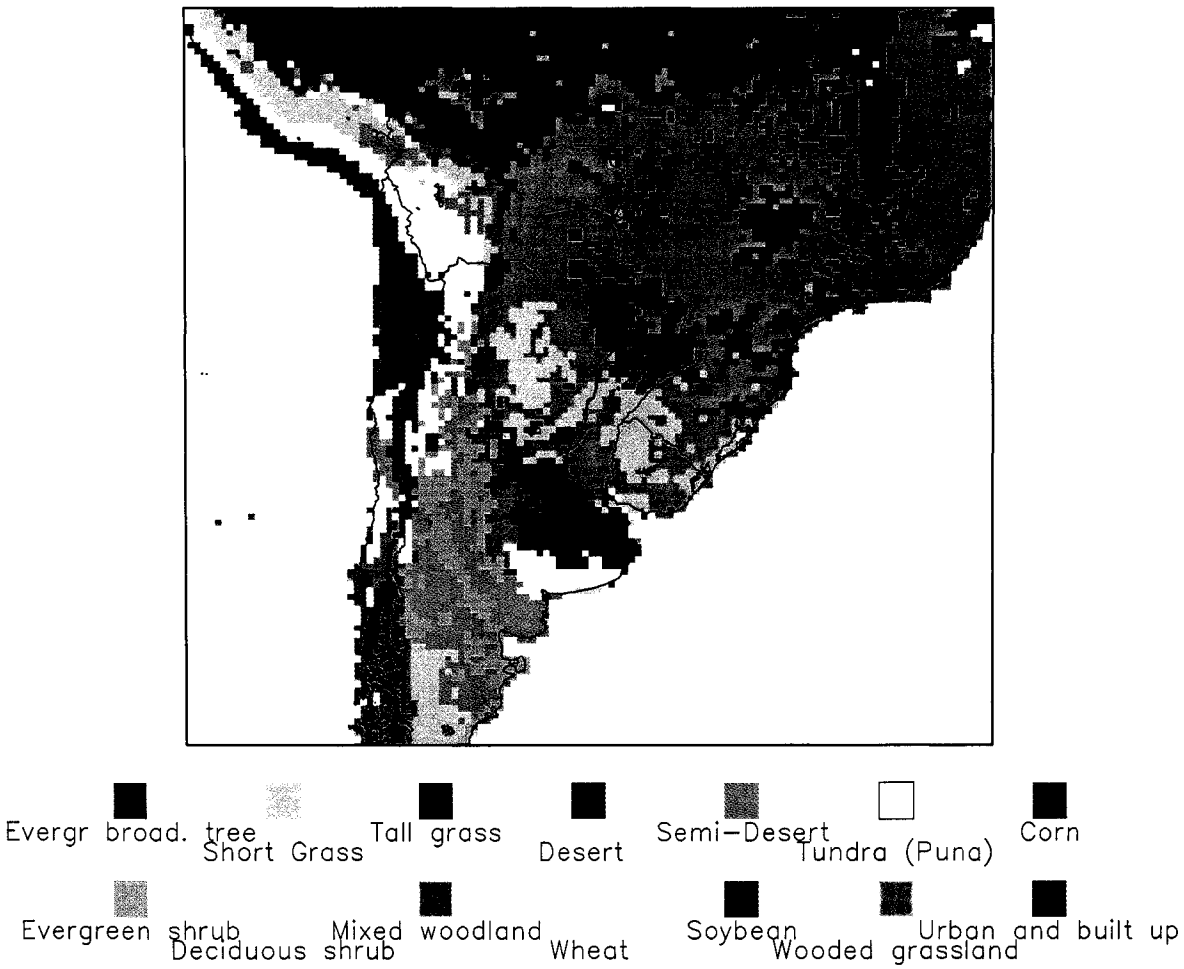

Figure 2.3. Vegetation cover for the simulation domain.

Reproduced with permission of the copyright owner. Further reproduction prohibited without permission.

Vegetation types are also distinguished by C_3 and C_4 photosynthesis pathways. Temperature, precipitation amount, and its distribution in the year, are the major controls of the relative proportion of C_3 and C_4 grasses (Paruelo et al. 1998). Cold C_3 grasses dominate the Patagonian region (Paruelo et al. 1998). The percentage of C_4 grasses increases towards the northwest. This corresponds to the Monte Province, with more than 75% of C_4 vegetation (Paruelo et al. 1998; Still et al. 2003). A C_4 type is assigned to this region. Although the grasslands in the Pampas is a mixture of C_3 and C_4 grasses (Soriano 1991), a C_3 type was assigned to this region these simulations. Grasslands north of 30°S latitude were assigned to a C_4 pathway based on Paruelo et al. (1998) and Still et al. (2003).

Leaf area index (LAI) was estimated using the Global Inventory Modeling and Mapping Studies Satellite Drift Corrected and NOAA-16 incorporated Normalized Difference Vegetation Index (GIMMS-NDVI) (Pinzon 2002; Pinzon et al. 2004; Tucker et al. 2005). A bimonthly maximum value composite of GIMMS-NDVI was available for South America for a 8 km × 8 km pixel footprint from July 1981 to December 2003. The algorithm proposed by Sellers et al. (1996) was applied on the GIMMS-NDVI data to calculate bimonthly LAI. Daily LAI values were obtained by linear interpolation. These data were then regridded to a GEMRAMS grid for each simulated September to January periods (1996-1997, 1997-1998 and 1999-2000). Figure 2.4 shows the initial LAI conditions for September 1st.

Some of the initial conditions for above and belowground biomass and root profiles were set up similarly to Eastman et al. (2001a). Total leaf biomass is related to LAI by the vegetation prescribed specific leaf area (SLA, m^2 kg^{-1}). Leaf biomass is then

Reproduced with permission of the copyright owner. Further reproduction prohibited without permission.

used to estimate stem biomass through a vegetation prescribed stem/leaf biomass ratio. An aboveground-belowground ratio is used to obtain initial conditions for root biomass. For woody species, initial root biomass is calculated from the maximum aboveground biomass (estimated from maximum LAI) for all the NDVI dataset. The total root biomass is distributed in the soil profile according to Schenk and Jackson (2002).

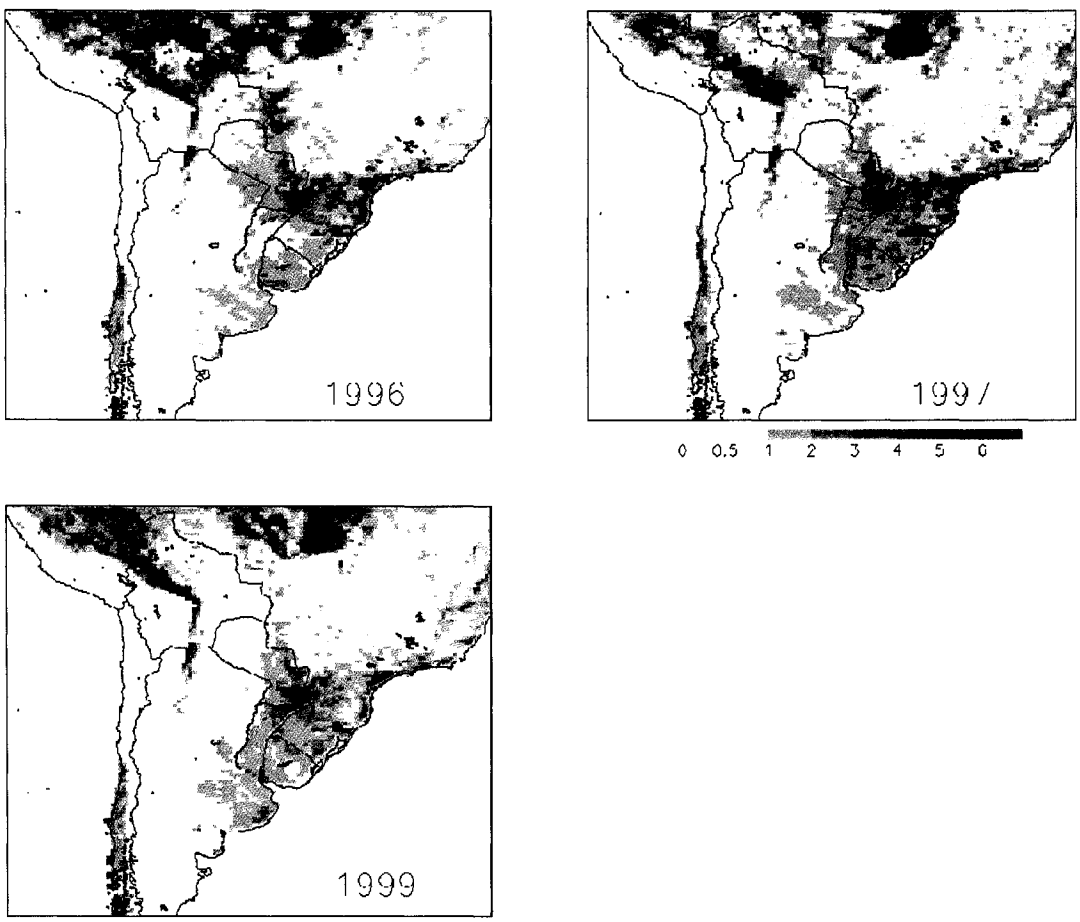

Figure 2.4. Initial conditions for the Leaf Area Index (m^2 m^{-2}) for September 1st.

Reproduced with permission of the copyright owner. Further reproduction prohibited without permission.

2.3 Model Configuration

The model was integrated over a domain covering the southern part of South America, approximately 8 to 45°S and 35 to 90°W. The 124 × 120 grid was centered at (28°S, 59.5°W), and had 35 km grid spacing (Figure 2.5). There were 32 vertical levels with a thickness of 120 m at the surface, stretching to 1 km from approximately 5.2 km to the domain top at 23 km. The soil model had 8 soil layers, with the bottom layer at 3.0 m. The time step for the model integrations was 30 s. The Mellor and Yamada (1982) parameterization was used for vertical diffusion and the modified Smagorinsky (1963) scheme for horizontal diffusion. The lateral boundary conditions were those of Klemp and Wilhelmson (1978). The short- and longwave radiative fluxes were parameterized by the Chen and Cotton (1983) radiation scheme. Large-scale precipitation processes were simulated with a "dump-bucket" parameterization scheme (Cotton et al. 1995). The convective precipitation parameterization employed was a modified Kain-Fritsch scheme (Castro et al. 2002; Kain 2004) which replaced the standard Kuo scheme in this RAMS version. The incorporation of the Kain-Fritsch scheme to RAMS greatly improves the amount and spatial distribution of precipitation in the simulations (Castro et al. 2002).

The experiments covered a 5 month period, from September to January (late winter-spring to early summer). Atmospheric lateral boundary conditions and initial atmospheric fields were provided by the European Centre for Medium-Range Weather Forecasts (ECMWF) 40 year reanalysis (ERA-40) data set. For the sensitivity experiments, these data were replaced by the NCEP/NCAR reanalysis (Kalnay et al. 1996). In both cases, the reanalysis data were assimilated every 6 h. Five gridpoints were used for the lateral boundary nudging. For internal nudging, a 24 h timescale was applied.

Reproduced with permission of the copyright owner. Further reproduction prohibited without permission.

Climatological sea surface temperature from NCEP global one-degree grid data base were used on a daily-basis update (Reynolds and Smith 1994).

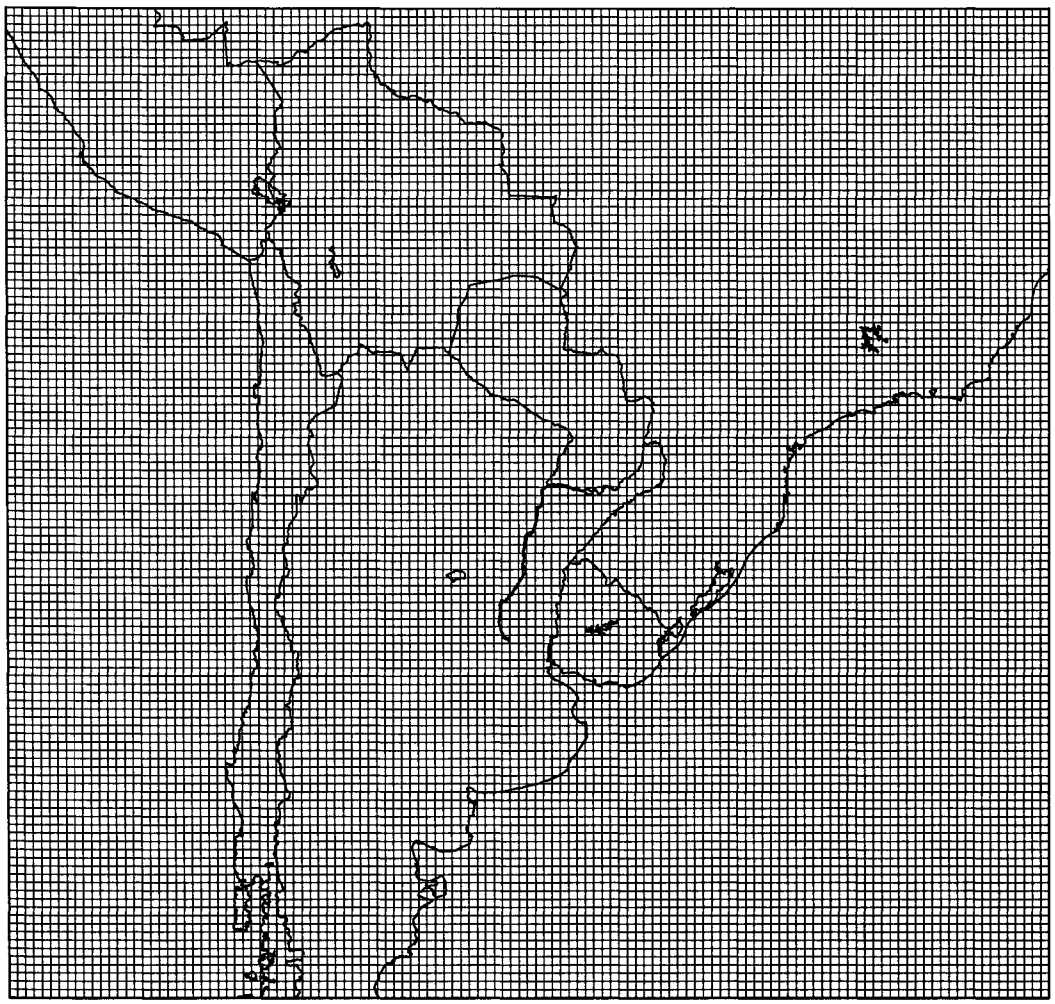

Figure 2.5. Grid used in all the South American simulations.

Reproduced with permission of the copyright owner. Further reproduction prohibited without permission.

Soil water content was initialized with the Soil Water Index (SWI; Wagner et al. 2003) derived from European Remote Sensing Satellites (ERS) scatterometer. The data are available at http://www.ipf/tuwien.ac.at/radar/ers-scat/home.htm, from 1992 to 2000, with a 10-day frequency and 28 km × 28 km grid spacing. This is a coarse-resolution active microwave product. Scatterometers transmit electromagnetic pulses and measure the energy scattered back from the observed surface. The intensity of the signal depends on the surface roughness that includes effects from the soil surface and from vegetation. Several studies have shown that scatterometer data are sensitive to surface soil moisture (e.g., Wagner et al. 1999a; Moeremans and Dautrebande 2000; Moran et al. 2000). These studies used a change detection approach: a backscatter coefficient representing a reference dry soil condition is subtracted from the actual measurements of the backscatter coefficient. In addition, Wagner et al. (1999b,c) improved the method to account for the effects of plant growth and decay. The retrieved information corresponds to the surface (< 5 cm) soil moisture content, representing the degree of saturation, scaled between zero soil moisture and saturation (1 or 100%). To estimate the moisture content in the soil profile, Wagner et al. (1999c) developed a semi-empirical modeling approach by considering a two-layer soil model. A relative measure of the area-averaged soil moisture content in a given layer can be estimated by a quantity called Soil Water Index which ranges between 0 and 1. When comparing to field measurements in different regions, the best correlations with SWI were observed for the 0-100 cm layer in Wagner et al. (1999c) and for the 0-25 cm layer in Ceballos et al. (2005). Wagner et al. (1999c) found a mean coefficient of determination R^2 of approximately 0.25 and a mean square error (RMS) of around 5 vol% for observed soil moisture in the 0-100 cm layer over Ukraine. Over the

Reproduced with permission of the copyright owner. Further reproduction prohibited without permission.

central part of the Duero Basin, Spain, Ceballos et al. (2005) found a R^2 of 0.75 for the averaged 0-100 cm soil moisture profile, and a root mean square error of 2.2 vol%. This indicates that at a global scale, the layer thickness corresponding to the SWI data may vary from region to region.

The SWI used to initialize RAMS simulations corresponds to a globally derived dataset from active microwave data (Wagner et al. 2003). Comparisons of this global monthly time series of SWI with modeled soil moisture of the 0 – 50 cm layer from the LPJ dynamic global vegetation model (Sitch et al. 2003), showed correlation coefficients higher than 0.61 for most of the climates. For dry climates correlation coefficients were generally below 0.5. Although the quality of this data was not strictly determined from that study, it constitutes an interesting new source of information that can be used to initialize soil moisture for climate modeling.

Wagner et al. (1999c) showed that SWI can be used to derive the plant available water content PAW:

$$PAW = \theta - \theta_{wp} = SWI\left(\frac{\theta_{fc} + \theta_{twc}}{2} - \theta_{wp}\right)$$

where θ, θ_{wp}, θ_{fc} and θ_{twc} are volumetric soil moisture, wilting point, field capacity, and total water capacity or porosity, respectively (all in units $m^3\ m^{-3}$). This is based on the idea that SWI values range between dry (e.g., wilting point) and wet conditions (e.g., mid-point between field capacity and porosity).

In all the simulations performed in this study, the three 10-day SWI data corresponding to September were averaged for the period 1992-2000 and, together with the values of θ_{wp}, θ_{fc} and θ_{twc} associated with each soil texture, were used to compute the

Reproduced with permission of the copyright owner. Further reproduction prohibited without permission.

initial soil water conditions. Vertically uniform soil moisture content was assumed throughout the soil profile. Initial soil moisture conditions range between 50-70% of saturation in the central-east decreasing to 10-20% in the arid-semiarid region (Figure 2.6). The highest values of soil moisture content were found in some grid cells in the Flooding Pampas, with 70 to 80% of saturation. No major floods occurred during the years chosen for this study, but initial soil moisture conditions presented the highest values in the Flooding Pampas mainly as a result of a relative wet 1992-2000 period. Standing water from 5 to 10 cm can be found in some areas during late winter (Soriano 1991), but no attempt was made to identify them (i.e., from satellite images). Those areas might also cover a small percentage of a grid cell.

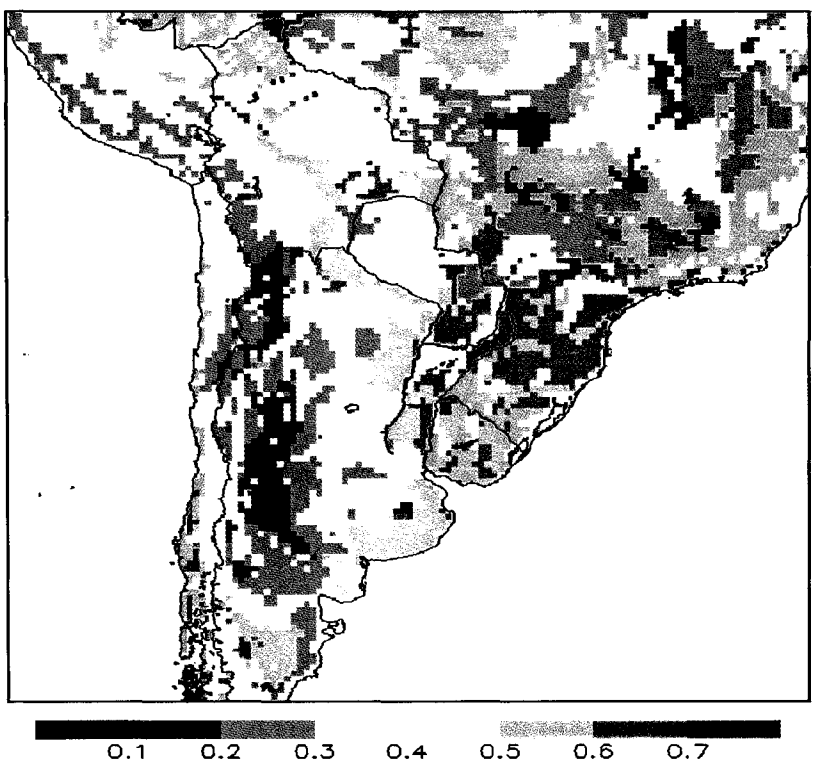

Figure 2.6. Initial soil moisture conditions (as a fraction of saturation) used as input to all the South American simulations.

Reproduced with permission of the copyright owner. Further reproduction prohibited without permission.

To evaluate simulated precipitation fields, different global gridded precipitation datasets were used. They are based on estimates from satellite over land and oceans and by rain gauge data over land. One corresponds to the 0.5° × 0.5° monthly 50-year Reconstruction dataset (Chen et al. 2002). This data is derived from the Global Historical Climatology Network version 2 (GHCN v.2) of NOAA/NCDC and the Climate Anomaly Monitoring System (CAMS) of NOAA/CPC. A second product used is the GPCP 1° × 1° daily data set (Huffman et al. 2001). These data extend from October 1996 to December 2001, and is a combination of several satellite estimates plus rain gauge observations over land and oceans. Monthly gridded data for temperature are based on the 0.5° × 0.5° dataset developed by Willmott and Matsuura (1995) from the GHCN v.2.

2.4 Experimental Design

Table 2.1 shows the different simulations carried out in this study. The first set of experiments comprises simulations performed with the uncoupled modeling system, RAMS, in which NDVI-derived LAI was ingested daily. The control experiments consisted on RAMS simulation for the non-ENSO period September 1996 - January1997. Two other periods were chosen for sensitivity tests because they correspond to different ENSO events: a 1997-1998 El Niño and a 1999-2000 La Niña. The 1999-2000 La Niña event was characterized by drought conditions from September 1999 to February 2000 in northeastern Argentina, resulting in crop damage and production losses in most of the region (Ravelo and Zanvettor 2000). The 1997-1998 year is considered one of the most important ENSO events (Camillioni and Barros 2001).

Reproduced with permission of the copyright owner. Further reproduction prohibited without permission.

Table 2.1. Experiment names, indicating the reanalysis product used as initial and boundary conditions (ERA_40 vs. NCEP) and the way LAI is obtained in each simulation.

Experiment	Lateral forcing	LAI
RAMS_ERA	ERA-40	NDVI-derived
RAMS_NCEP	NCEP	
GEMRAMS	ERA-40	Prognosed

Another sensitivity experiment considered the use of different atmospheric forcing conditions. Differences in initial conditions in large-scale forcing can have a significant effect on regional climate simulations (Miguez-Macho and Paegle 2000; Wu et al. 2005). The NCEP reanalysis and ERA-40 are the two most common products used to initialize regional atmospheric models. Wang and Paegle (1996) and Min and Schubert (1997) found differences in the regional moisture flux in northeastern Argentina between those two datasets, mainly because of differences in the low-level jet and large-scale circulation patterns. Simulations using the NCEP reanalysis were performed from September to January for the three periods 1996-1997, 1997-1998, and 1999-2000.

In the second part, the fully coupled modeling system, GEMRAMS, was used with the same configuration and initial conditions as the uncoupled model. ERA-40 reanalysis were used in the coupled simulations. LAI values for September 1st for each year were used to initialize the model (see Figure 2.4). Results were compared to RAMS_ERA simulations.

Reproduced with permission of the copyright owner. Further reproduction prohibited without permission.

2.5 Results of the Uncoupled Simulations

The results from the control RAMS_ERA simulations are introduced here. The objective in this exercise was to evaluate RAMS ability to simulate spatial and temporal variation of pressure fields, precipitation, near-surface temperature, and fluxes using ERA-40. Sensitivity experiments of changes in large-scale forcing (RAMS_NCEP) are discussed in Section 2.6. Lastly, the results for RAMS_ERA and RAMS_ NCEP for the additional wet and dry years are analyzed in Section 2.7.

2.5.1 Pressure Fields and Winds

Because of the interior nudging applied, it is expected upper-level height and winds to be close to the corresponding reanalysis data. The large-scale features were maintained but temporal and spatial differences were found. Simulated 850 hPa geopotential height fields tended to be lower than the corresponding ERA-40 reanalysis (Figure 2.7). Nevertheless, they reproduced the characteristic features associated with the summer climate in this region: two centers of high pressure in the Pacific and Atlantic subtropical oceans, and low pressure around north of Argentina, Paraguay, and center of Bolivia and south of 39°S (Figure 2.7). Associated winds to these patterns include southerlies along the coast of Chile, northeasterlies from the Atlantic that penetrate up to the center of the domain, and northwesterlies along the Andes.

Reproduced with permission of the copyright owner. Further reproduction prohibited without permission.

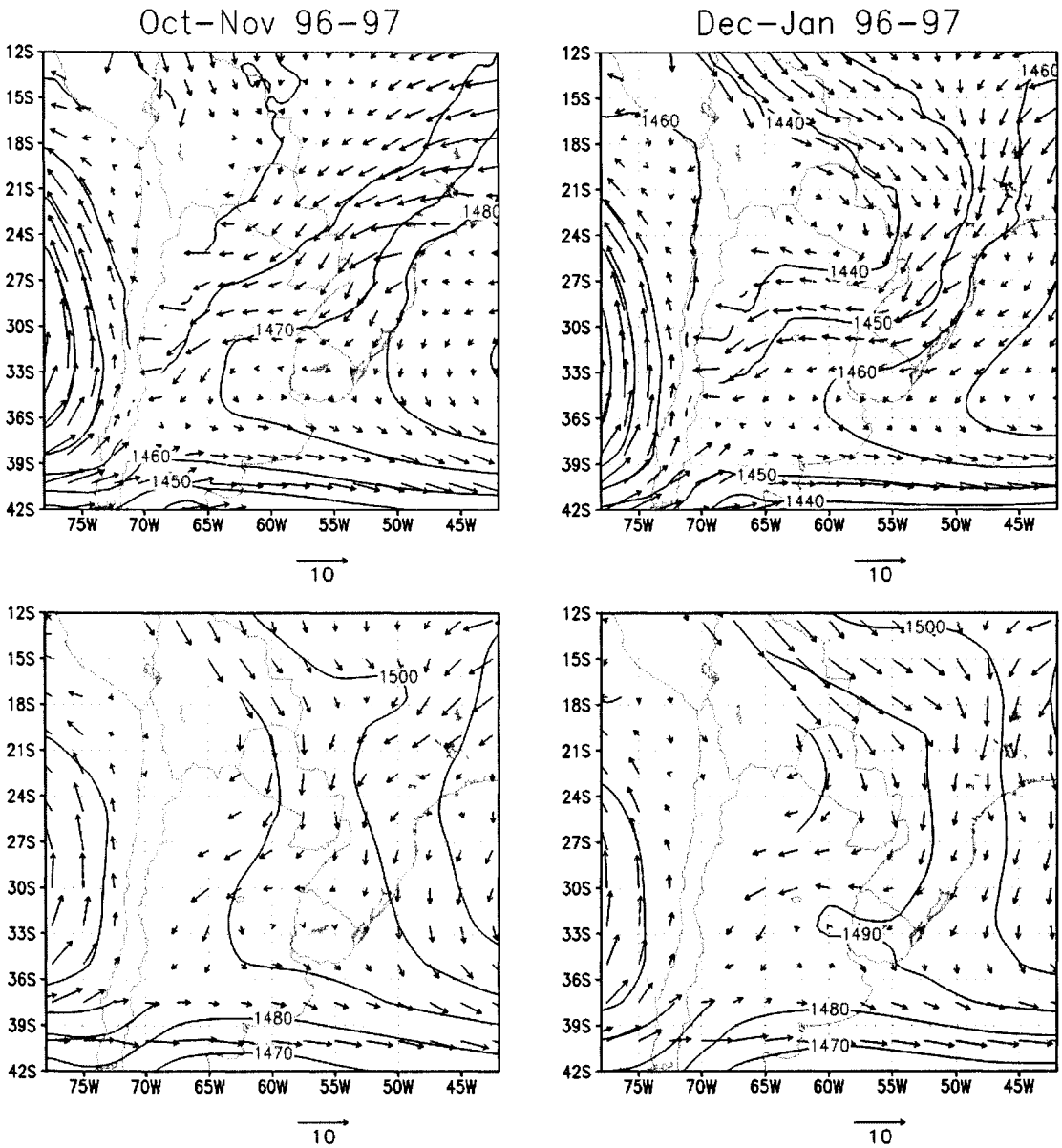

Figure 2.7. Simulated RAMS_ERA (top) and observed from ERA-40 (bottom) 850 hPa geopotential heights and wind patterns.

Reproduced with permission of the copyright owner. Further reproduction prohibited without permission.

Simulated geopotential heights and winds tended to be closer to the reanalysis in summer than in spring. During spring, northeasterlies around (18°S, 45°W) in the reanalysis were easterlies in the simulations. Also in this season, northwesterlies along the Andes north of 21°S were underestimated, compared to the reanalysis. During summer, a small cyclonic circulation close to the Andes around (21°S, 64°W) appeared in the simulation which was not found in the reanalysis. The low-level circulation in Bolivia was better captured in this season.

The predominant feature in the 250 hPa streamlines (Figure 2.8) is the Bolivian High (Lenters and Cook 1997). During spring, its simulated and observed center was located around (10°S, 60°W) close to the border of the model domain (not shown). During summer, its center shifted southward, but it was slightly displaced eastward with respect to the ERA-40 fields.

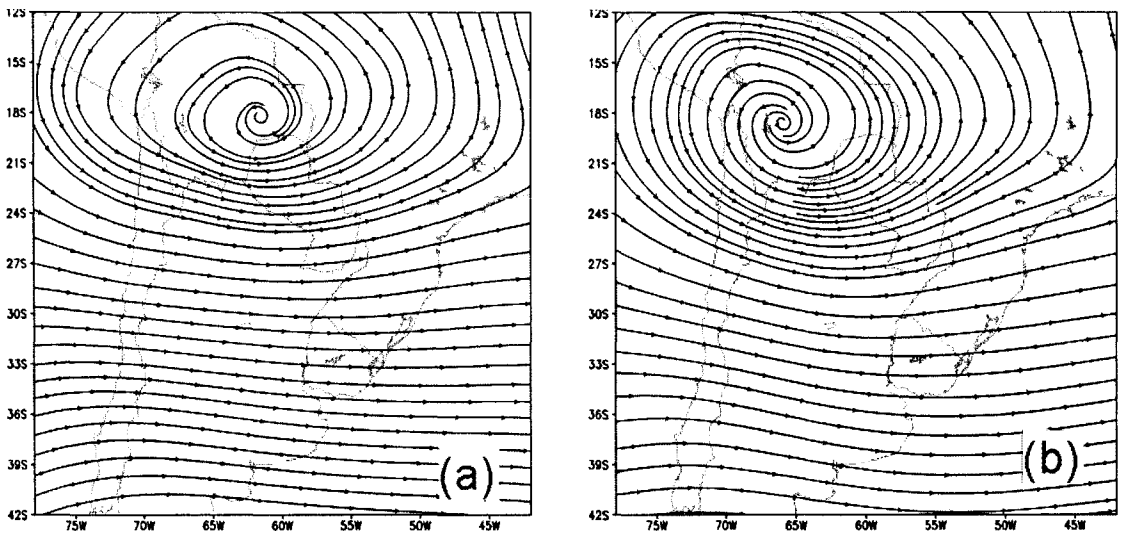

Figure 2.8. Simulated RAMS_ERA (left) and observed from ERA-40 (right) 250 hPa streamlines.

Reproduced with permission of the copyright owner. Further reproduction prohibited without permission.

2.5.2 Precipitation Fields

Figure 2.9 shows the observed (at 0.5° × 0.5 °, from Historical database), simulated (at 35 × 35 km) and ERA-40 precipitation fields (2.5° × 2.5°). Their own grid cell sizes were retained, so small features that appeared in the simulated fields are associated with the small grid spacing. Maximum values are observed on the northern and eastern part of the domain and along the Andes, north of 24°S, in both seasons. Over land, minimum values are found west of the Andes in an area oriented northwest-southeast, more noticeable during spring. In summer, another area with relative minimum values extended from the eastern part of Bolivia, around 60°W, through central Argentina to Uruguay.

Simulated precipitation patterns showed that over land, the model was able to capture the main features of the observed precipitation, although in general the values were overestimated (Figure 2.9). Because of the relatively weak central nudging used in the simulations, similar moisture convergence is expected between RAMS and ERA-40. Model configuration like nudging, convective parameterization and grid spacing may also greatly affect precipitation estimations. Over the Atlantic Ocean simulated precipitation was underestimated, although a simulated relative maximum appeared around (27°S, 47°W) extending in a NW-SE direction from the coast of Brazil. This deficit of precipitation over land was also found by Chou et al. (2002) and Misra et al. (2002a) with the Eta model. In spring, simulated maximum values on the northern part of the domain were overestimated, and the observed maximum over the NE tip of Argentina underestimated. In summer, the maximum in southeastern Brazil was relatively well

Reproduced with permission of the copyright owner. Further reproduction prohibited without permission.

collocated with observed values, although it was overestimated. A simulated secondary minimum area, around 60°W-65°W, was also well corresponded with the observations.

There are some observed features that are missing in the simulations. One is a relative maximum in the center of the Pampas, around (36°S, 60°W). In spring, this maximum was not simulated, while in summer it covered a smaller area than the observations and it was shifted to the west. The observed maximum around 40°S on Chile was also misrepresented. These last two underrepresented features may be associated with the parameterization of the large-scale (non-convective) precipitation. According to ERA-40 the large-scale precipitation represented a large portion of the total precipitation in the southern part of the domain during spring (not shown), but in the model only represented approximately less than 10% of the total precipitation. The simple "dumpbucket" type of scheme to simulate large-scale precipitation may be responsible for this behavior. Large-scale precipitation is simple computed based on a fixed precipitation efficiency applied over the supersaturation an air parcel. Preliminary results showed that a relatively low efficiency value has to be used to avoid anomalous high amounts of precipitation over some areas.

Reproduced with permission of the copyright owner. Further reproduction prohibited without permission.

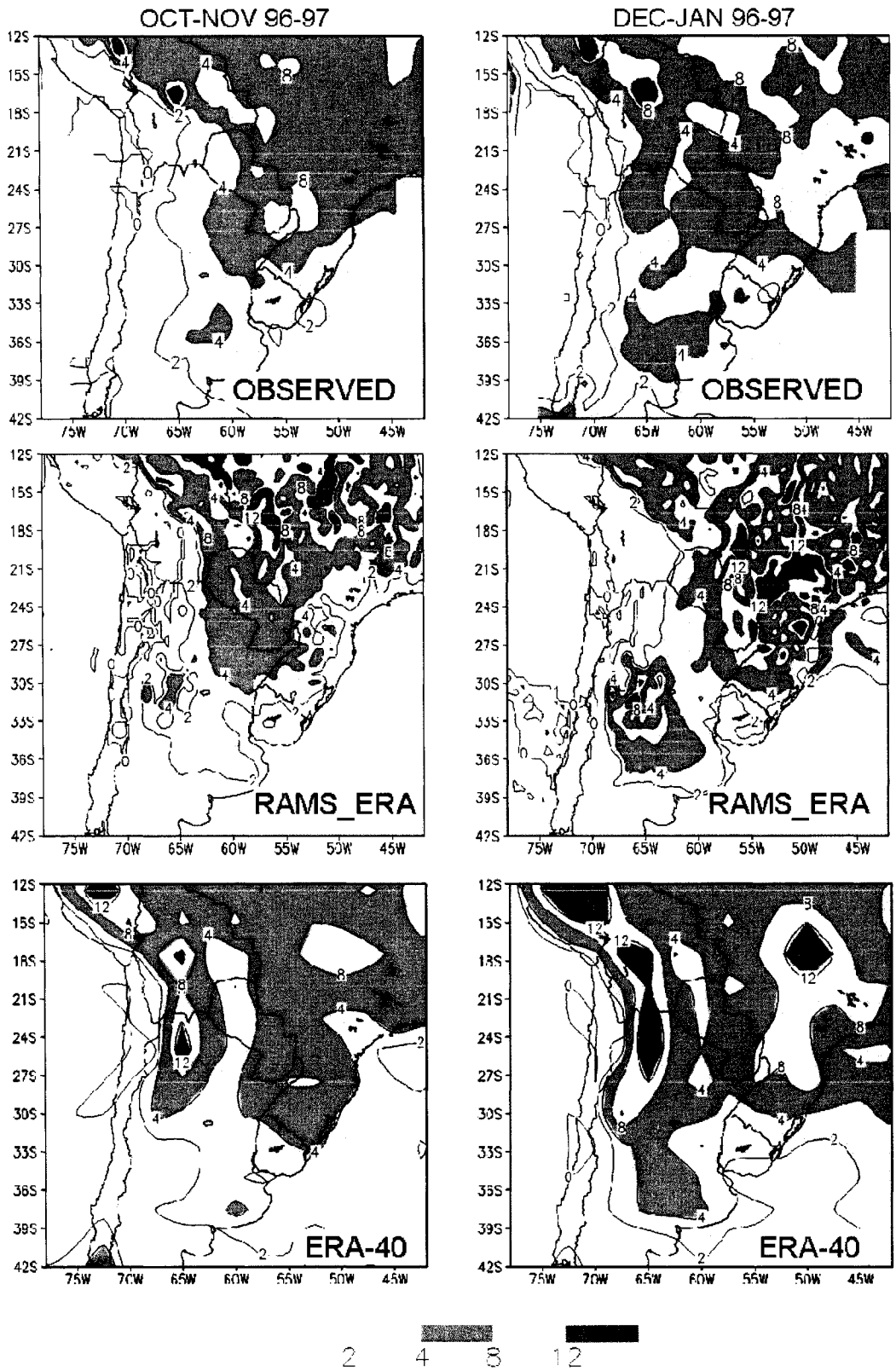

Figure 2.9. Mean precipitation (mm day^{-1}) for the 1996-1997 period: observed (top), simulated RAMS_ERA (middle), and ERA-40 reanalysis (bottom).

Reproduced with permission of the copyright owner. Further reproduction prohibited without permission.

Another feature that was not well represented in RAMS during summer was the maximum observed precipitation along the Andes, northward of 27°S. Although this observed maximum may be overestimated, precipitation data from stations located in this area show very characteristic maximum values during these two months (not shown). This feature may be related to deficiencies associated with the Kain-Fritsch convective parameterization and representation of terrain. In general, models tend to produce excessive precipitation along the Andes (e.g., Nicolini et al. 2002a,c; Misra et al. 2002a,b). In RAMS, some of the parameters in the convection scheme were adjusted to limit the orographic precipitation (Castro et al. 2002). The selection of the values of these parameters is a compromise between a general well behavior of the model over the steep terrain and over the plains. Some overestimation was found in intermediate elevations. A simulated maximum, around (30°S, 66°W) was not present in the observations. This maximum persisted throughout the simulation and may be related to a small topographic feature located in that area (see Figure 2.1).

Misrepresentation of some of the observed features was also found in the ERA-40 fields, especially with the maximum values (Figure 2.9). For example, maximum precipitation areas along the Andes were overestimated in magnitude and extension in both averaged periods. Although the position of the maximum in Brazil was better represented in summer than in spring, the value was overestimated. Due to the weak interior nudging used in the simulations, RAMS tended to produce precipitation fields similar to the corresponded reanalysis, modulated by the model physics, parameterizations (e.g., the adjustments introduced in the convection scheme to account for topography) and model configuration (e.g., domain size and grid spacing).

Reproduced with permission of the copyright owner. Further reproduction prohibited without permission.

Two selected regions were chosen within the eastern part of the domain to characterize the daily patterns of precipitation, based on the location of the land-cover changes to be discussed in Chapter 3. One of the areas, the Pampas (PA), is located between 39°S and 30°S and the land area east of 65°W is a region mostly covered by crops (Figure 2.9). The northeast (NE) comprises the land area located east of 62°W, between the latitudes 30°S and 17°S, mostly covered by wooded grasslands, with higher precipitation than the Pampas (Figure 2.9). Simulated RAMS_ERA and observed area-averaged daily precipitation are plotted in Figure 2.10 from October to January. Simulated and observed averaged values were 2.9 mm day^{-1} and 3.8 mm day^{-1} for the PA region and 6.2 mm day^{-1} and 6.5 mm day^{-1} for the NE region. Daily variability was relatively well captured in both areas, although in general RAMS tended to underestimate the peaks of heavy precipitation events, and overestimate the smaller precipitation events.

Reproduced with permission of the copyright owner. Further reproduction prohibited without permission.

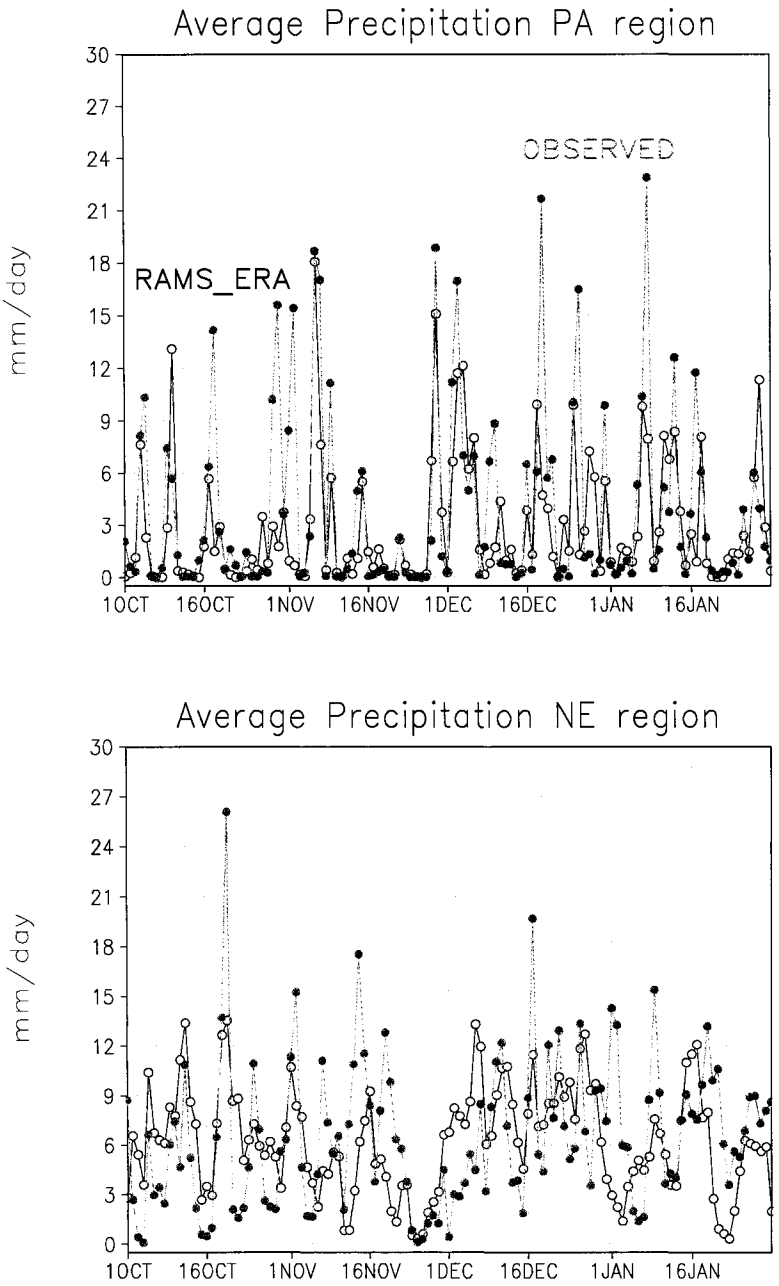

Figure 2.10. Area-average precipitation (mm day^{-1}) for 1996-1997 period for: NA region (top), and NE region (bottom), for RAMS_ERA and observed.

Reproduced with permission of the copyright owner. Further reproduction prohibited without permission.

2.5.3 Near-Surface Temperature and Fluxes

Main temperature patterns, described by Schwerdtfeger (1976), are well reproduced by RAMS (Figure 2.11). Areas with low temperatures were associated with elevated areas, like the Andes and southern Brazil, and high latitudes. Warmer areas were located in the north of the domain, with a tongue of maximum temperatures between 65°W and 60°W that advanced from the tropics towards the center of the domain as the summer season progresses. Maximum temperatures higher than 27°C were observed centered in Bolivia and western Paraguay in spring, extending to northern Argentina and Paraguay in summer. Simulated temperatures tended to be colder than the observed temperatures (Figure 2.11). On an area-averaged basis, the cold biases at the first model level (~57 m) were -1.5°C and -1.7°C in spring and summer, respectively. This bias decreased to -1.0°C and -1.1°C when the 2 m simulated temperatures were considered (not shown). This bias may be overestimated because of the different methods used to compute averaged temperatures, from monthly maximum and minimum temperatures in the case of observed data, and from 3 hourly outputs in the case of the model results. In these RAMS simulations, this cold bias is not directly affecting the vegetation, because LAI is updated from NDVI-derived data. It is found that this cold bias is amplified in GEMRAMS simulations, particularly in the center of the domain (see Section 2.9.3, Figure 2.28). In this case, vegetation growth might be affected by this colder temperature. Mean monthly temperatures computed using the maximum and minimum temperatures have been found to be up to 0.8°C warmer than the ones computed as the average of observations at fixed times, i.e., every 3 hours (Collison and Tabony 1984; Weber 1993; Trewin 2004). The areas with differences higher than -2°C were located around 18°S,

Reproduced with permission of the copyright owner. Further reproduction prohibited without permission.

extended to the east, and around 30°S close to the Andes, increasing the area in summer. This may be related to an overestimation of simulated precipitation. In these RAMS simulations, this cold bias is not affecting directly the vegetation, because LAI is updated from NDVI-derived data. It is found that this cold bias is amplified in GEMRAMS simulations, particularly in the center of the domain (see Section 2.9.3, Figure 2.28). In this case, vegetation growth might be affected by this colder temperature.

Temperatures higher than observed were found in the tip of NE Argentina-Brazil, central Argentina and in a small area in the northern part of the domain around 60°W. Nicolini et al. (2002a) also reported a general cold bias in a January climatology obtained with the CSIRO Division of Atmospheric Research limited area model (DARLAM) over South America. On the other hand, summertime simulations with the Regional Spectral Model (RSM) (Misra et al. 2002b) and regional ETA model (Chou et al. 2000, 2002) showed a generalized warm bias, of up to 6°C in the case of RSM.

Regional validation of the surface short and longwave radiation and latent and sensible heat fluxes components is a difficult task because those data are not commonly measure at the regular synoptic network. Monthly mean maps of global solar radiation are available for South America south of 10°S (Grossi Gallegos et al. 1987). Updated values of those data for Argentina (Grossi Gallegos 1998; Grossi Gallegos personal communication), together with the simulated values are shown in Figure 2.12.

Reproduced with permission of the copyright owner. Further reproduction prohibited without permission.

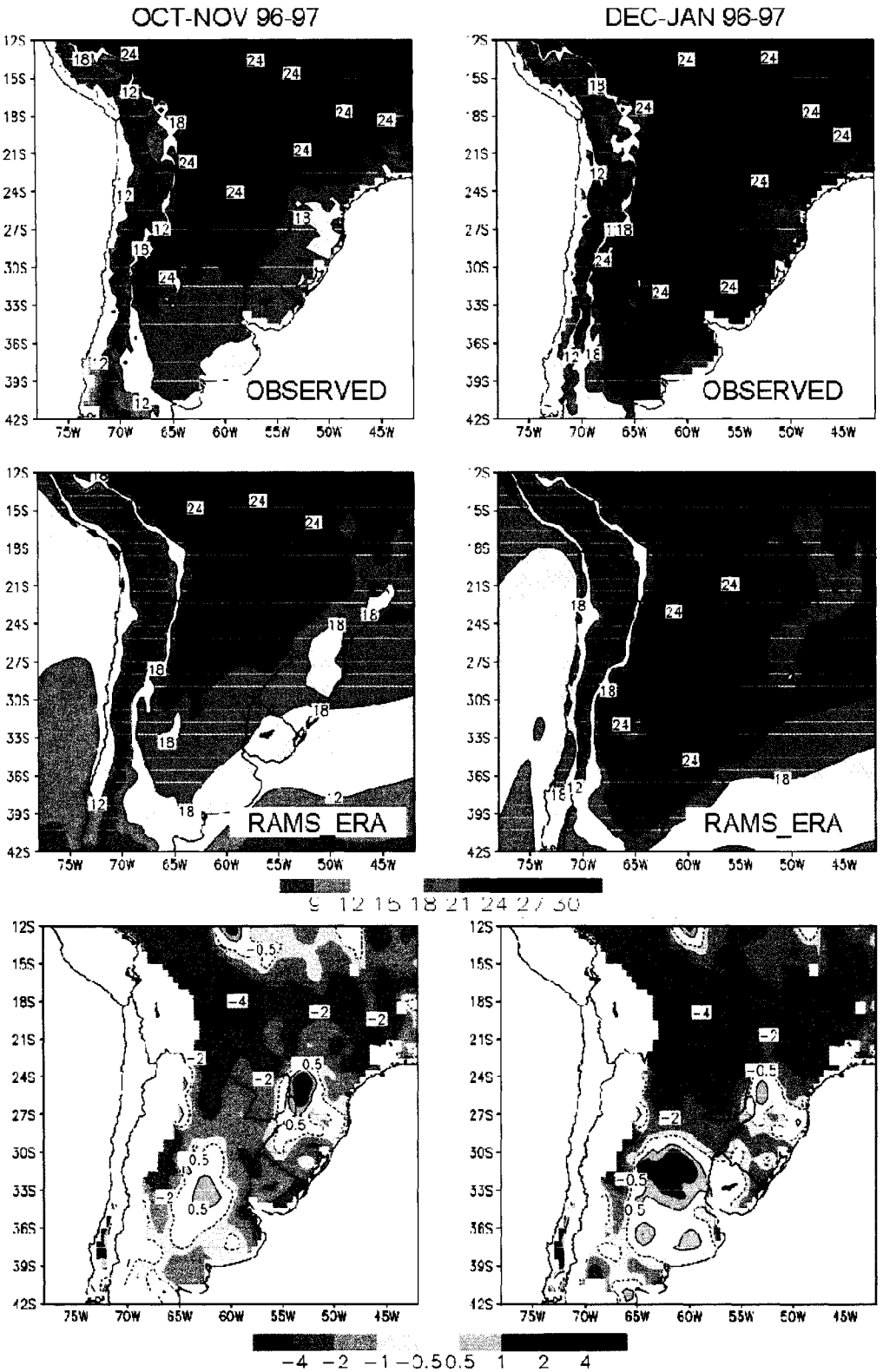

Figure 2.11. Mean temperature (°C) for 1996-1997 period: observed (top), RAMS_ERA (middle), and difference RAMS_ERA – observed (bottom).

Reproduced with permission of the copyright owner. Further reproduction prohibited without permission.

Minimum values were found in the areas of high precipitation, along the Andes and in the northern part of the domain. Values over central Argentina approximately agreed with the observed values. Over southern Brazil, the excess of rainfall and cloudiness produced a strong underestimation of the shortwave radiation received at the surface that may be responsible for the very cold bias in temperature.

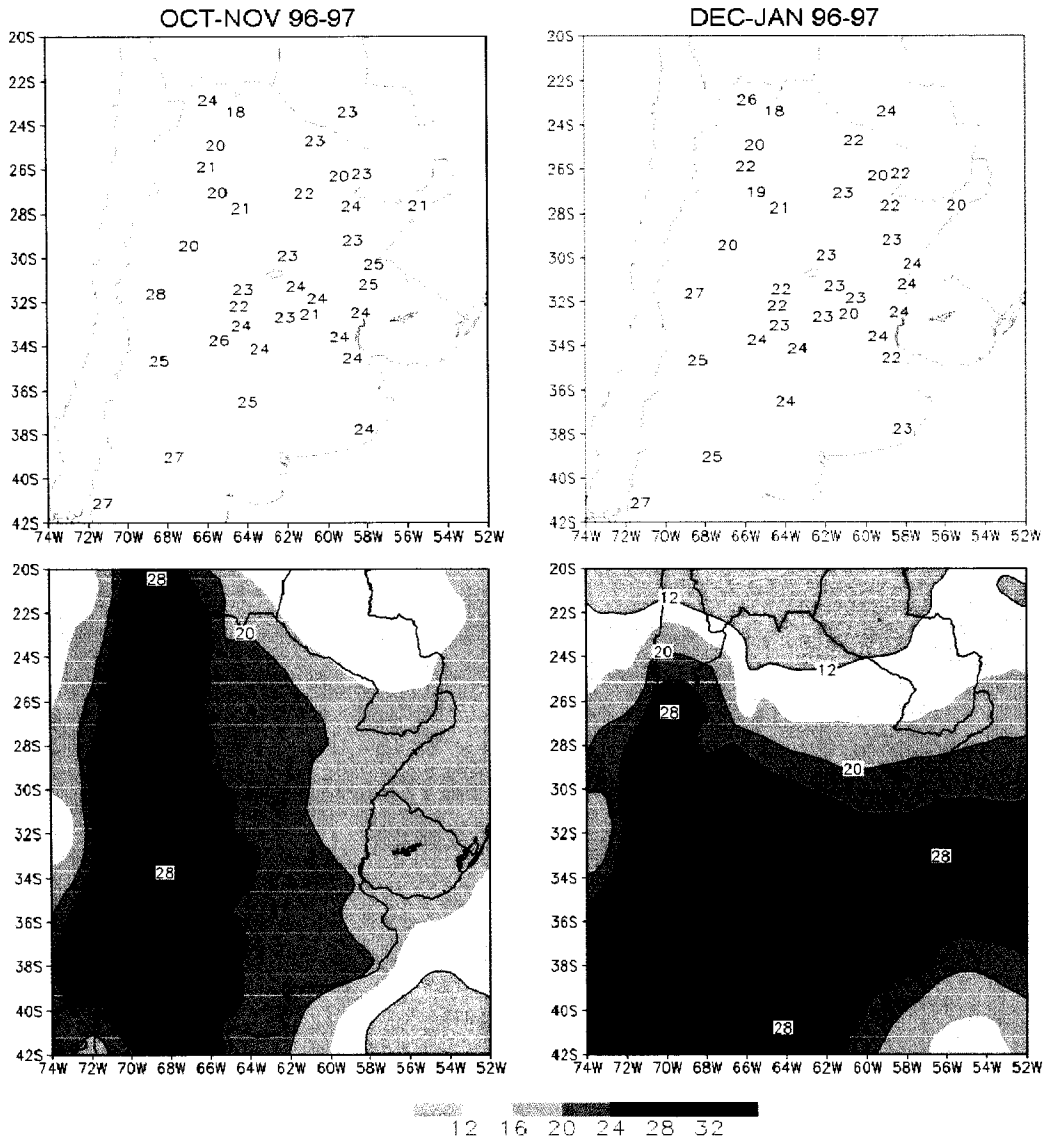

Figure 2.12. Observed (top) and simulated (bottom) solar global radiation (MJ m^{-2} day^{-1}).

Reproduced with permission of the copyright owner. Further reproduction prohibited without permission.

Lack of observations or intensive field campaigns like the ones undertaken in the Amazonia region makes the validation of the surface fluxes difficult to carry out. However, RAMS could capture the diurnal variations in the surface fluxes, with magnitudes in the range of typical values (see for example Jones 1994; Larcher 1995; Chou et al. 2002). Examples of simulated diurnal evolution of sensible (SH) and latent heat (LH) fluxes for different vegetation types are given in Figure 2.13. The top two figures correspond to a grid cell centered at (29°02', 64°W) with soybean as vegetation cover. The left panel represents two clear days after a rain and the right panel two days after several days without rain. The main difference between the two panels is how energy was partitioned between SH and LH. With good levels of soil moisture, most of the energy was dissipated as LH, approximately 83% of the net radiation (left panel), while during a drying period, LH was 36% of net radiation and most of the energy was dissipated as SH (right panel). For a site located at (31°49'S, 63°46'W), approximately 210 km west of the grid point, Pereyra (1988) found that LH on a soybean field represented 93% and 69% of net radiation for days under adequate and lower soil water conditions, respectively.

The bottom panels correspond to the energy balance of two grid cells 125 km apart around (25°S, 54°W), one classified as broadleaf tree and the other one as wooded grasslands, with similar soil water content levels and for the same days. The major differences between the two sites were the values of latent and sensible heat. Latent heat represented 92% and 38% of the net radiation for trees and wooded grasslands, respectively.

Reproduced with permission of the copyright owner. Further reproduction prohibited without permission.

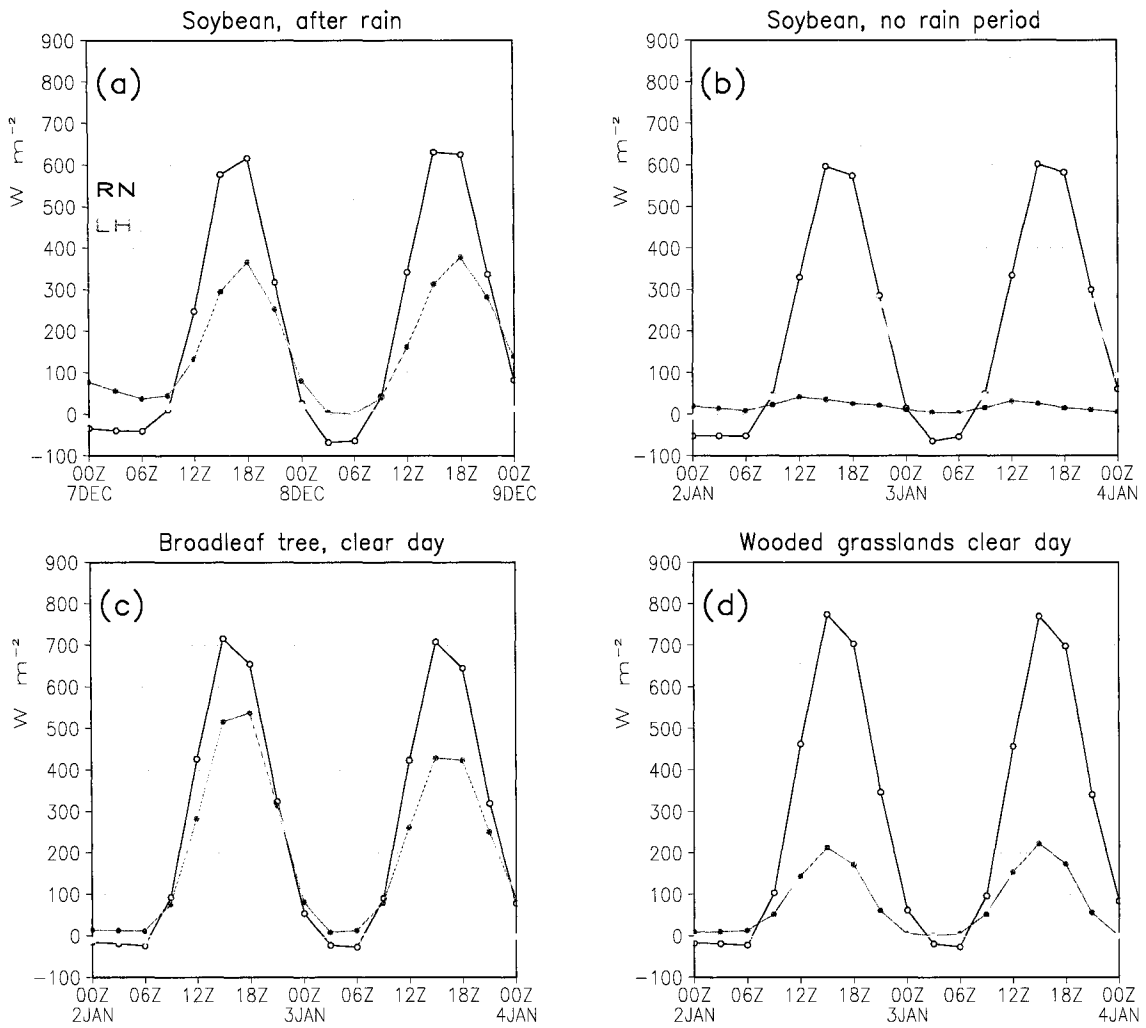

Figure 2.13. Evolution of net radiation (RN), latent heat (LH), and sensible heat (SH) for grid cells classified as: soybean (a) and (b), broadleaf tree (c), and wooded grasslands (d).

Reproduced with permission of the copyright owner. Further reproduction prohibited without permission.

2.6 Sensitivity to Atmospheric Lateral Boundary Conditions: Use of NCEP Reanalysis

Differences in large-scale forcing can have a significant effect on regional climate simulations (Wang and Paegle 1996; Miguez-Macho and Paegle 2000; Chou et al. 2002; Wu et al. 2005). Small differences in geopotential fields can lead to differences in moisture fluxes, which may turn out in differences in precipitation fields. The NCEP reanalysis and ERA-40 are the two most common products used to initialize regional atmospheric models. Small inherent differences can be seen in the 850 hPa heights and wind patterns between the two reanalysis products (Figure 2.14, top). NCEP reanalysis 850 hPa geopotential heights tended to be higher than ERA-40, with the maximum differences up to 8 m on the eastern side of the Andes at around 24°S in summer. This generated a slight cyclonic anomaly in the wind field, with a northerly anomaly component in ERA-40 around 55°W and a southerly anomaly close to the Andes around 65°W, between 24°S and 27°S. In general, RAMS_NCEP simulations (Figure 2.14, middle panel) were similar to RAMS-ERA simulations shown in Figure 2.7. A closer look at the differences between these two runs (Figure 2.14, bottom panel) revealed that differences found between the two reanalysis are shifted slightly eastward and enhanced. Largest differences in wind speed were found close to the Andes, around 21°S. In RAMS_NCEP simulations, northwesterlies close to the Andes around 15°S are stronger than in RAMS_ERA simulations. They tended to hug the Andes and penetrate northern Argentina with a northerly direction around 21°S and 65°W. On the other hand, in RAMS_ERA simulations, the flow had a WNW direction around 15°S and entered northern Argentina around 55°W (Figure 2.7).

Reproduced with permission of the copyright owner. Further reproduction prohibited without permission.

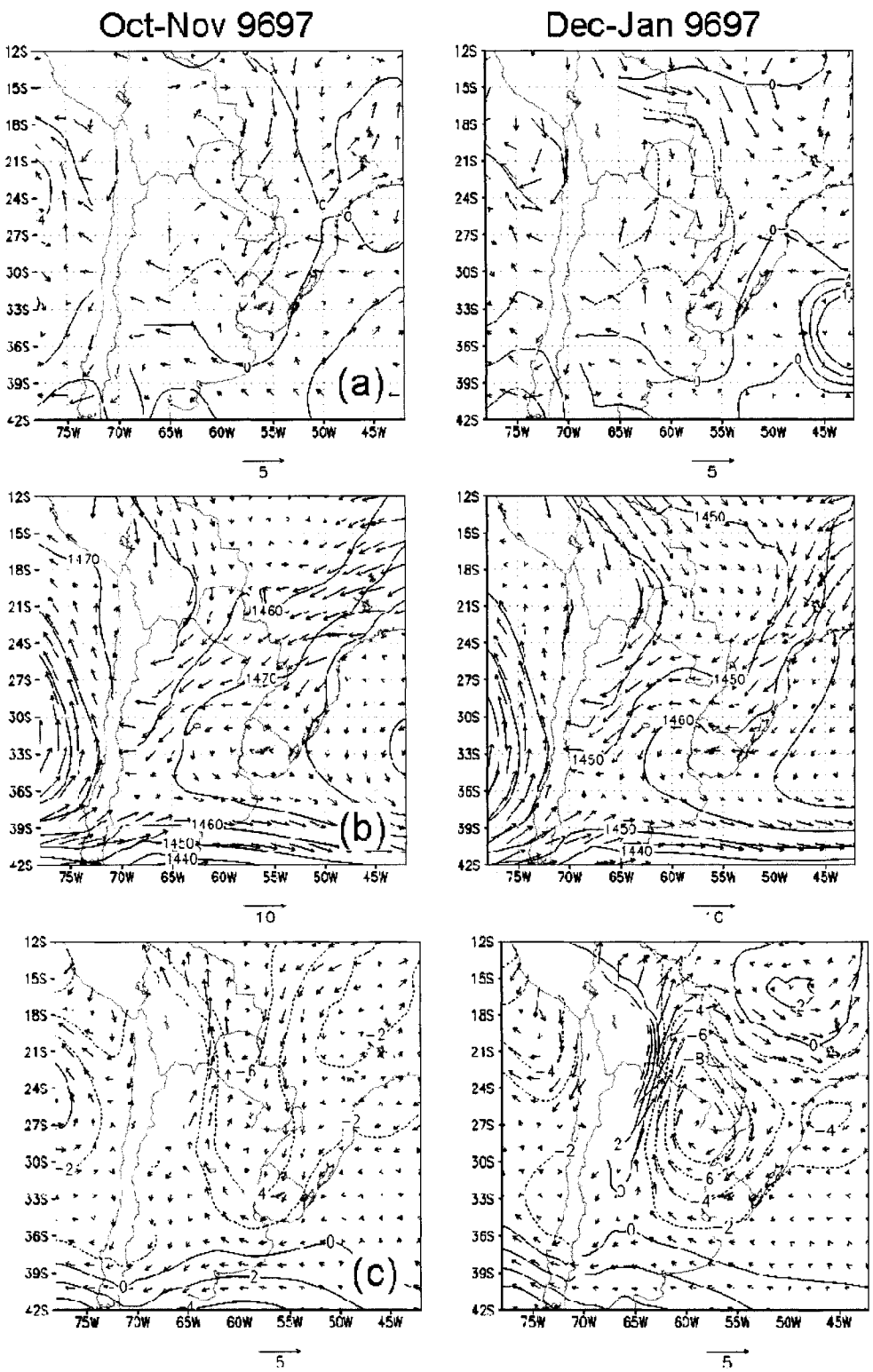

Figure 2.14. 850 hPa geopotential heights and winds: (a) Difference between reanalysis ERA-40 and NCEP, (b) Simulated RAMS_NCEP, (c) Difference between RAMS_ERA and RAMS_NCEP.

Reproduced with permission of the copyright owner. Further reproduction prohibited without permission.

The center of the Bolivian high, as seen in the 250 hPa streamlines in RAMS_NCEP simulations, was displaced eastward with respect to the observed NCEP reanalysis (Figure 2.15) and slightly westward with respect to RAMS_ERA simulations (compared to Figure 2.8).

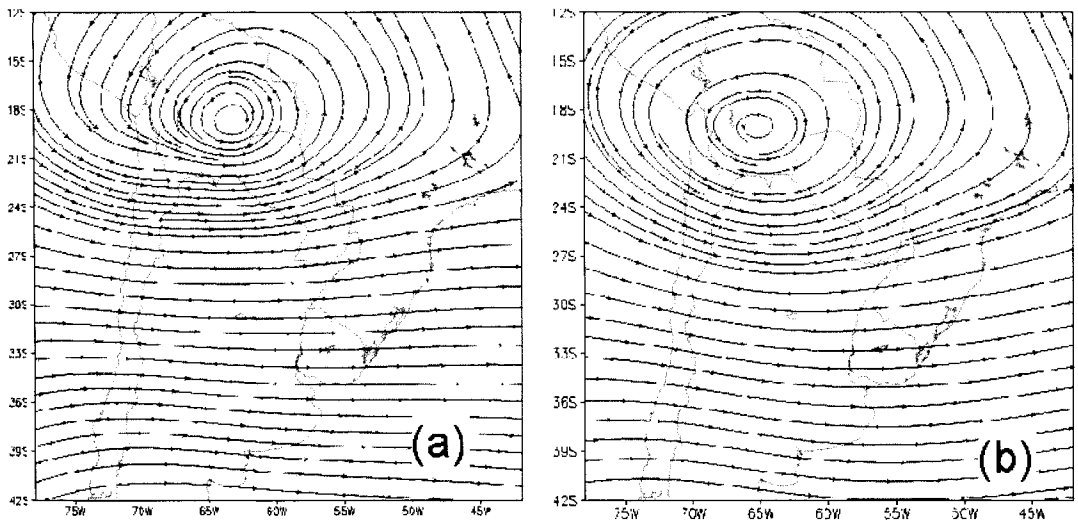

Figure 2.15. 250 hPa streamlines: (a) Simulated RAMS_NCEP, (b) NCEP reanalysis for Dec-Jan 1996-1997.

Figure 2.16 shows the 1996-1997 precipitation fields for RAMS_NCEP simulations together with the corresponding NCEP reanalysis and the difference between RAMS_ERA and RAMS_NCEP modeled precipitation. Precipitation simulated with RAMS_NCEP underestimated the observed values (see Figure 2.9 top) in the central and southern part of the domain and over the oceans. Similar to RAMS_ERA simulations, precipitation tended to be overestimated in the northeastern part of the domain over Brazil, and along the base of the slope in the northern Andes. Clearly it can be seen that, except for the maximum precipitation along the Andes, RAMS_NCEP simulations tended to closely resemble the NCEP reanalysis fields, similar to the RAMS-ERA

Reproduced with permission of the copyright owner. Further reproduction prohibited without permission.

simulations (see Figure 2.8 bottom). The last panel of Figure 2.15 shows the differences between the two simulations. In most of the central region, precipitation simulated by RAMS_ERA was higher that the one simulated by RAMS_NCEP, except for an area along the Andes and in the northeastern part of the domain, in Brazil. Another area with positive differences was the Pampas region, south of 30°S, where RAMS_ERA tended to have a better performance than RAMS_NCEP.

Deficiencies in simulated precipitation using NCEP reanalysis can also be seen in the daily area-averaged for Pampas and Northeast regions (Figure 2.17). On an area basis, RAMS_NCEP precipitation only represents 55% and 81% of RAMS_ERA in PA and NE regions (Table 2.2). Most of the rainfall events in RAMS-NCEP were underestimated, especially in the PA region.

Dataset	PA	NE
Observed	3.8	6.5
RAMS_ERA	2.9	6.2
RAMS_NCEP	1.6	5.0

Table 2.2. Area-averaged precipitation (mm day^{-1}) from RAMS_ERA, RAMS_NCEP and observations for PA and NE areas.

Using NCEP reanalysis as large-scale forcing led to a warm bias with respect to the observed temperatures (Figure 2.18). The areas with positive anomalies, with respect to observations, at the center of the domain found in RAMS_ERA simulations (see Figure 2.11) were enhanced. In summer, a wide area with positive anomalies, larger than 4°C, extended in a north-south direction immediately east of the Andes, collocated with the area with negative anomalies in precipitation (Figure 2.16). Warm bias in temperature

Reproduced with permission of the copyright owner. Further reproduction prohibited without permission.

was also found by Misra et al. (2002b), of as much as 6°C over the Pampas using NCEP reanalysis as boundary atmospheric conditions.

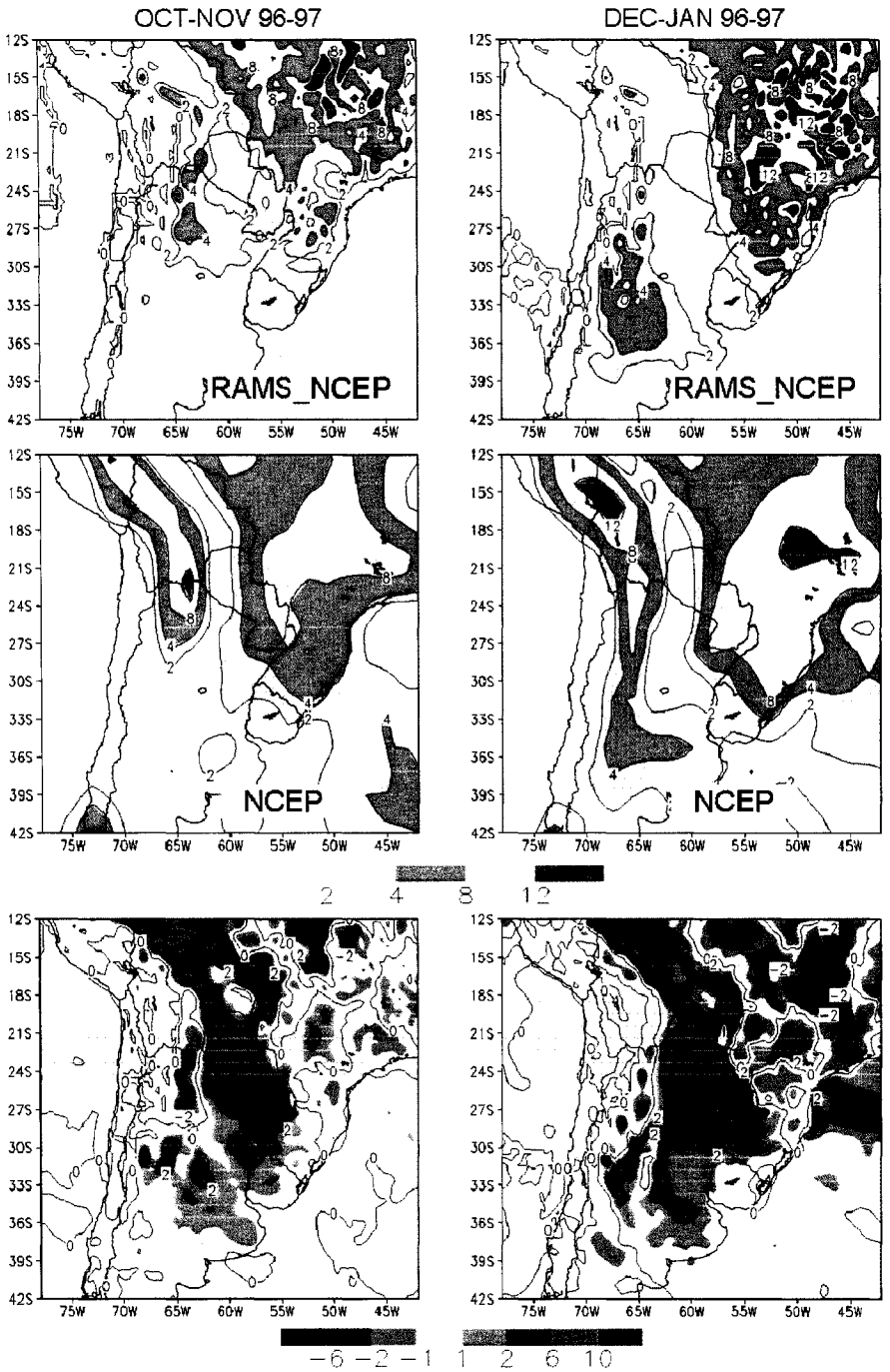

Figure 2.16. Mean precipitation (mm day^{-1}) for the 1996-1997 period: RAMS_NCEP simulated (top), NCEP reanalysis (middle), and differences between RAMS_ERA and RAMS_NCEP (bottom).

Reproduced with permission of the copyright owner. Further reproduction prohibited without permission.

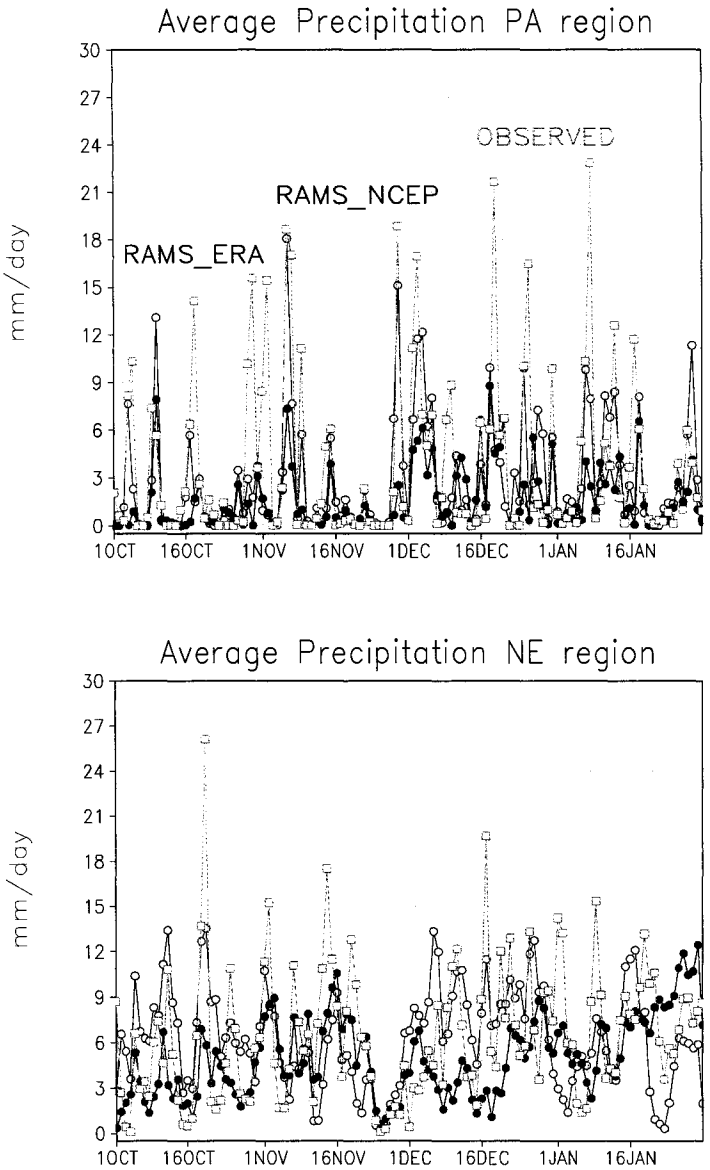

Figure 2.17. Area-average precipitation (mm day^{-1}) for the 1996-1997 period for: NA region (top), and NE region (bottom) for RAMS_ERA (black), RAMS_NCEP (red), and observed (green).

Reproduced with permission of the copyright owner. Further reproduction prohibited without permission.

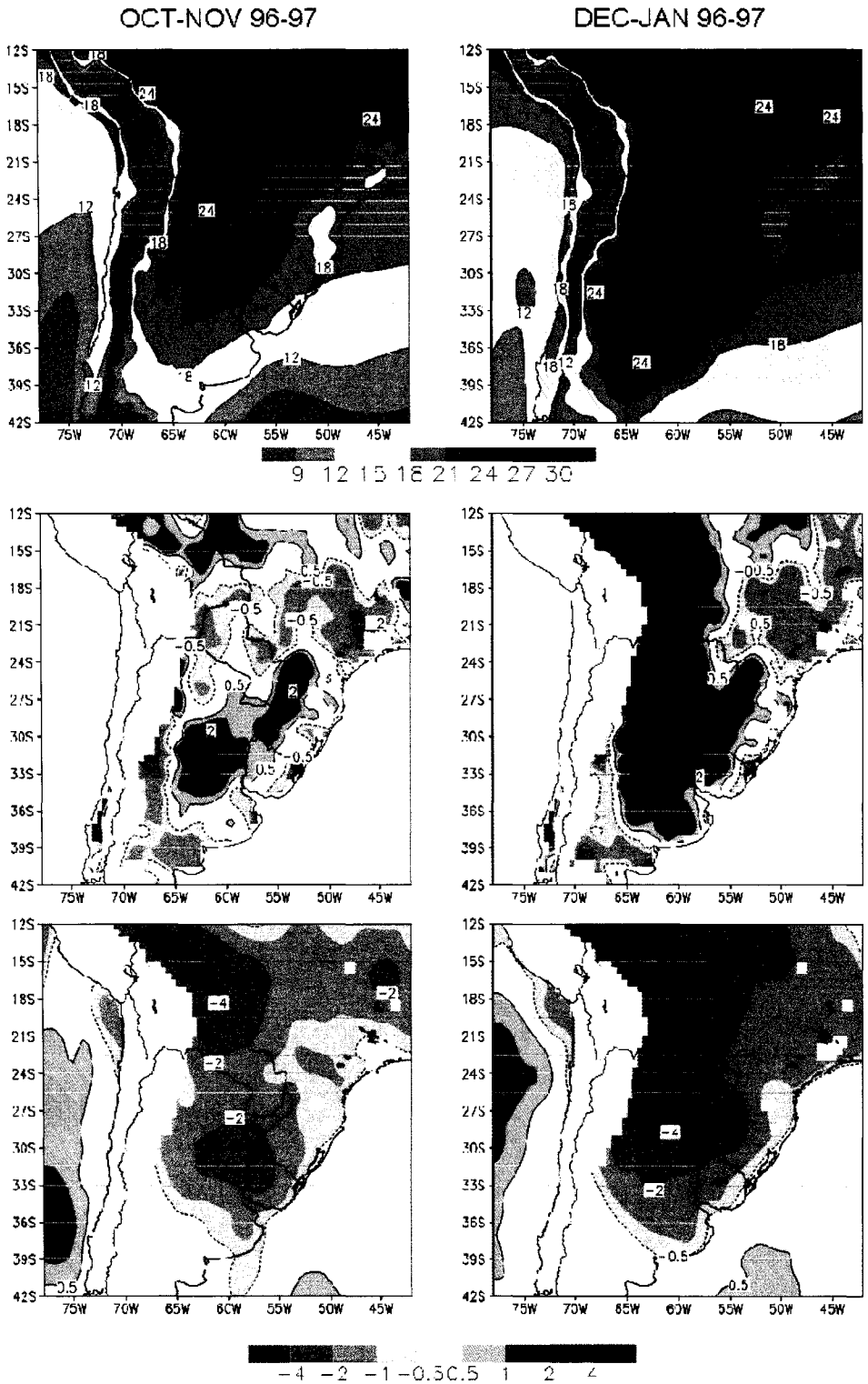

Figure 2.18. Mean temperature (°C) for the 1996-1997 period: RAMS_NCEP (top), difference RAMS_NCEP – Observed (middle), and difference RAMS_ERA – RAMS_NCEP (bottom).

Reproduced with permission of the copyright owner. Further reproduction prohibited without permission.

2.7 Sensitivity to Interannual Variability: El Niño and La Niña Years

RAMS simulations of 850 hPa winds and geopotential heights reproduced the major features found in the reanalysis products for both ENSO years. Only the simulated fields are shown. These simulations were examined based on the 1996-1997 RAMS_ERA and RAMS_NCEP simulations. During the El Niño year (1997-1998), simulations using both reanalysis (Figure 2.19) showed stronger northwesterlies in Bolivia along the northern Andes than in the control run (Figures 2.7 and Figure 2.14). In addition, most of the flow entering northern Argentina originated in the Amazon region. The Atlantic high shifted towards the northeast with respect to the control run, and then northeasterlies ran almost along the coast in southern Brazil with an anticyclonic turn between 50°W and 55°W. Differences in 850 hPa winds and geopotential heights between RAMS_ERA and RAMS_NCEP were slightly enhanced respect to the control simulation (see Figure 2.14 bottom panel), especially during spring.

During 1999-2000, corresponding to a La Niña year, northwesterlies along the northern Andes tended to be weaker than in the other two years (Figure 2.20), in particular in RAMS_ERA simulations. Easterlies and northeasterlies from the Atlantic high penetrated through northern Argentina around 27°S. Similar to the 1997-1998 results, 850 hPa geopotential heights were higher in RAMS_NCEP than in RAMS_ERA, and also enhanced with respect to the control 1996-1997 simulation.

Reproduced with permission of the copyright owner. Further reproduction prohibited without permission.

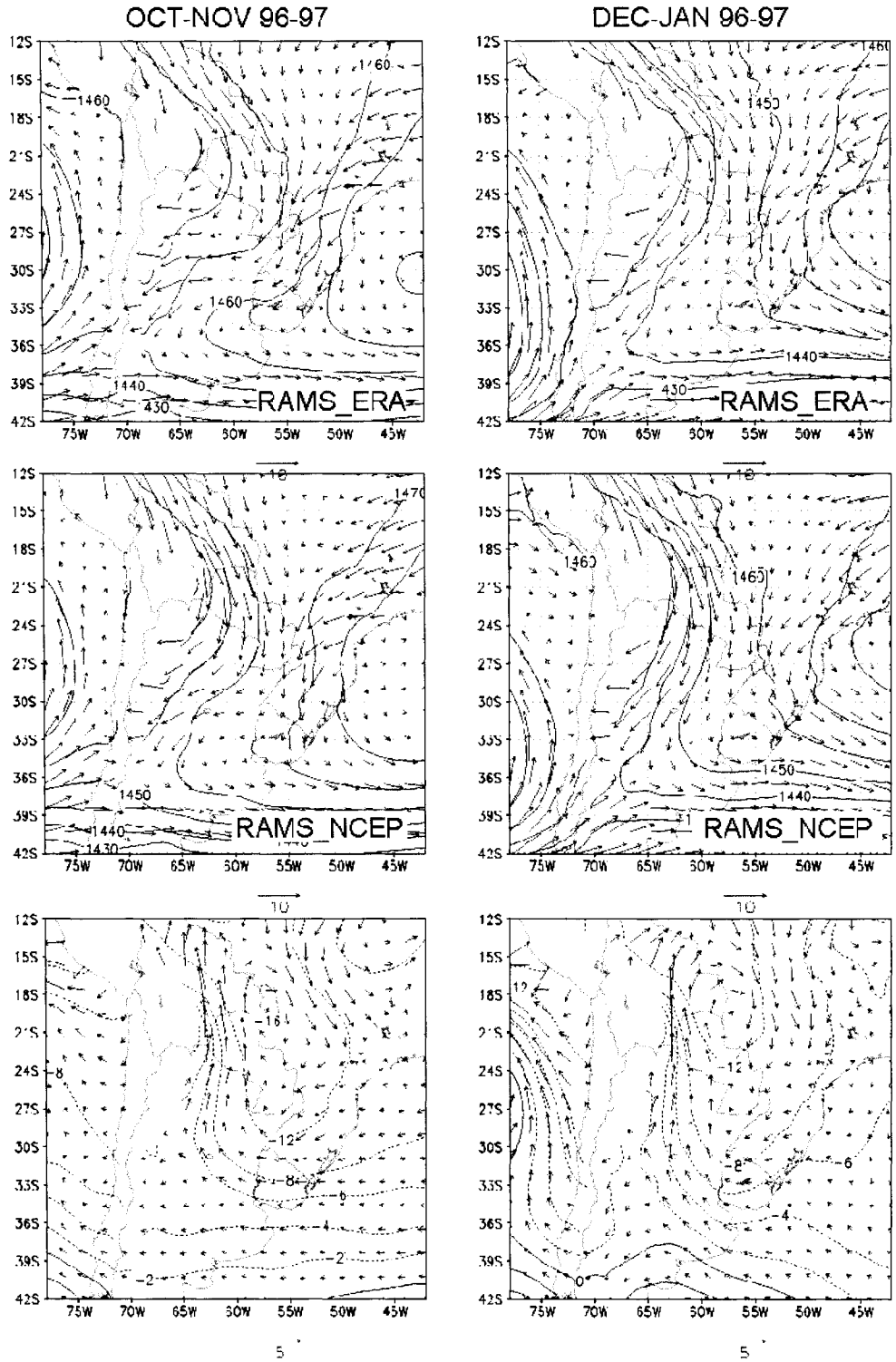

Figure 2.19. Simulated 850 hPa geopotential heights and wind patterns for the 1997-1998 period: RAMS_ERA (top), RAMS_NCEP (middle), difference RAMS_ERA – RAMS_NCEP (bottom).

Reproduced with permission of the copyright owner. Further reproduction prohibited without permission.

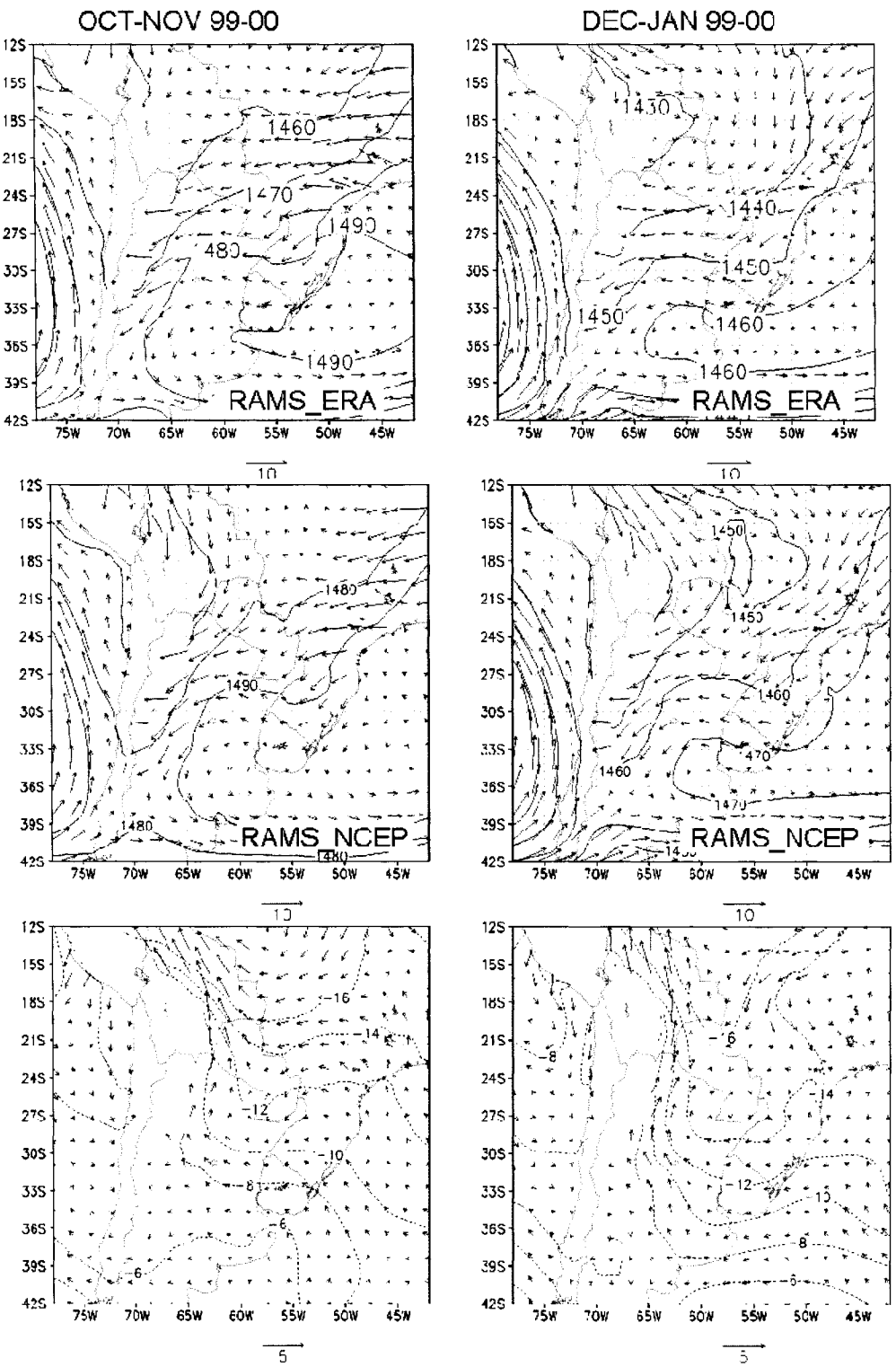

Figure 2.20. Simulated 850 hPa geopotential heights and wind patterns for the 1999-2000 period: RAMS_ERA (top), RAMS_NCEP (middle), difference RAMS_ERA – RAMS_NCEP (bottom).

Reproduced with permission of the copyright owner. Further reproduction prohibited without permission.

The observed differences in the 250 hPa streamlines between the ENSO years were also reproduced by RAMS (not shown). During summer 1997-1998, the anticyclone over Bolivia shifted slightly northwestward from its 1996-1997 position, in agreement with Lenters and Cook (1997). On the other hand, in 1999-2000, the Bolivian High is enhanced and displaced slightly eastward from its 1996-1997 position.

Differences in observed and simulated precipitation fields for 1997-1998 and 1999-2000 are shown in Figures 2.21 and 2.22. Spatial patterns were better represented when using the ERA-40 as boundary conditions than with NCEP reanalysis, similar to the control 1996-1997 simulations. Interannual variability can be observed between both ENSO years with 1997-1998 being relatively wet compared to 1999-2000. This variability was better captured by RAMS in spring than in summer with RAMS_ERA reproducing better the observed precipitation fields than RAMS_NCEP. Nevertheless, there were spatial differences. In spring for the El Niño year, RAMS_ERA overestimated the excess of precipitation over the northeastern part of the domain, but over the Pampas it performed relatively better than RAMS_NCEP. In summer, both simulations failed to represent the observed maximum over northern Uruguay and southern Brazil area. A similar result was found by Zhou and Lau (2002). A poor representation of the LLJ may have caused this underestimation. During a La Niña year, noticeable low precipitation was observed on the eastern part of the domain in spring and between 36°S and 27°S in summer. RAMS_NCEP underestimate the observed precipitation south of 24°S during this year.

Reproduced with permission of the copyright owner. Further reproduction prohibited without permission.

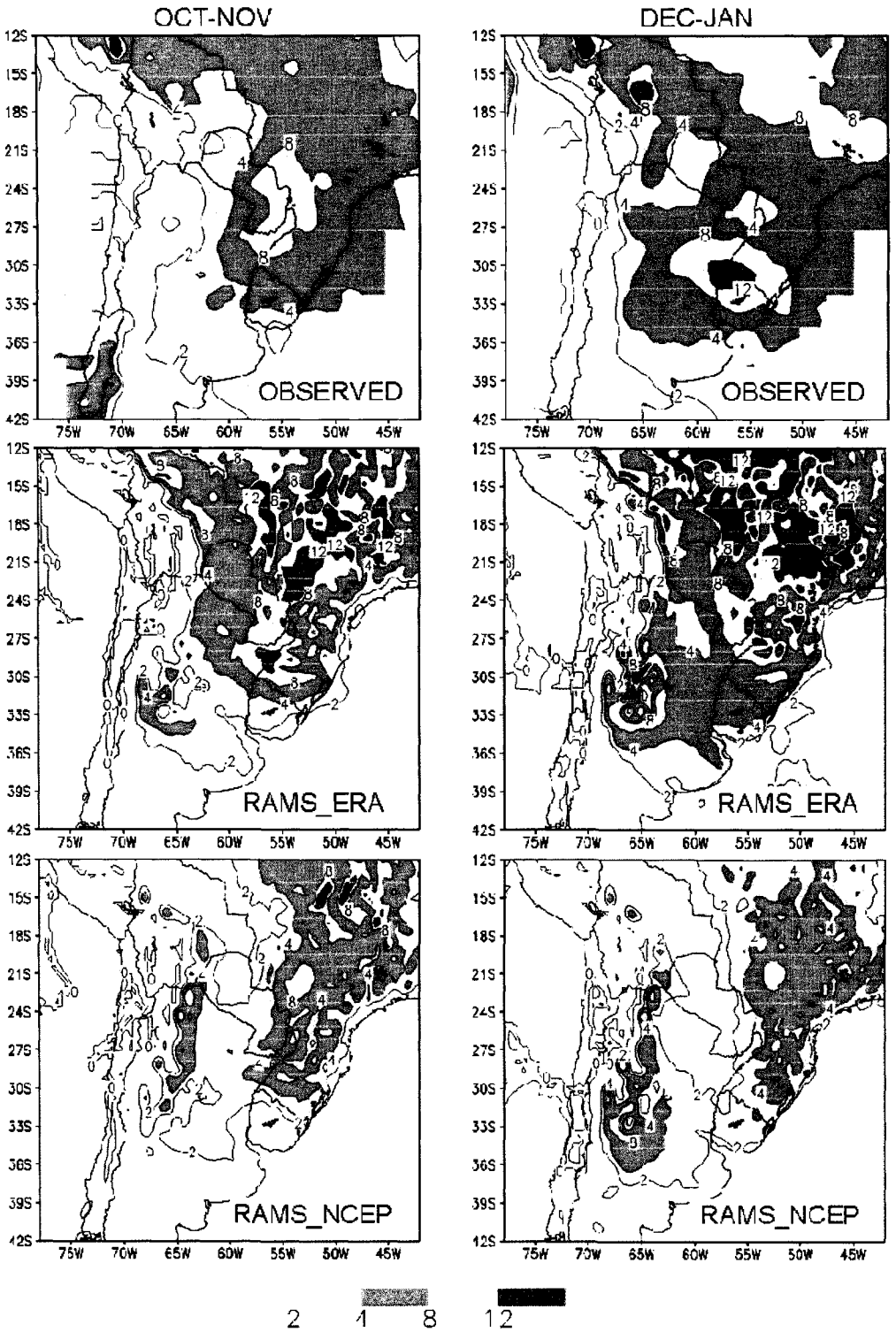

Figure 2.21. Precipitation (mm day^{-1}) during 1997-1998 for: observed (top), RAMS_ERA (middle), and RAMS_NCEP (bottom).

Reproduced with permission of the copyright owner. Further reproduction prohibited without permission.

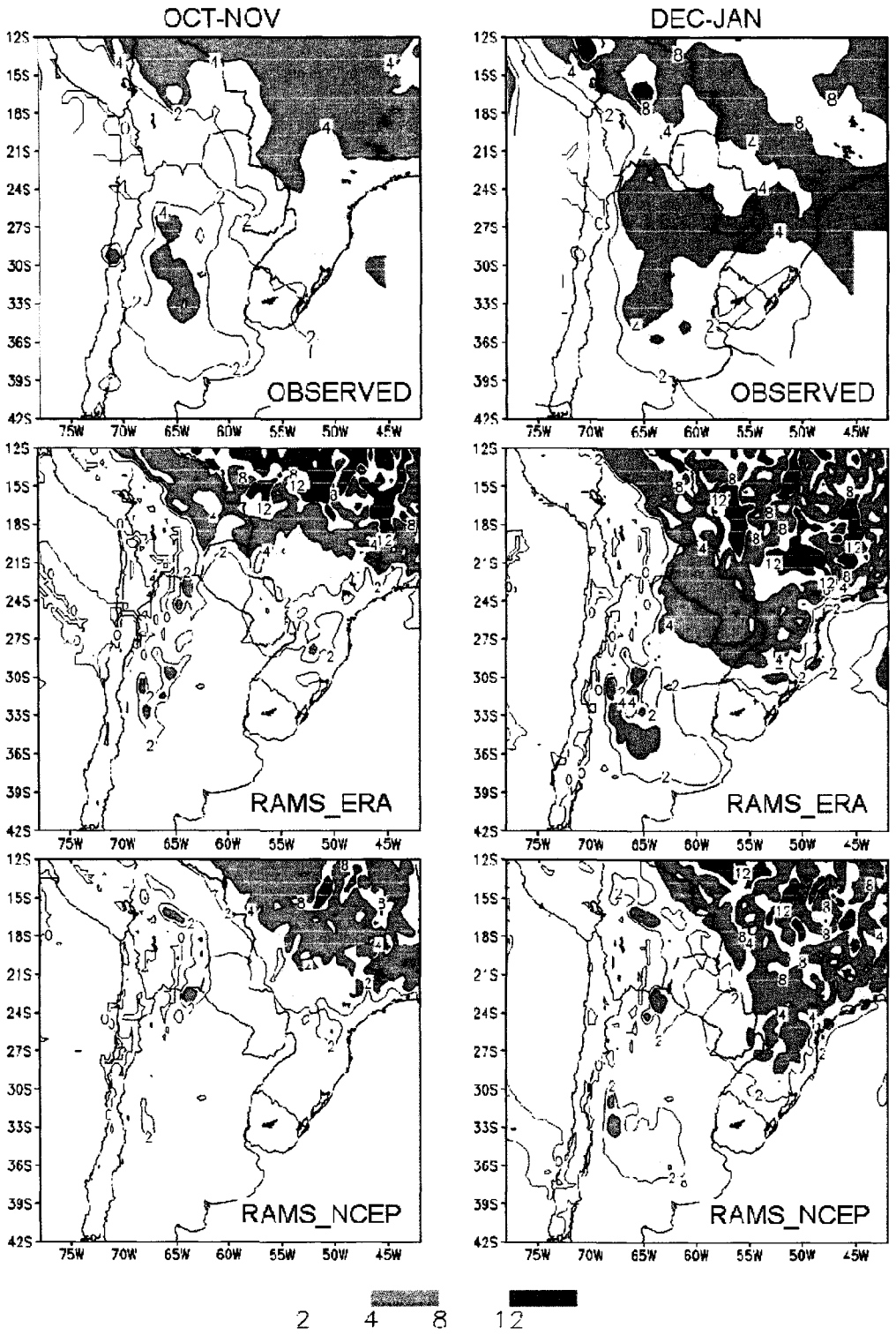

Figure 2.22. Precipitation (mm day^{-1}) during 1999-2000 for: observed (top), RAMS_ERA (middle), and RAMS_NCEP (bottom).

Reproduced with permission of the copyright owner. Further reproduction prohibited without permission.

2.8 Summary and Conclusions of Uncoupled Simulations

Several five-month long simulations were carried out over a domain with a 35 km grid spacing comprising southern South America. Simulations were performed for the spring-summer austral season from September to January. The goal was to assess the performance of RAMS in simulating the atmospheric circulation and the spatial and temporal variation of near surface temperature, energy fluxes and precipitation. Two of the most commonly used reanalysis products, ERA-40 and NCEP reanalysis, were used as initial and boundary atmospheric conditions.

RAMS was able to capture the main features of the low-level circulation. One noticeable feature is the northwesterlies in Bolivia along the Andes. They constitute the South America low-level jet and they represent one of the main sources of water vapor into central Argentina, southern Brazil and Uruguay. Differences in the 850 hPa field that exist between the reanalysis were amplified in the simulations. The largest differences in the low-level wind field, between the two simulations, and between each simulation and its corresponding lateral forcing, were located immediately east to Andes. The LLJ plays a major role in the precipitation in central Argentina (Misra et al. 2002b; Nicolini et al. 2002a).

In simulating spring-summer precipitation processes, most of the regional atmospheric models tend to produce an excess of precipitation over the Andes, around northwestern Argentina and Bolivia (e.g.. Misra et al. 2002b with RSM; Chou et al. 2002 with Eta/SSiB; Saulo et al. 2000 with Eta/CPTEC; Berbery and Collini 2000 with Eta; Roads et al. 2003 with several regional models). They also tended to underestimate precipitation over the Pampas region. The simulations performed with RAMS in this

Reproduced with permission of the copyright owner. Further reproduction prohibited without permission.

study also share some of those problems, although simulated precipitation was closer to the observation when ERA-40 reanalysis were used.

Temperature biases were also influenced by the large-scale forcing reanalysis. RAMS exhibited a generalized cold bias with ERA-40 and a warm bias with NCEP reanalysis throughout the domain. The largest colder values were found in the northern part of the domain and may be related to an excess of precipitation in that area found with ERA-40. The largest warmer values were found in the central part of the domain, between 55°W and 65°W, associated with a noticeable deficit in precipitation values found with NCEP reanalysis.

Sensitivity to interannual variability of large-scale atmospheric conditions was also tested for two years which corresponded to different ENSO events. Results were not intended to be conclusive about RAMS characterization of ENSO events, because only two years were considered. They rather represent two years characterized by very different precipitation conditions, in particular over the Pampas region. RAMS was able to simulate the interannual variability in precipitation. Similarly to the control experiment, spatial patterns and absolute values of rainfall were better simulated when using the ERA-40 dataset.

Large-scale forcing played a major role in the simulated climate. In agreement with other regional modeling studies (e.g.; Miguez-Macho and Paegle 2000; Rojas and Seth 2003; Wu et al. 2005) these results demonstrated that quality of the global analysis (i.e., reanalysis or AGCM) is the critical factor to reproduce the low-level circulation and near surface climate. In particular for SSA, Wang and Paegle (1996) found that the moisture budget over a domain centered on Del Plata Basin was convergent when the

Reproduced with permission of the copyright owner. Further reproduction prohibited without permission.

operational UKMO analyses were used and divergent when NCEP analyses were used. Similar deficiencies were also found by Min and Schubert (1997). In these RAMS simulations, the differences in the low-level pressure fields found between the two reanalysis were enhanced by the model.

Simulated precipitation closely resembled the corresponding reanalysis fields, and then precipitation errors passed to the simulations. RAMS simulations using ERA-40 compared better with observations than with NCEP in the central part of the domain. However, in the northeastern part of the domain, i.e., southern Brazil, NCEP reanalysis simulated better the absolute amounts of precipitation.

The use of ERA-40 reanalysis as large-scale forcing gave a more accurate description of temperature and precipitation fields and daily variability than with the NCEP reanalysis for this southern South America domain. Therefore, the next set of simulations with the coupled model system GEMRAMS will be performed using ERA-40 reanalysis as initial and boundary atmospheric conditions.

2.9 Results of Coupled Simulations

In the coupled modeling system, temperature, radiation, and moisture calculated by LEAF-2 in RAMS drives biomass growth in GEMTM, through photosynthesis processes. At each time step, stomatal conductance and leaf area index for sunlit and shaded leaves are computed by GEMTM and passed to LEAF2 in RAMS to generate latent and sensible heat fluxes. LAI is updated at the end of the day using a prescribed vegetation-specific specific leaf area. In these simulations, initial, lateral, and boundary conditions are given by the ERA-40 dataset.

Reproduced with permission of the copyright owner. Further reproduction prohibited without permission.

2.9.1 Leaf Area Index Estimations

A recent compilation of LAI global field measurements (Scurlock et al. 2001) shows only two published references with data south of 5°S, Trapani et al. (1992) and Madonni and Otegui (1996), both for crops. Additional published field observations of LAI were found in Asner et al. (2003) for shrublands, Soriano (1991) and Sala et al. (1986) for grasslands, and Calderini et al. (1997) and Miralles and Slafer (1997) for wheat. Table 2.3 shows the observed from measurements, NDVI-derived and GEMRAMS-simulated LAI values. For each vegetation type, maximum and mean LAI were computed for the surrounded grid cells with the same vegetation type around the one that corresponds to the observation ("Closest" column in Table 2.3) and for all the grid cells with the same vegetation type ("All cells" column in Table 2.3). Figure 2.23 shows all the maximum LAI values for major crops cited in Scurlock et al. (2001). In general, GEMRAMS-simulated LAI tended to be slightly higher than the measurements and NDVI-derived values, but overall, they are within a range of reasonable values. For shrublands, NDVI-derived values were underestimated compared to observed and simulated LAI values. On the other hand, observed LAI for grasslands are lower than NDVI-derived and simulated LAI.

Reproduced with permission of the copyright owner. Further reproduction prohibited without permission.

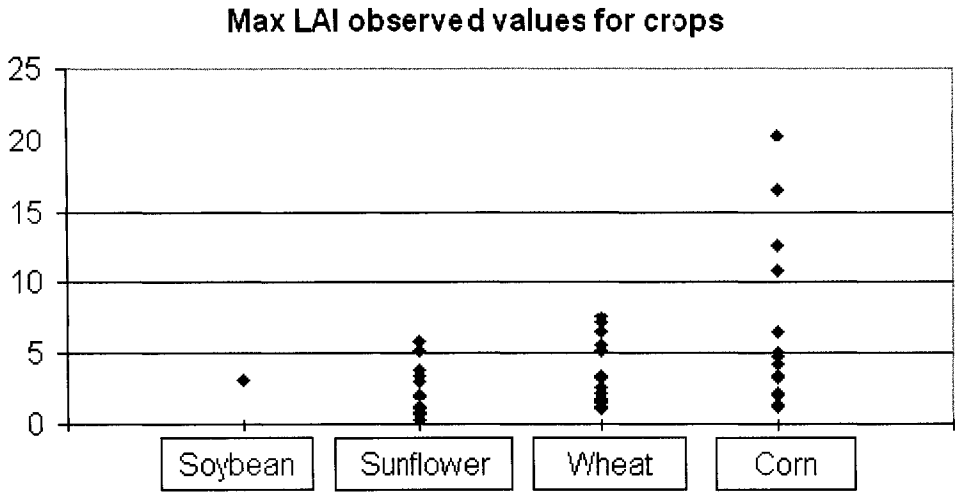

Figure 2.23. Maximum observed LAI values for crops, according to Scurlock et al. (2001).

	Source	Lat (S)	Long (W)	Time	Observed	NDVI-derived		GEMRAMS Simulated	
						Closest	All cells	Closest	All cells
Corn	(1)	34°07'	60°58'	Dec to Feb	4.9	4.5 (1.6)	4.5 (2.0)	6.2 (5.0)	6.0 (4.0)
Corn	(2)	37°45'	58°18'	Oct to Mar	5.5; 1.5				
Sunflower	(3)	34°33'	60°33'	End Jan	5.4	---	---	---	---
Sunflower	(3)	34°35'	58°29'	Begin Feb	3.5	---	---	---	---
Wheat	(4)	34°35'	58°29'	---	7.2 ± 1.4	---	4.8 (1.6)	---	5.9 (3.4)
Wheat	(5)	34°35'	58°29'	---	7.9 ± 0.2	---		---	
Soybean	---	---	---	---	---	---	5.0 (2.1)	---	6.1 (4.1)
Shrublands	(6)	34°02'	67°58'	Feb	1.7	1.6 (0.7)	2.1 (0.5)	3.6 (1.7)	4.0 (2.2)
Grasslands	(7)	36°01'	58°07'	Nov	0.9	5.0 (3.6)	5.0 (2.8)	2.8 (2.1)	3.2 (2.9)

Table 2.3. LAI values from measurements ("Observed"), NDVI-derived and GEMRAMS-simulated LAI. Observed values are maximum LAI for crops and mean LAI for shrublands and grasslands. In the last four columns, values are LAI maximum and mean LAI in parenthesis. LAI values for sunflower and soybean were included in the table, although sunflower was not present in the simulation domain and no published observed values were found soybean for this region. Sources: (1) Madonni and Otegui, 1996; (2) Gardiol et al. 2003; (3) Trapani et al. 1992; (4) Calderini et al. 1997; (5) Miralles and Slafer, 1997; (6) Asner et al. 2003; (7) Soriano, 1991; Sala et al. 1986.

Reproduced with permission of the copyright owner. Further reproduction prohibited without permission.

Temporal evolution of GEMRAMS-simulated LAI for the main vegetation type also shows a relatively good agreement with the NDVI-derived LAI (Figure 2.24). For evergreen shrubs and semidesert simulated LAI tended to be higher than NDVI-derived values. The parameters used in the algorithm to estimate LAI from NDVI may be affected by the high percentage of bare soil associated with those vegetation types.

Variability within each vegetation type can be high. As an example, Figure 2.25 shows GEMRAMS-simulated LAI for all cells with the given crop. The seasonal variations for each of the crops are reasonably well described, although simulated values tended to be concentrated towards high LAI values.

A strict comparison of the simulated LAI with observations is a difficult task. LAI measurements at a plot level may not be representative of all the possible range of values for a given vegetation type. They also are affected by local conditions, like soils, experimental settings, like irrigation and fertilization in the case of crops, and methodology used in the measurements. Nevertheless, they provide approximate "ground-truth" values for the LAI estimates. Other uncertainties associated with LAI comparisons include the NDVI-LAI conversion algorithm, the NDVI dataset used (Buermann et al. 2002) and different spatial scales associated with the different estimations (i.e., plot: ≤ 10 m^2; satellite pixel: from 10^5 to 10^8 m^2; model grid-cell: 10^9 m^2). Overall, simulated GEMRAMS and NDVI-derived LAI are in generally qualitative agreement with observed LAI.

Reproduced with permission of the copyright owner. Further reproduction prohibited without permission.

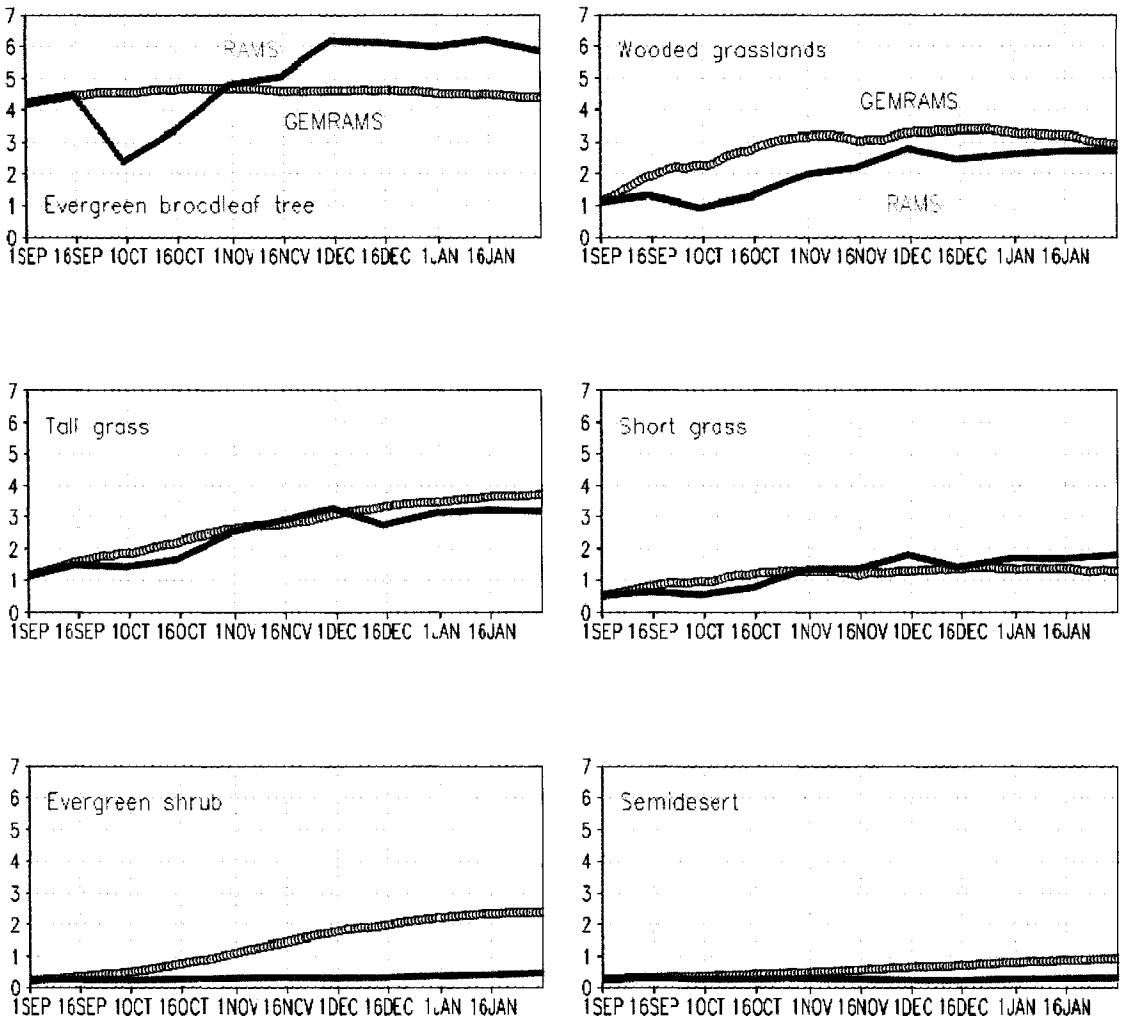

Figure 2.24. NDVI-derived (RAMS) and simulated by the fully coupled model (GEMRAMS) LAI-averaged over evergreen broadleaf trees, wooded grasslands, grasslands, evergreen shrub, and semidesert.

Reproduced with permission of the copyright owner. Further reproduction prohibited without permission.

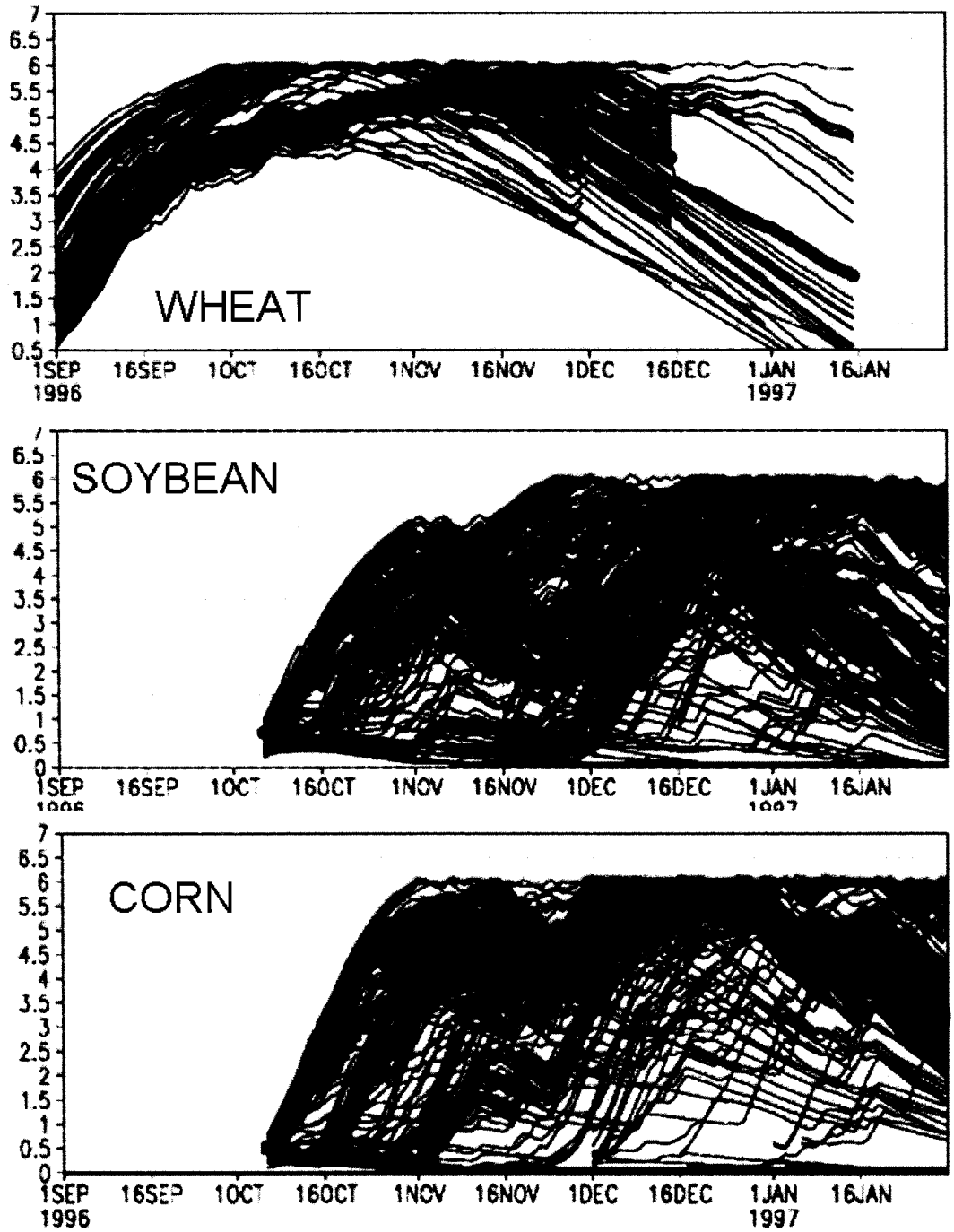

Figure 2.25. Simulated LAI by GEMRAMS for all the grid cells corresponding to wheat, soybean, and corn (black lines) and the average (red).

Reproduced with permission of the copyright owner. Further reproduction prohibited without permission.

2.9.2 Precipitation

Precipitation patterns simulated with GEMRAMS (Figure 2.26) were similar to RAMS_ERA (Figure 2.9). Although overall GEMRAMS precipitation tends to be higher than RAMS_ERA, it is in closer agreement to the observations in the Pampas region (see also Figure 2.9, top). Maximum positive differences between GEMRAMS and RAMS concentrate mainly along the Andes, Paraguay, and south of Brazil in spring and over the center of the domain in summer. Only in the northern part of the domain, GEMRAMS precipitation tended to be lower than RAMS. Positive differences tended to be collocated with enhanced moisture flux convergence (MFC) between GEMRAMS and RAMS_ERA on the western part of the domain. In summer, some areas with increased precipitation were collocated with an increase in LH, associated with increase in an LAI (see next section). The use of the coupled model enhanced precipitation over most of the domain. Nevertheless these differences are smaller when compared to the differences found using the two atmospheric boundary products (see Figure 2.16). In this sense, the large-scale forcing remains the main factor that affects the behavior of this regional atmospheric modeling system.

Figure 2.27 shows the time evolution of daily precipitation in the PA and NE regions. GEMRAMS enhanced precipitation in the pampas region especially in summer. The number of rainy days remained the same but GEMRAMS simulated a general increase in the amount of precipitation in each of the events. On an area-averaged basis, GEMRAMS precipitation was closer to observations than RAMS-ERA in the PA region and slightly overestimated in the NE region (Table 2.4).

Reproduced with permission of the copyright owner. Further reproduction prohibited without permission.

Dataset	PA	NE
Observed	3.8	6.5
GEMRAMS	3.7	6.9
RAMS_ERA	2.9	6.2

Table 2.4. Area-averaged precipitation (mm day^{-1}) from GEMRAMS, RAMS_ERA, and observations for PA and NE areas.

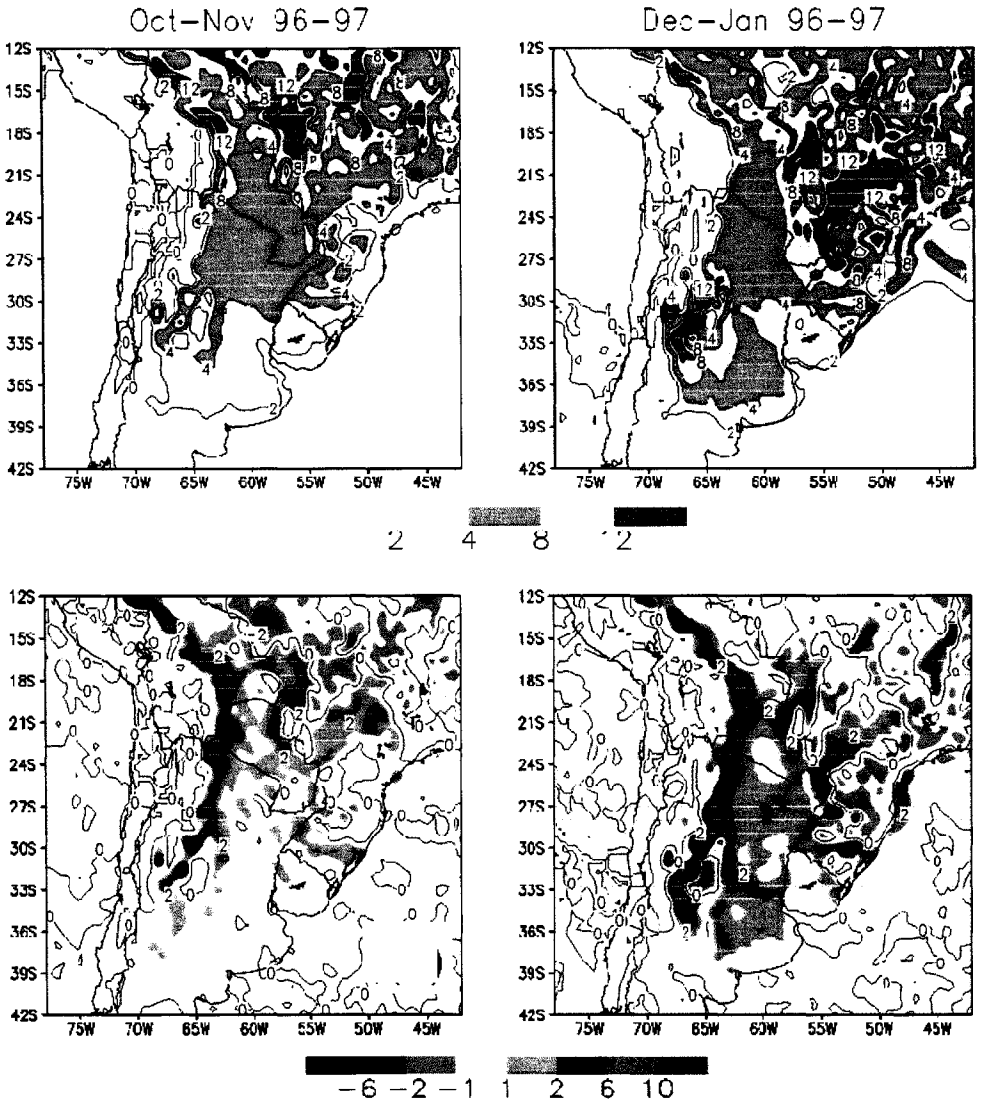

Figure 2.26. Mean precipitation (mm day^{-1}) simulated by GEMRAMS (top) and difference GEMRAMS - RAMS_ERA (bottom) for the 1996-1997 period.

Reproduced with permission of the copyright owner. Further reproduction prohibited without permission.

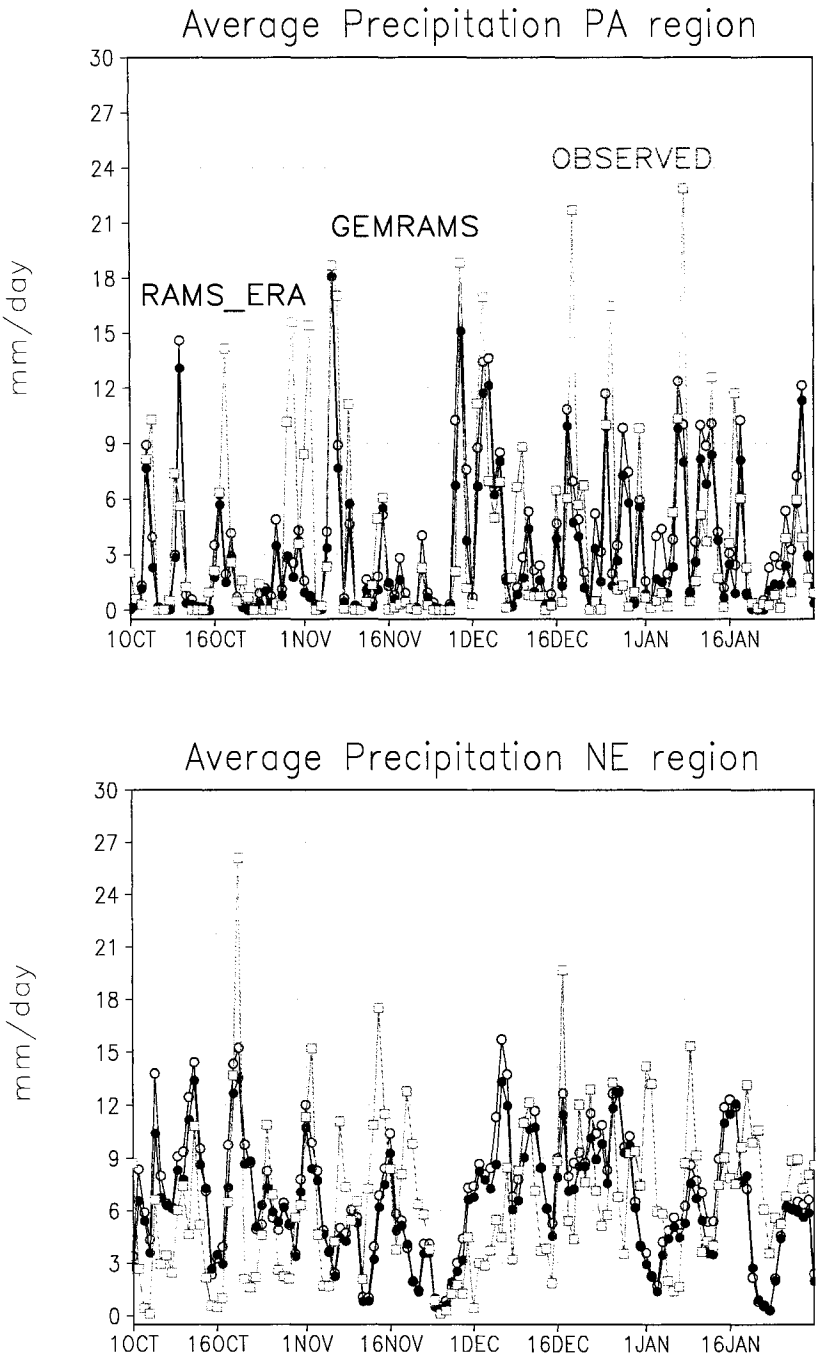

Figure 2.27 Area-averaged precipitation (mm day^{-1}) for 1996-1997 period for: NA region (top), and NE region (bottom), for GEMRAMS, RAMS_ERA, and observations.

Reproduced with permission of the copyright owner. Further reproduction prohibited without permission.

2.9.3 Near-Surface Temperature and Fluxes

On an area-basis, temperatures simulated by GEMRAMS were the coldest of all the simulations performed (Table 2.5). The simulation with the warmest bias with respect to observations was RAMS_NCEP. The absolute differences between RAMS_ERA and RAMS_NCEP were higher than between GEMRAMS and RAMS_ERA. This indicates the first-order impact of the atmospheric boundary conditions on the simulated climate.

Model	Spring	Summer
Observations	22.5	24.5
GEMRAMS	19.9	21.8
RAMS_ERA	20.7	22.6
RAMS_NCEP	22.2	25.1

Table 2.5. Simulated and observed area-averaged first model level temperatures (over land) for spring (Oct-Nov) and summer (Dec-Jan) of the 1996-1997 period for all the simulation.

The GEMRAMS temperature pattern was similar to RAMS_ERA, with cooler temperature over most of the domain (Figure 2.28). The highest differences were found along the Andes and in central Chile, and also in central Pampas and Uruguay in summer up to -2°C. This cold pattern tends to be reduced when 2 m temperatures are considered (not shown).

Reproduced with permission of the copyright owner. Further reproduction prohibited without permission.

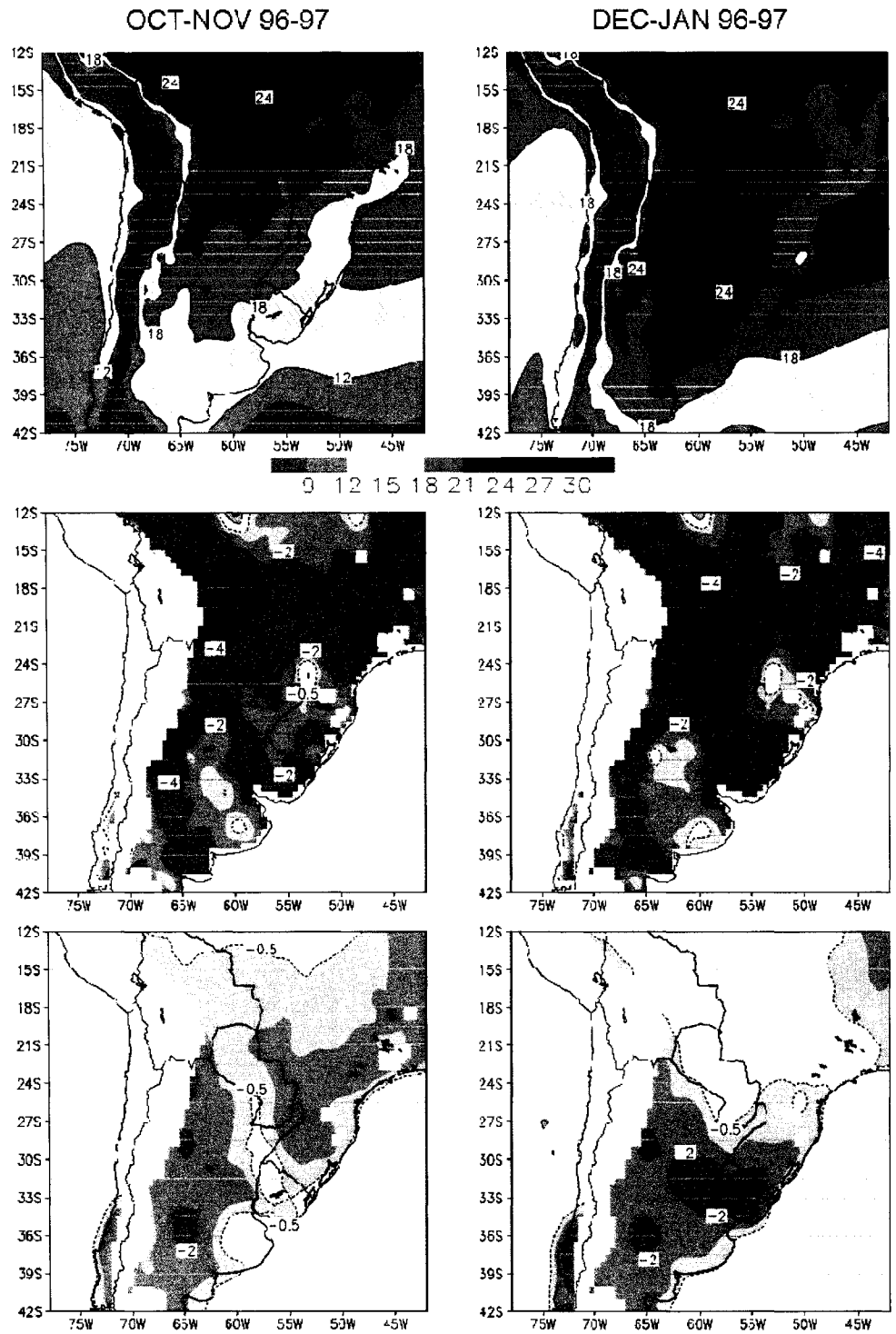

Figure 2.28. Mean temperature (°C) for 1996-1997 period: GEMRAMS (top); difference GEMRAMS – observations (only over land) (middle); difference GEMRAMS - RAMS_ERA (bottom)

Reproduced with permission of the copyright owner. Further reproduction prohibited without permission.

The spatial differences between GEMRAMS and RAMS_ERA were mostly associated with surface latent heat (LH) flux differences: higher (lower) LH in GEMRAMS than in RAMS_ERA was related to cooler (warmer) temperatures (Figure 2.28 and 2.29). In most of the domain, LH was higher in GEMRAMS than in RAMS_ERA, except for small areas on the eastern part of the Pampas. LH differences tended to be related to mean LAI differences (Figure 2.29), especially in the southern part of the domain: higher (lower) LAI favored higher (lower) LH. Changes in LH were mainly due to changes in transpiration. In the northern part of the domain, in the areas where LAI decreased between GEMRAMS and RAMS_ERA, soil evaporation increased and caused positive differences in LH in spite of the decrease of LAI.

In the northern part of the domain, cooler temperatures were mostly due to overestimation of precipitation. Lu et al (2001), using a previous version of RAMS coupled with the CENTURY model, also found a cold bias in the coupled model in boreal summer when compared to observations and the uncoupled RAMS, due to the excessive rainfall simulated by the coupled model.

Differences in surface fluxes strongly controlled the differences in near-surface temperatures between the coupled and uncoupled models. As an example for the PA region, Figure 2.30 the temporal evolution of LH and first level temperature. Initially the differences were smaller. As the warm season progresses, higher LAI induced higher LH and consequently lower temperatures in the coupled model than in the uncoupled model.

Reproduced with permission of the copyright owner. Further reproduction prohibited without permission.

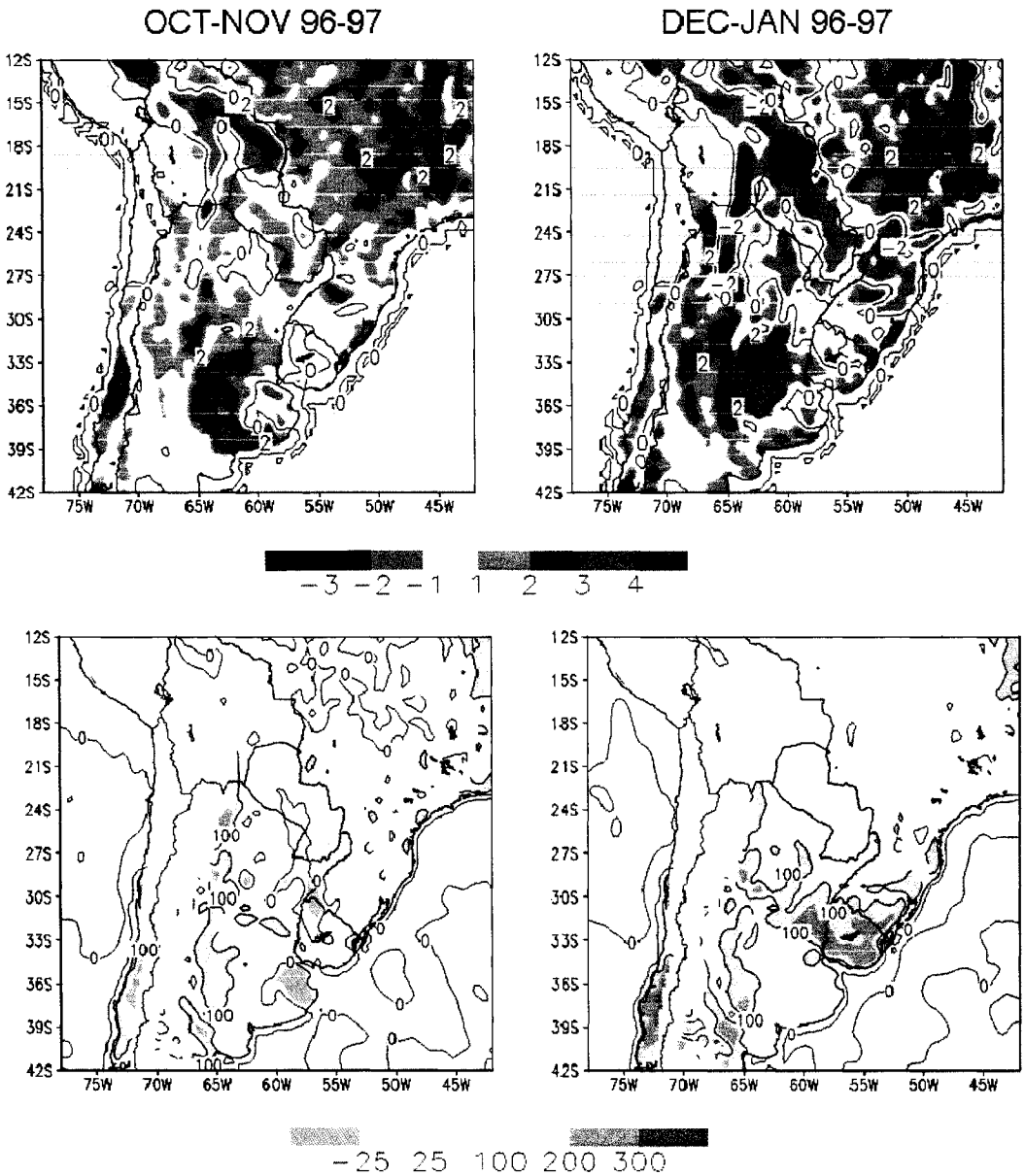

Figure 2.29. Differences of mean LAI (top) and LH (bottom) between GEMRAMS and RAMS_ERA for the 1996-1997 period.

Reproduced with permission of the copyright owner. Further reproduction prohibited without permission.

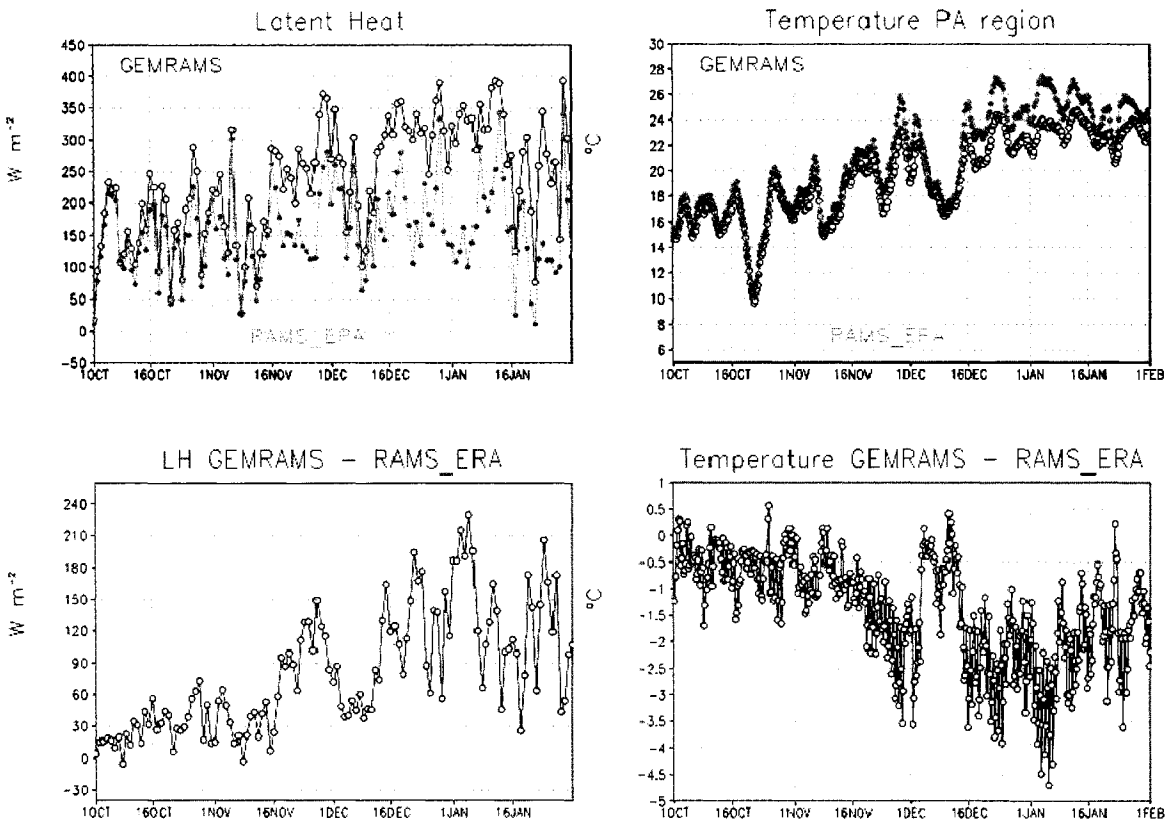

Figure 2.30. Temporal evolution of daytime area-average LH (left) and first-level temperature (right) for GEMRAMS and RAMS_ERA.

Reproduced with permission of the copyright owner. Further reproduction prohibited without permission.

2.9.4 Sensitivity to Interannual Variability

Simulated spring and summer precipitation patterns from the fully coupled simulations for the 1997-1998 and 1999-2000 periods (Figure 2.31) were similar to the uncoupled model (compared to Figures 2.19 and 2.20). The fully coupled model simulated higher precipitation than the uncoupled model in most of the domain, except for the north and northeastern part of the domain. Overall, the difference in the area-averaged precipitation between the two models is highest in the "wet" year 1997-1998 and lowest in the "dry" year 1999-2000.

In general, the coupled modeling system was able to capture the observed spatial and temporal interannual differences in precipitation between 1997-1998 and 1999-2000. The temporal behavior of the simulated precipitation depends on the region considered within the simulation domain. Figures 2.32 and 2.33 show the temporal evolution of area-averaged precipitation for PA and NE simulated by GEMRAMS, RAMS_ERA, and the observations. Observed area-averaged precipitation during the 1999-2000 period was half the one during 1997-1998 in the PA region and slightly higher in the NE region. The number of rainy days was overestimated in the NE region with both RAMS_ERA and GEMRAMS. On the other hand, in the PA region, differences in area-averaged precipitation between observations and simulations were lower for GEMRAMS than for RAMS_ERA.

Reproduced with permission of the copyright owner. Further reproduction prohibited without permission.

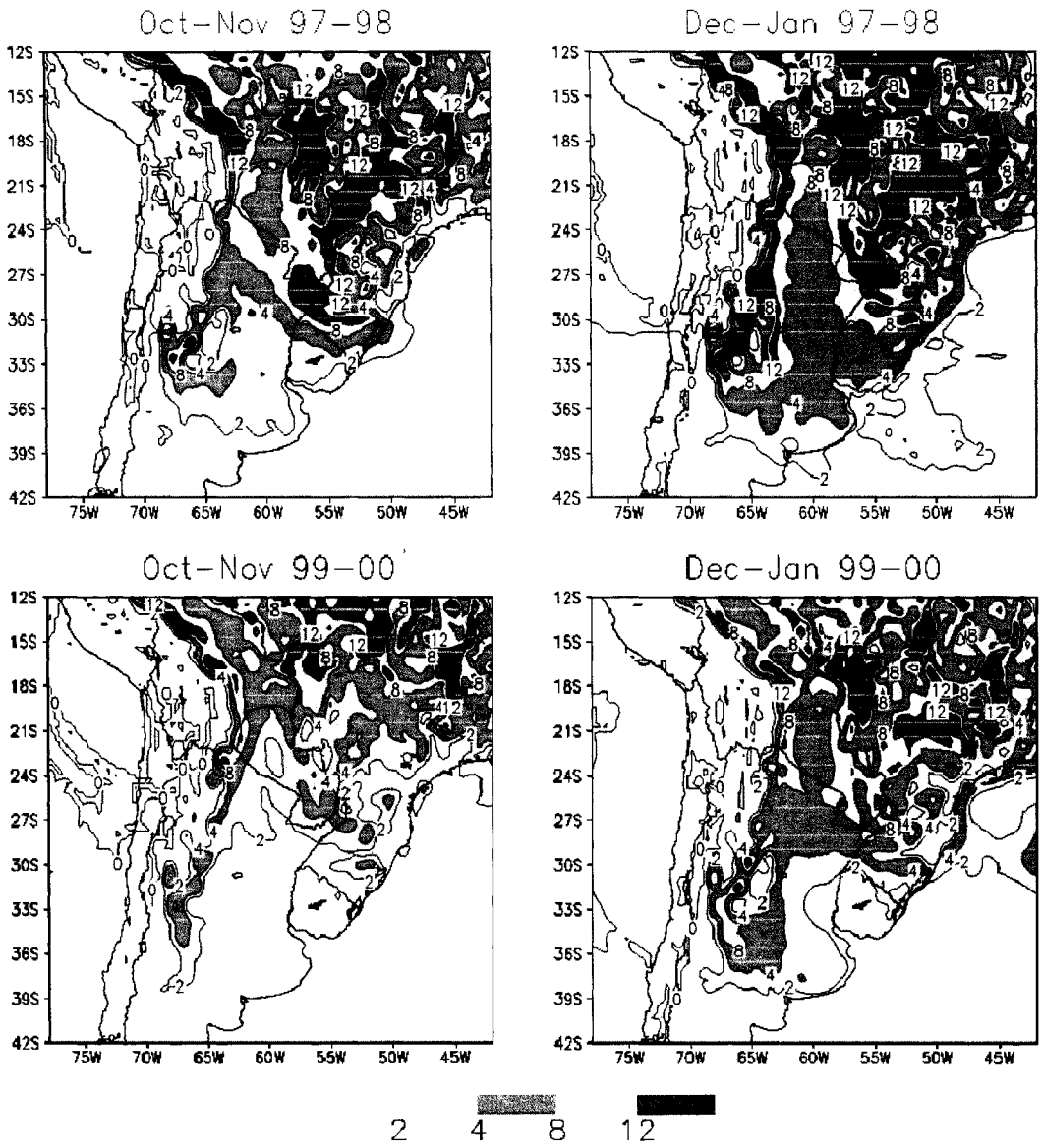

Figure 2.31. Mean simulated GEMRAMS precipitation (mm day^{-1}) for 1997-1998 (top) and 1999-2000 (bottom).

Reproduced with permission of the copyright owner. Further reproduction prohibited without permission.

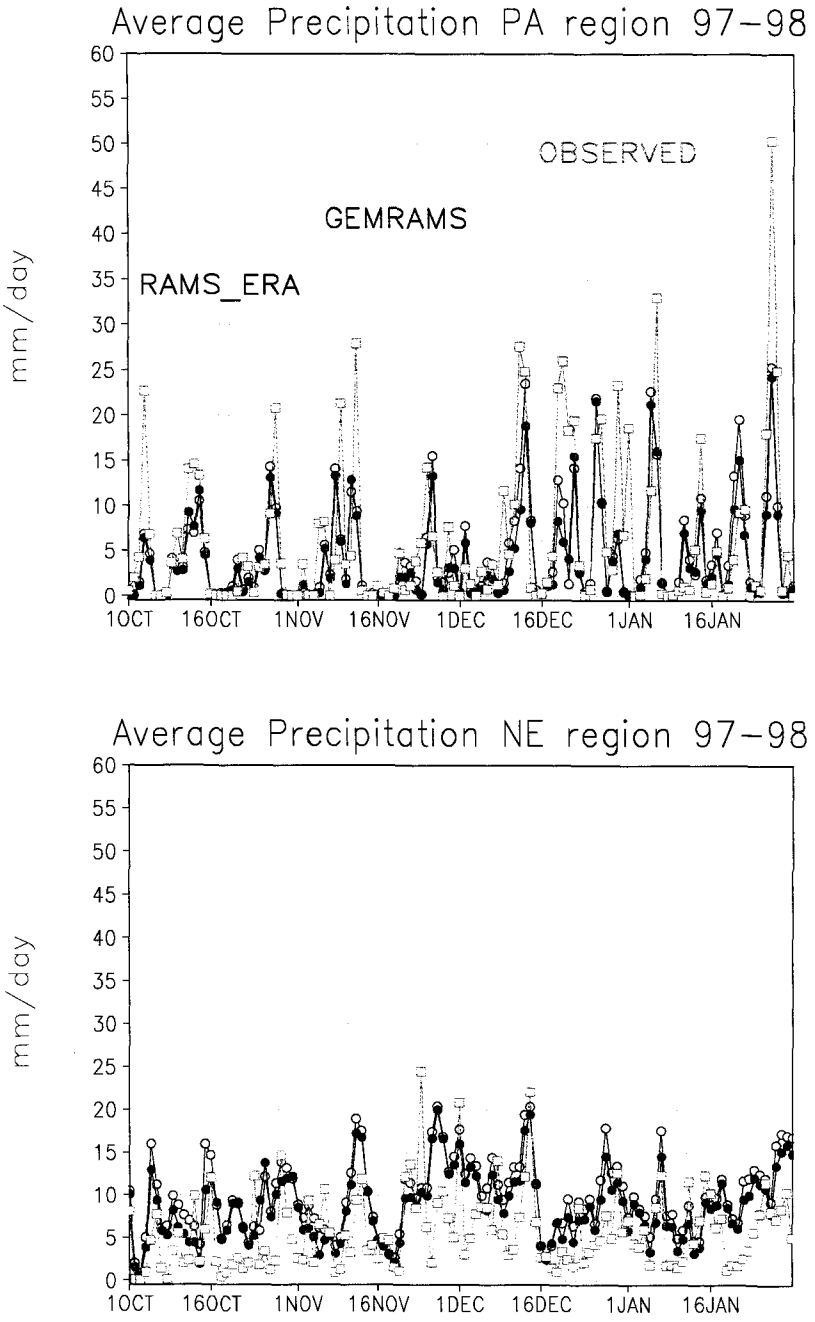

Figure 2.32. Area-averaged precipitation (mm day-1) for the 1997-1998 period for: NA region (top) and NE region (bottom), for GEMRAMS, RAMS_ERA, and observed.

Reproduced with permission of the copyright owner. Further reproduction prohibited without permission.

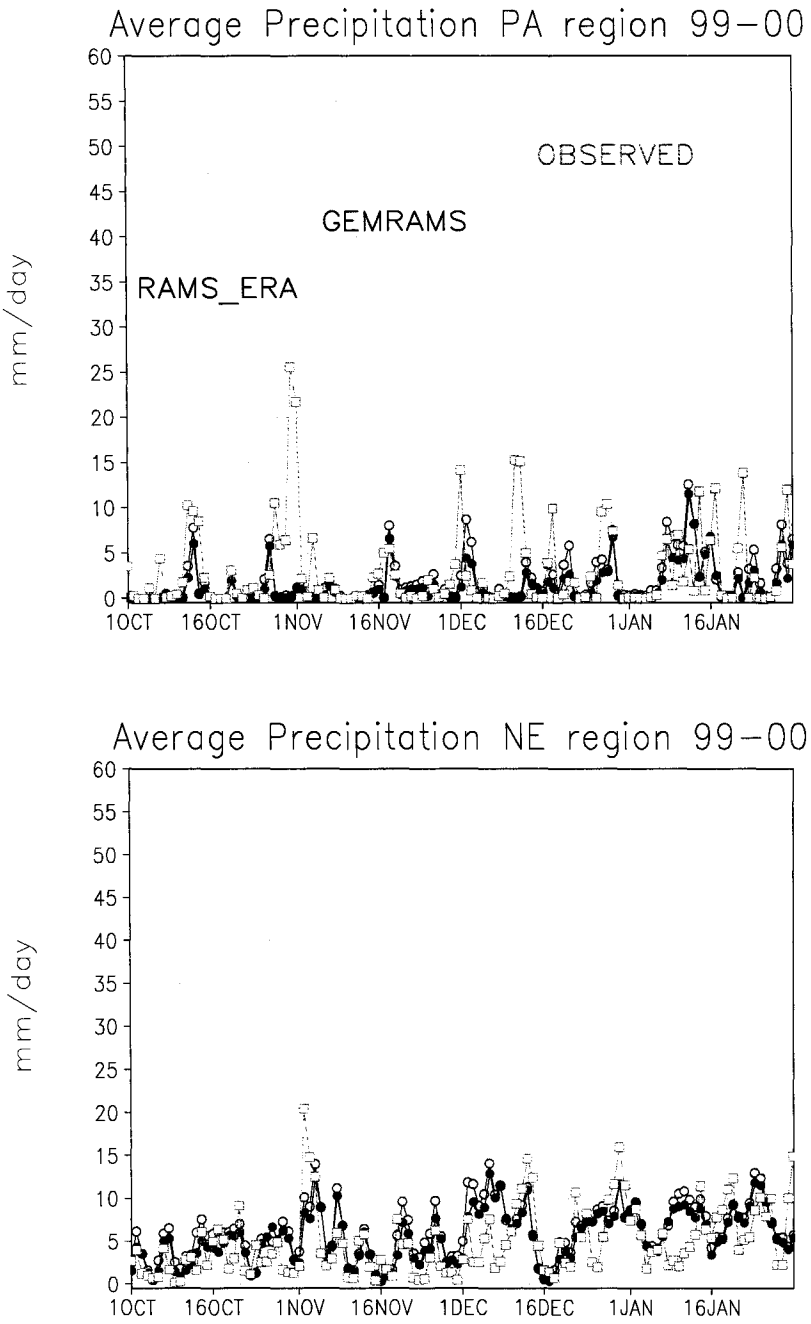

Figure 2.33. Area-averaged precipitation (mm day-1) for the 1999-2000 period for: NA region (top) and NE region (bottom), for GEMRAMS, RAMS_ERA, and observed.

Reproduced with permission of the copyright owner. Further reproduction prohibited without permission.

A nonlinear response of the vegetation to the interannual variability in precipitation was found in these simulations. When averaging by vegetation type, simulated LAI tended to be higher in the wet year, 1997-1998, than in the other two years, but the response also depended on the spatial pattern of precipitation associated with the spatial distribution of vegetation. Similar response could be also seen in NDVI-derived LAI values. For example, almost no difference in NDVI-derived LAI was found for evergreen broadleaf trees. On the other hand, mean NDVI-derived LAI for short grass at the end of January was 2.3 m^2 m^{-2} and 1.5 m^2 m^{-2} for the wet and dry year, respectively. These values for GEMRAMS-simulated LAI were 1.8 m^2 m^{-2} and 1.4 m^2 m^{-2} respectively. Similar results applied for other vegetation types. This indicates that interannual differences are smaller than the corresponding NDVI-derived values, when averaging by vegetation type. Similar results were also found by Lu et al. (2001).

Nevertheless, interannual variability in precipitation could be seen in the Pampas region, and also relatively well represented by the model. Therefore, when the LAI area-average for that region is considered, interannual variability in simulated LAI was very similar to the one found in NDVI-derived LAI (Figure 2.34). On the other hand, in the NE region, where GEMRAMS produced an excess of precipitation in both years, interannual variability in LAI was overestimated compared to NDVI-derived values (Figure 2.34).

Reproduced with permission of the copyright owner. Further reproduction prohibited without permission.

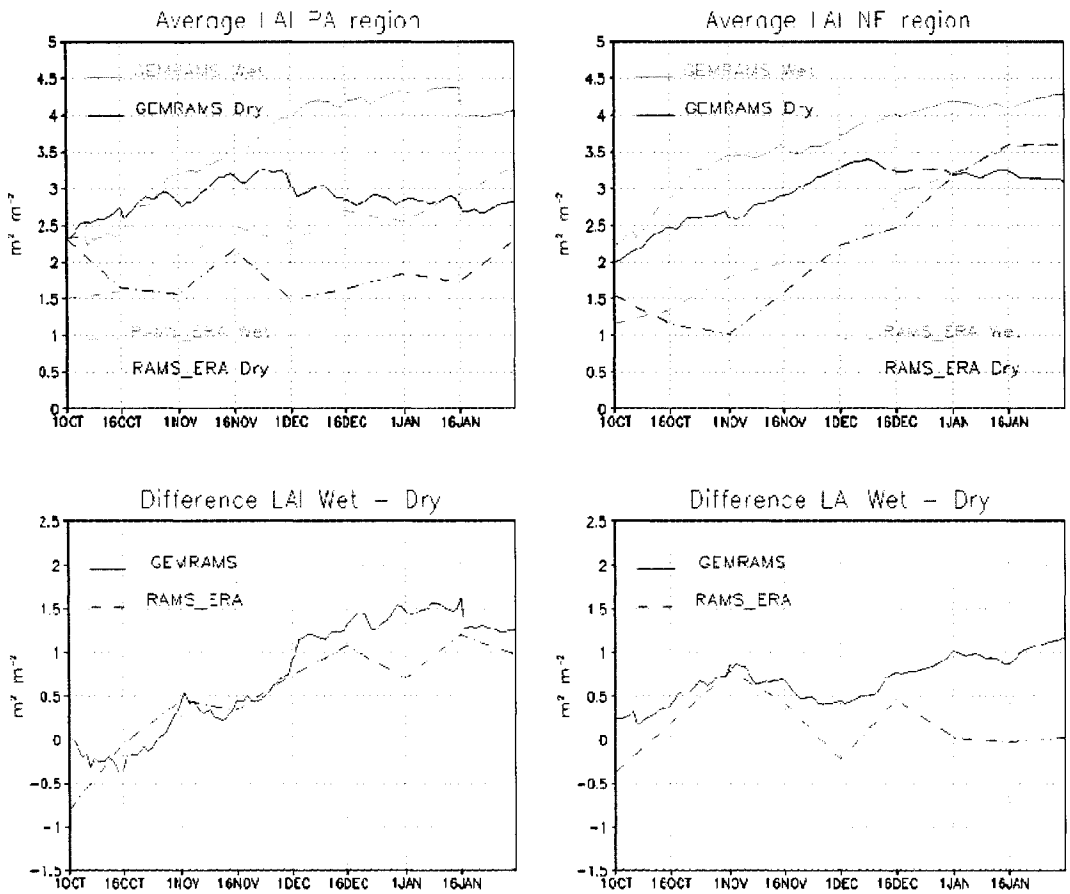

Figure 2.34. Area-averaged LAI (m^2 m^{-2}) for 1997-1998 (wet year) and 1999-2000 (dry year) for NA region (left) and NE region (right), for GEMRAMS and RAMS_ERA.

Reproduced with permission of the copyright owner. Further reproduction prohibited without permission.

2.10. Summary and Conclusions of Coupled Simulations

These experiments showed that the coupled modeling system was able to respond to atmospheric variables, and vice versa, atmospheric variables, through the surface fluxes responded to the vegetation differences. A general validation of the LAI with observed values indicated that values and seasonal variation were relatively well simulated. The response of LAI to interannual variability depended on the spatial location of the interannual signal. In particular, ENSO signal is important in the Pampas region. Even though only two years were considered, they represented clearly two different rainfall patterns. Interannual variability in simulated LAI is similar to the NDVI-derived variability, in particular over the Pampas. On the other hand, over the NE region, excess of precipitation had a positive feedback on plant growth and temperature. This modeling system proved to be able to respond to spatial differences in interannual variability.

A generalized cold bias was found in the coupled simulations. The largest differences in temperature between the coupled and uncoupled model tended to be collocated with increase in LAI and LH. In spite of this cold bias and the relatively high LAI, GEMRAMS realistically represented precipitation patterns and responded also to interannual variability. This indicates that GEMRAMS is suitable to be used in long-term climate simulations, in particular to study sensitivity to land-cover/land-vegetation changes.

Reproduced with permission of the copyright owner. Further reproduction prohibited without permission.

Chapter 3

MODEL SENSITIVITY TO LAND-USE/LAND-COVER CHANGES

Results from simulations conducted over southern South America using a land-cover specification that corresponds to current conditions were analyzed in Chapter 2. In this Chapter and Chapter 4, simulations performed with a modified vegetation cover are discussed. The objective was to examine the possible effects of land-use/land-cover changes on the near-surface atmospheric variables. Several case studies were considered. Results from five month-long simulations carried out over southern South America, with focus on the Pampas region are shown in this Chapter. Sensitivity experiments of near-surface climate to historical vegetation changes that have occurred in a semiarid area located in the northern Chihuahuan Desert in North America are discussed in Chapter 4.

3.1. Land-Use/Land-Cover Changes in Southern South America

Southern South America comprises a wide range of vegetation (Figure 2.3) and soil types (Figure 2.2) closely related to the spatial and temporal mean climatic characteristics. However, at a local and regional scale, vegetation, and soils can affect the overlying atmosphere, through two-way interactions.

Urbanization and conversion of natural areas to agriculture/animal husbandry are two of the main land-use changes in the past 100 years in the Pampas region. The area in

Reproduced with permission of the copyright owner. Further reproduction prohibited without permission.

Argentina dedicated to cropland increased from $6{:}10^6$ ha in the 1910's to $27{:}10^6$ ha in 1997 (FAO 1998). The introduction of domestic herbivores by Europeans has modified the landscape in Patagonia (Soriano et al. 1983) and Pampas (Hall et al. 1992; Viglizzo et al. 1997). Overgrazing in Patagonia has had an impact on vegetation cover, reducing grass cover and increasing shrub cover (León and Aguiar 1985). Land-cover change associated with agriculture has had an important effect on the structure and functioning of temperate ecosystems in this area (Paruelo et al. 2001, 2004; Guerschman et al. 2003; Guerschman and Paruelo 2005). Disturbances, such as grazing, fire, and weather variability strongly affect the structure and function of grasslands and savannas (Oesterheld et al. 1999) and other ecosystems in the region (Villalba and Veblen 1997).

In temperate South America (Argentina, Chile, Uruguay), as well as in subtropical southern South-America (Bolivia, Brazil, Paraguay), natural forests have been drastically reduced since the beginning of the 20th Century (FAO 2001a). Large areas were converted to agriculture and pasture. The rate of conversion varies among the countries, higher in Bolivia and Brazil than in Chile (FAO 2001b). Reforestation plans started in Chile, Uruguay, and Argentina in the last two decades supported through government economic incentives or subsidies (World Bank 2000). Afforestation may affect the hydrological cycle (Engel et al. 2005; Farley et al. 2005; Nosetto et al. 2005).

Most of the modeling studies addressing the impacts of land-cover/land-use changes in South America are centered on tropical regions, particularly deforestation on the Amazon basin and desertification in northeast Brazil (e.g., Sud and Fennessy 1982; Nobre et al. 1991; Hahmann and Dickinson 1997; Hoffmann and Jackson 2000; Baidya Roy and Avissar 2002; Oyama and Nobre 2004). The impact of LULC on the near-

Reproduced with permission of the copyright owner. Further reproduction prohibited without permission.

surface climate of southern South America has not yet been fully explored on the regional scale.

The increase in atmospheric carbon dioxide (CO_2) levels is another process that could alter near-surface temperatures in a long-term time scale (Houghton et al. 2001). The terrestrial biosphere responds to this increase through photosynthesis, transpiration, and respiration processes. Short- and long-term effects in the physiological and structural response of plants are observed. Stomatal conductance (g_s) and leaf area index (LAI) are the vegetation characteristics that respond to this CO_2 increase, and in addition provide the link between plants and the atmosphere through energy and water exchanges. In the short term, increased photosynthesis in C_3 plants (whose photosynthesis rate is not CO_2 saturated at current atmospheric levels) and a general decrease in stomata aperture are the generally expected response to the CO_2 enrichment (e.g., Morison 1987; Field et al. 1995; Owensby et al. 1997; Wullschleger et al. 2002) although there are still uncertainties in the stomata behavior (Morison 2001). The reductions in g_s vary between 20-50% depending on the type of life form or other environmental conditions, e.g., water status of the plants (Morison 2001).

In a long-term term exposure (i.e., after several seasons or years) to high CO_2 levels, acclimation of photosynthesis sometimes occurs. Generally, this translates in a "down-regulation" of photosynthesis, with the same light-saturated photosynthesis values in both elevated and ambient CO_2 (Drake et al. 1997). Nutrient and water availability might also control the occurrence or degree of this down-regulation (e.g.,,Gunderson and Wullschleger 1994; Huxman et al. 1998). Several studies have shown little or no evidence of down-regulation in trees (e.g., Curtis and Wang 1998; Herrick and Thomas

Reproduced with permission of the copyright owner. Further reproduction prohibited without permission.

2001). In addition, under elevated CO_2 levels, stomata may acclimate in parallel with photosynthesis acclimation (i.e., a signal from the mesophyll controls stomatal aperture), independently of it (i.e., a signal directly from the guard cells, Frechilla et al. 2002), or maintain the same sensitivity as in normal CO_2 levels (Santrucek and Sage 1996). Anatomical and morphological changes, like stomatal number or frequency and/or size may also occur (Woodward 1987). The structural response includes an increase in carbon assimilation and in biomass (Bazzaz 1990; Poorter 1993). LAI behavior as a result of higher CO_2 concentrations is not clear. Water status in grasslands (Owensby et al. 1999) and degree of canopy closure in forest systems (Hymus et al. 2002; Norby et al. 2003) may affect elevated CO_2 on the leaf dynamics.

Bounoua et al. (1999) addressed this long-term physiological effect using SiB2 coupled with a global land-ocean-atmospheric model, with unchanged vegetation structure, i.e., LAI. Betts et al. (1997) incorporates LAI dynamics together with the physiological effects in a GCM. In the present study, only the short-term response of increased CO_2 on the near-surface atmosphere is addressed, and down-regulation in photosynthesis or stomatal conductance were not considered. Also, changes in species composition and community structure due to long-term (i.e., more than decades) effects of elevated CO_2 are beyond the scope of this study.

Complex nonlinear interactions between atmosphere and biosphere under increasing CO_2 levels exist at a regional and seasonal level. Eastman et al. (2001a) and Narisma and Pitman (2004) explored the effects of CO_2 and land-cover changes with GEMRAMS for central U.S. and Australia, respectively. In the present study,

Reproduced with permission of the copyright owner. Further reproduction prohibited without permission.

GEMRAMS sensitivity to doubled CO_2 levels and land-cover change is investigated over southern South America.

3.2 Experimental Design

To address the effects of LULC changes on atmospheric processes in the South America region, two sensitivity experiments were performed using GEMRAMS (Table 3.1). The first sensitivity experiment, NAT, represents the conditions before the European settlement. Croplands were replaced by tall grass, wooded grasslands, or evergreen broadleaf forest, depending on their geographical location (Figures 3.1 and 3.2). The vegetation maps of Matthews (1983), Küchler (2000), and Cabrera and Willink (1980) were used to perform the replacement of croplands.

Experiment name	LULC scenario
CTRL	Current
CO2, CO2bio	Current
NAT	Natural
AFFOR	Afforestation

Table 3.1. Land-use/land-cover scenario that corresponds to each of the experiments.

Reproduced with permission of the copyright owner. Further reproduction prohibited without permission.

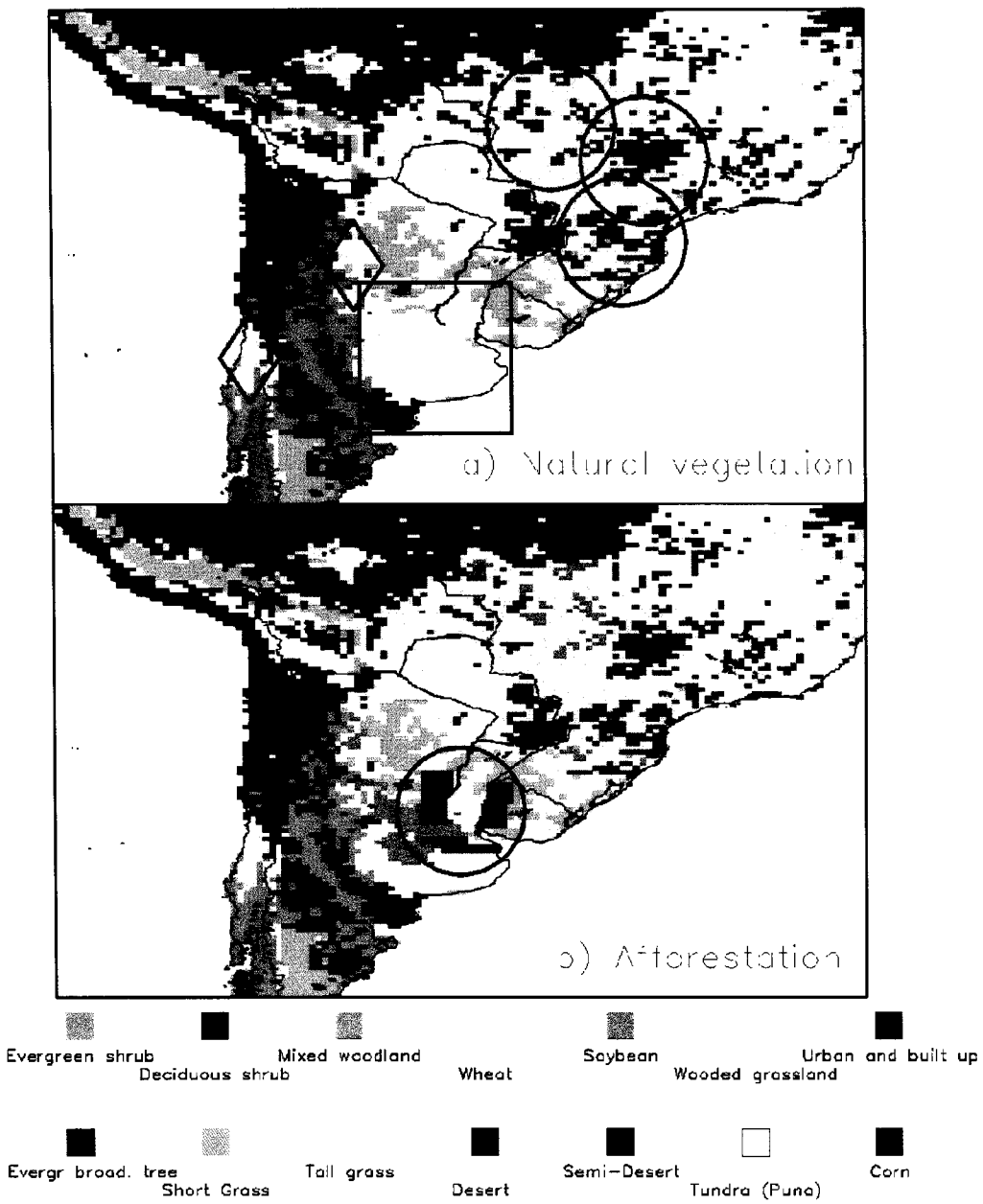

Figure 3.1. Vegetation types for each of the land-cover/land-use experiments. a) "Natural vegetation" experiment: replacement of crops by tall grass (red square), wooded grasslands (red circle), and Evergreen broadleaf tree (red diamond). b) "Afforestation" experiment: in the red circle are the "new" Evergreen broadleaf tree grid cells.

Reproduced with permission of the copyright owner. Further reproduction prohibited without permission.

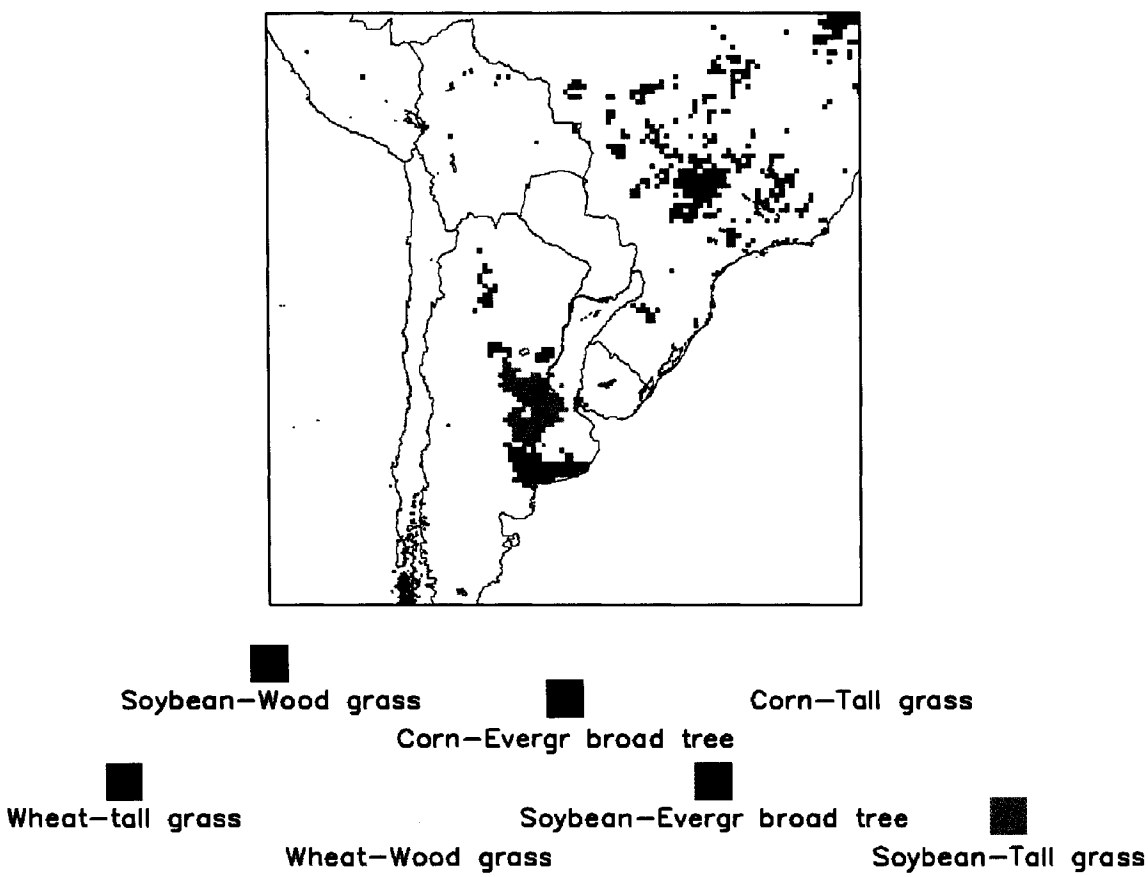

Figure 3.2. Areas with changes in vegetation for the "historic" land-cover/land-use experiment.

Reproduced with permission of the copyright owner. Further reproduction prohibited without permission.

The second LULC change experiment, AFFOR, corresponds to an attempt to simulate a potential future "afforestation" scenario. Several grid cells were replaced by evergreen broadleaf trees based on the areas studied by Nosetto et al. (2005) and SAGYPA (2000) (Figure 3.1). Conversion was from grasslands (70%), wooded grasslands (29%), and wheat (1%). Vegetation cover corresponded to current conditions in the rest of the model domain. The control simulations, CTRL, were the ones performed with the current land-cover scenario discussed in Chapter 2.

Sensitivity experiments to doubled CO_2 concentrations were also performed using the current vegetation cover for the period 1996-1997. In one experiment, both CO_2 available for the plant (i.e., biological CO_2) and atmospheric CO_2 affecting the radiative fluxes were increased from 360 ppm to 720 ppm (CO2 in Table 3.1). In a second experiment, only the biological CO_2 was doubled (CO2bio in Table 3.1). Both doubled CO_2 experiments had the same initial LAI conditions than the CTRL. In addition, the same large-scale forcing was used in the doubled CO_2 experiments. As mentioned in Section 3.1, these are sensitivity experiments only to the short-term effects of elevated CO_2 on the near-surface atmosphere.

Sensitivity experiments to doubled CO_2 concentration were also performed using the current vegetation cover for the period 1996-1997. In one experiment, both CO_2 available for the plant (i.e., biological CO_2) and atmospheric CO_2 that affects the radiative fluxes were increased from 360 ppm to 720 ppm (CO2 in Table 3.1). In a second experiment, only the biological CO_2 was doubled (CO2bio in Table 3.1).

To isolate the effects of the land-cover and CO_2 changes, simulations were performed using the same current atmospheric boundary conditions, namely the ERA-40

Reproduced with permission of the copyright owner. Further reproduction prohibited without permission.

dataset, from September to January of 1996-1997 and 1999-2000. Results are presented as the difference of the averages for both periods between the current cover simulation and each of the LULC experiments, grouped in austral spring (October-November) and summer (December-January) seasons. Statistical significance of the differences between CTRL and NAT experiments in the seasonal means was assessed with a Z-test (accounting also for autocorrelation) (Wilks 1995).

3.3 Results

3.3.1 "Natural Vegetation" Scenario

Two main areas with vegetation changes are identified in Figure 3.2. The largest converted area is located in southern Brazil, where broadleaf trees were assumed to be replaced by corn in 42% of the modified grid cells and by soybean in 15% (Table 3.2). The other area is located over the Pampas region, with a 20% and 12% of the changed grid cells converted from tall grass to soybean and wheat respectively.

	Vegetation conversion	%	z_o
1	Wheat - tall grass	12	---
2	Wheat - wooded grasslands	5	- 0.4
3	Soybean - evergreen broadleaf tree	15	- 1.9
4	Soybean - tall grass	20	---
5	Soybean - wooded grasslands	5	- 0.4
6	Corn - evergreen broadleaf tree	42	- 1.9
7	Corn - tall grass	1	---

Table 3.2. Percentage of grid cells associated with the NAT experiment and changes in roughness length (z_o) for each of the vegetation changes. The name of the vegetation conversion corresponds to Current vegetation – "Natural" vegetation.

Reproduced with permission of the copyright owner. Further reproduction prohibited without permission.

These conversions have associated changes in vegetation characteristics, like leaf area index (LAI), albedo and roughness length, that may affect the partition of available energy (Table 3.2). Albedo and LAI differences between current and "natural" vegetation cover were computed and averaged over the grid cells with the same vegetation changes, for austral spring and summer (Figure 3.3). Albedo increased in all the vegetation conversions: albedo of current vegetation was higher than that of natural vegetation. Differences were lower in spring than in summer when the vegetation changes included summer crops, like soybean and corn. In the grid cells with wheat as the current crop, differences in albedo were higher in spring than in summer. Wheat is harvested mid-December to early January (Hall et al. 1992), and vegetation is assuming to shift to tall grass after that event. On the other hand, in the case of summer crops, sowing is around mid-October, and the growing season extends throughout all the simulation period (see Figure 2.25). Harvest dates for these crops are around March and April for corn and soybean respectively (Hall et al. 1992; Guerschmann et al. 2003).

The different seasonal behavior of the crops is also reflected in LAI differences between CTRL and NAT experiments. Figure 3.4 shows the spatial pattern of the changes in albedo and LAI between CTRL and NAT experiment. Conversion from natural vegetation to winter crops (i.e., wheat) increased LAI during spring and decreased LAI in summer, after harvest. LAI decreased, for both spring and summer seasons, in the grid cells that converted from broadleaf trees and wooded grasslands to summer crops.

Reproduced with permission of the copyright owner. Further reproduction prohibited without permission.

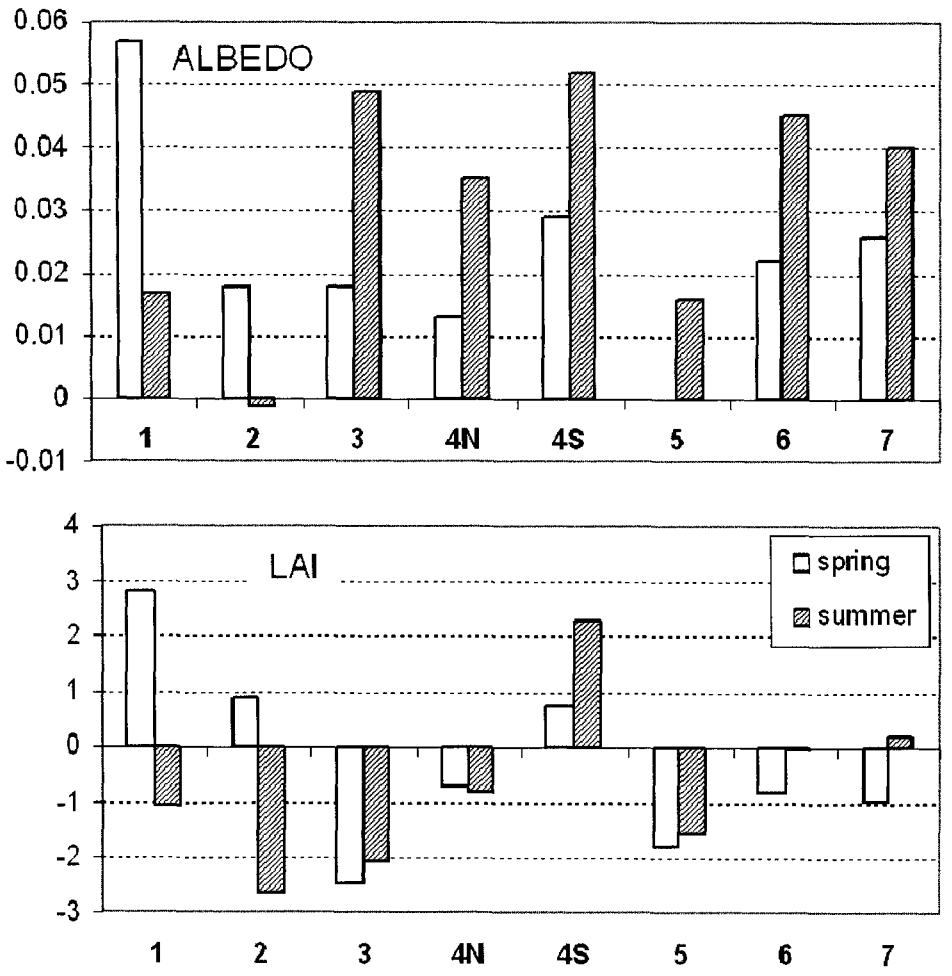

Figure 3.3. Differences in area-averaged albedo and LAI between the NAT and CTRL experiments. See Table 3.2 for the vegetation conversions. 4N and 4S are the northern and southern grid cells of the conversion # 4, soybean to tall grass.

Reproduced with permission of the copyright owner. Further reproduction prohibited without permission.

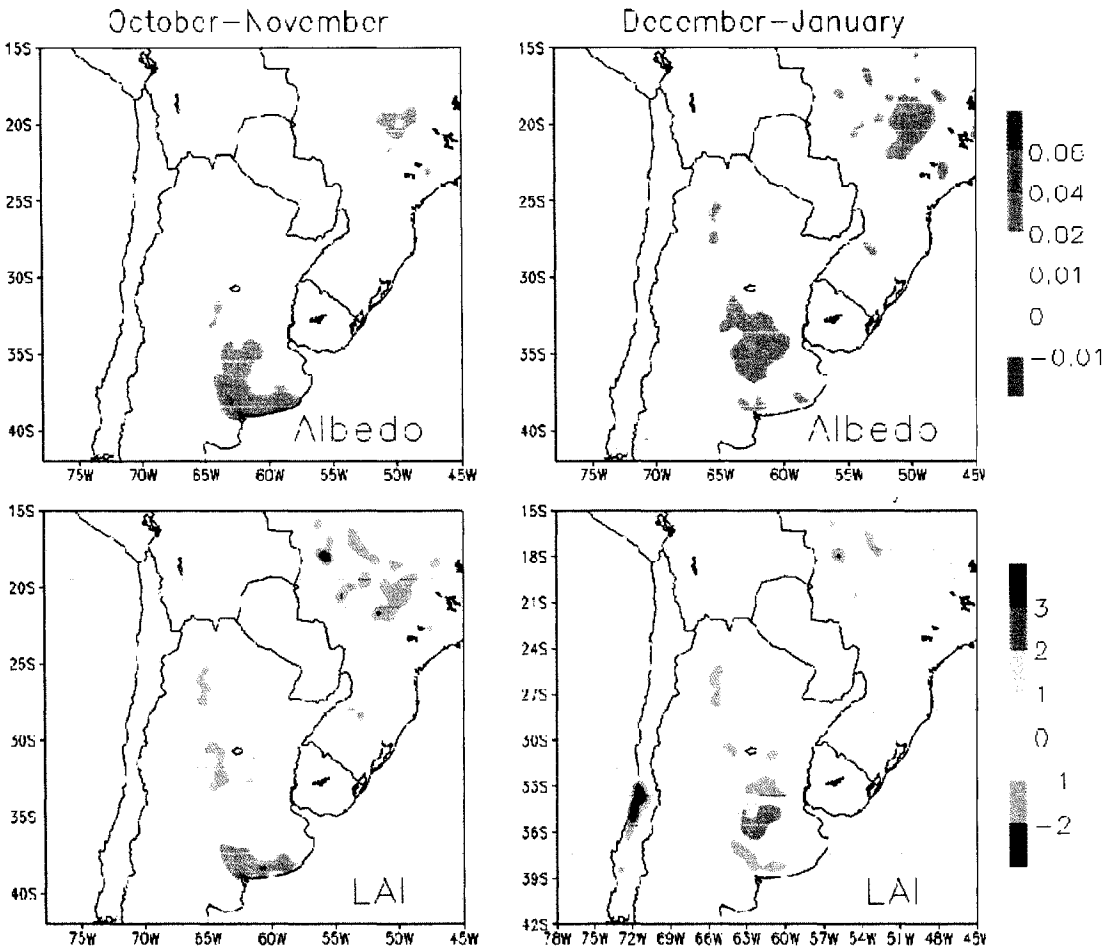

Figure 3.4. Spatial changes in albedo and LAI averaged for spring (October-November) and summer (December-January) computed as CTRL - NAT experiments, i.e., "current" – "natural" vegetation.

Reproduced with permission of the copyright owner. Further reproduction prohibited without permission.

Within the grid cells that converted from tall grass to soybean in the Pampas region, two areas of opposite behavior were found. In the northern part (4N conversion in Figure 3.3), where grasslands were assumed to have a C_4 photosynthetic pathway, LAI was slightly higher in the NAT experiment than under current conditions. On the other hand, in the southern part, grasslands were assumed to be C_3 (4S conversion in Figure 3.3). In this case, LAI was higher in the CTRL than in NAT experiment.

Another parameter associated with the vegetation changes is the roughness length. The largest decreases in roughness length concentrated in Brazil associated with the tree-to-crop conversion followed by the wooded grasslands-to-crop conversion (Table 3.2).

Changes in LULC had a direct impact on the near-surface latent and sensible heat fluxes (Figures 3.5 and 3.6). The combined effect of changes in albedo and LAI can be associated with those impacts. Areas with noticeable changes in the surface fluxes were collocated with the areas that experienced the land-cover change. During the entire simulation, sensible heat decreased when crops replaced natural vegetation in most of the domain. Largest SH differences (i.e., lower than -40 W m^{-2}) were found in the southern portion of the grid cells that converted from tall grass to soybean, and in the ones converted to wheat in the southern Pampas during spring. The same areas had almost opposite changes in LH between CTRL and NAT simulations. Over wheat fields, LH were higher and SH lower than with the natural vegetation cover during spring, switching to lower values in summer, when most of the wheat was already harvested. In the grassland-to-soybean grid cells, LH was higher in CTRL than in NAT simulations during both seasons, associated with LAI differences. Less noticeable changes in LH and SH were found in the other vegetation conversions, although the direction of the changes can

Reproduced with permission of the copyright owner. Further reproduction prohibited without permission.

be related to changes in albedo and LAI. A general slight decrease in available energy (SH plus LH) was found over the domain, associated with the overall increase in albedo.

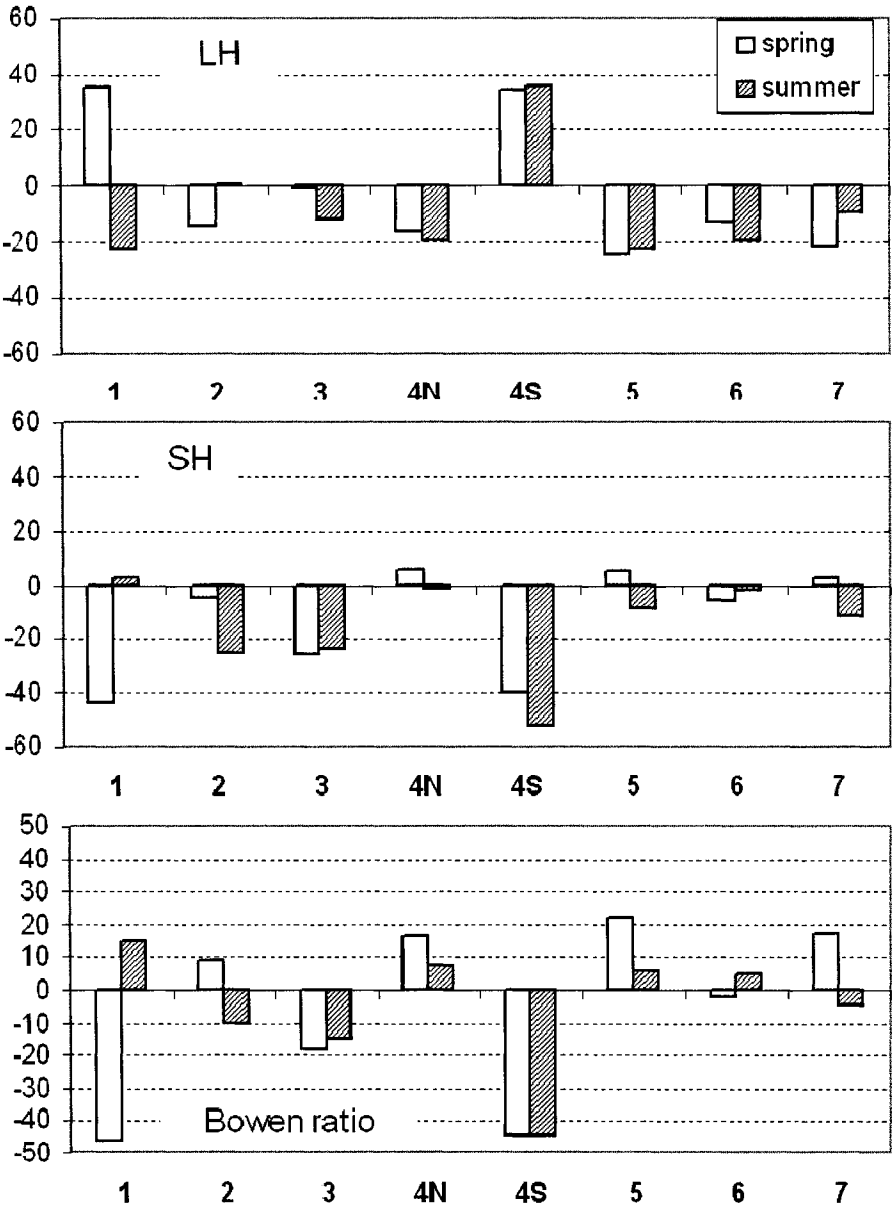

Figure 3.5. Changes in latent heat (LH) flux, sensible heat (SH) flux and Bowen ratio (SH/LH) between the current (CTRL case) and natural vegetation cover (NAT case). Values are in W m^{-2} for the fluxes. Changes in SH/LH are in percentage with respect to the natural cover.

Reproduced with permission of the copyright owner. Further reproduction prohibited without permission.

Bowen ratio values (β=SH/LH), calculated for each of the vegetation changes, varied between 0.4 and 1.4, indicating that in general the available energy is mostly used in transpiration and evaporation. There was also a seasonal variation in β, with values generally lower in summer than in spring. The shift from natural to current vegetation led to changes in how the energy is partitioned between LH and SH (Figure 3.5). Spatial and seasonal variations were found associated with the behavior in LH and SH in each of the simulated vegetation cover changes (Figure 3.6). The largest changes in Bowen ratio values, up to 46%, corresponded to a decrease in β from natural to current vegetation cover. They occurred in spring in the grid cells located in the Pampas with wheat and soybean as current vegetation cover. This indicates more energy is now being used in transpiration and evaporation than in heating the near-surface atmosphere, and a net cooling effect is expected in those grid cells. The largest positive change, of 22%, was also found in spring in the few grid cells that changed from wooded grasslands to soybean. Absolute changes in summer tended to be similar or lower than in spring.

Changes in near-surface fluxes led to changes in near-surface temperature and water vapor (Figure 3.7). A cooler (warmer) near-surface atmosphere was found with current vegetation cover associated with higher (lower) LH and lower (higher) SH fluxes. Near-surface temperatures decreased when crops (i.e., wheat and soybean) replaced C_3 grasslands, like in the southern Pampas. Increases in temperature were found when crops replaced evergreen trees and wooded grasslands (e.g., in Brazil), and C_4 grasslands (e.g., in the central region of the Pampas). The coolest (up to -0.8°C) and warmest (higher than 0.6°C) 2 m temperature differences appeared in the spring averages.

Reproduced with permission of the copyright owner. Further reproduction prohibited without permission.

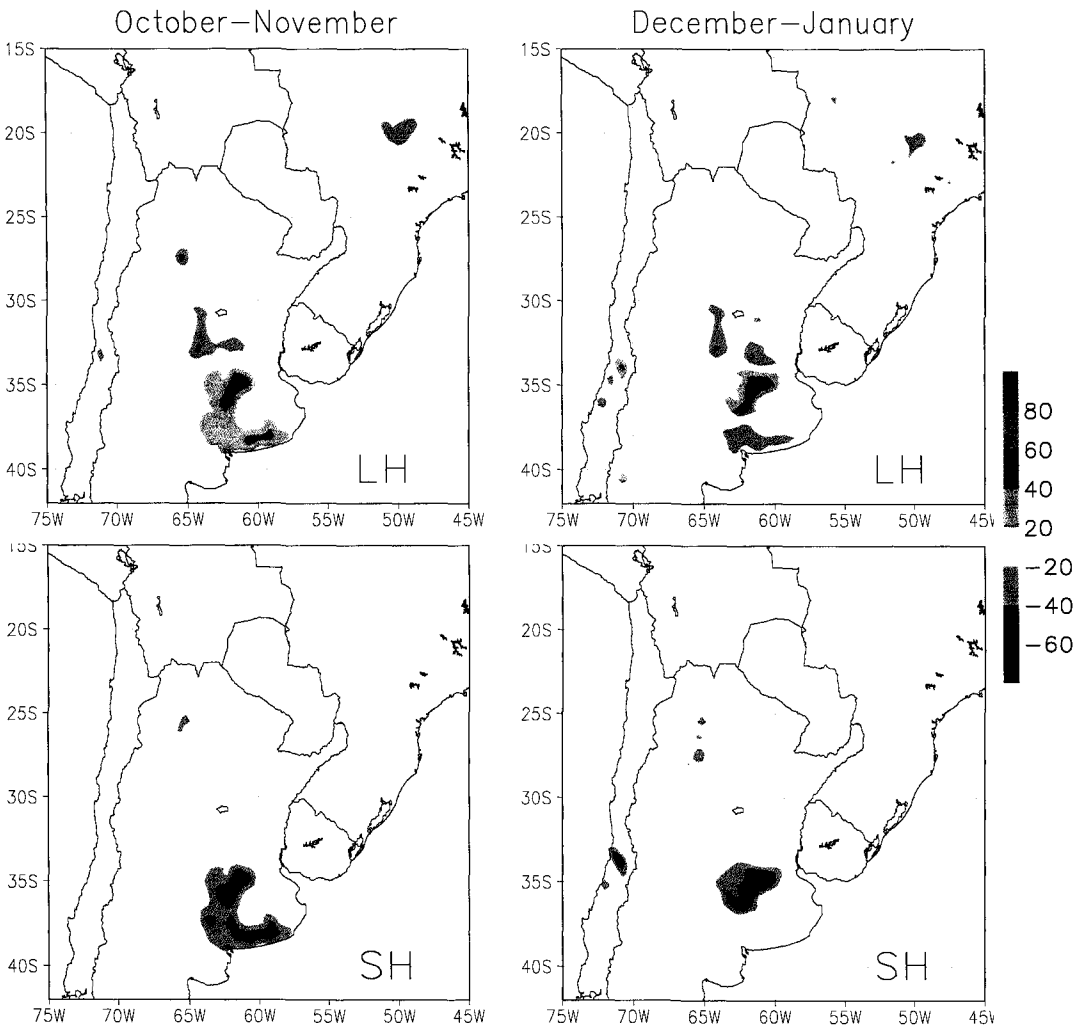

Figure 3.6. Spatial changes in latent heat (LH) and sensible heat (SH) fluxes averaged for spring (October-November) and summer (December-January).

Reproduced with permission of the copyright owner. Further reproduction prohibited without permission.

The shelter-level temperature (at 2 m), calculated using similarity theory, is to a certain extent affected by the model parameterization. First model level temperatures (approximately at 57 m) may be more reliable. At that level, differences between current and natural cover became smaller, but the spatial pattern remained, in particular in the Pampas region during all the simulation time (Figure 3.7). Changes in mean temperatures could be seen up to approximately 1000 m. Changes in humidity were less noticeable (Figure 3.7, bottom), but tended to be consistent with the changes in LH fluxes: moister (drier) near-surface atmosphere was found with increases (decreases) in LH.

Temperature changes between current and natural vegetation had a diurnal variation (Figure 3.8). Maximum temperatures, considered as the temperature at 18Z (15 LST), presented a larger decrease than minimum temperatures, considered as temperatures at 12Z (LST). Minimum temperatures slightly increased in summer in the southern Pampas. This means also a decrease in the diurnal amplitude of temperature.

Slight changes were found in precipitation between the current and natural scenarios (not shown). In the southern Pampas in spring, an area with a decrease in precipitation under current land-cover conditions was found collocated with the grid cells that presented an increase in LH and temperature. Absolute mean values were 0.5 mm day^{-1} for spring that represent around 10-20% with respect to the value simulated for the natural scenario. In summer, a small area with a reduction in precipitation was found in the center of the Pampas associated with a decrease in LH. Nevertheless, differences were less noticeable during summer.

Reproduced with permission of the copyright owner. Further reproduction prohibited without permission.

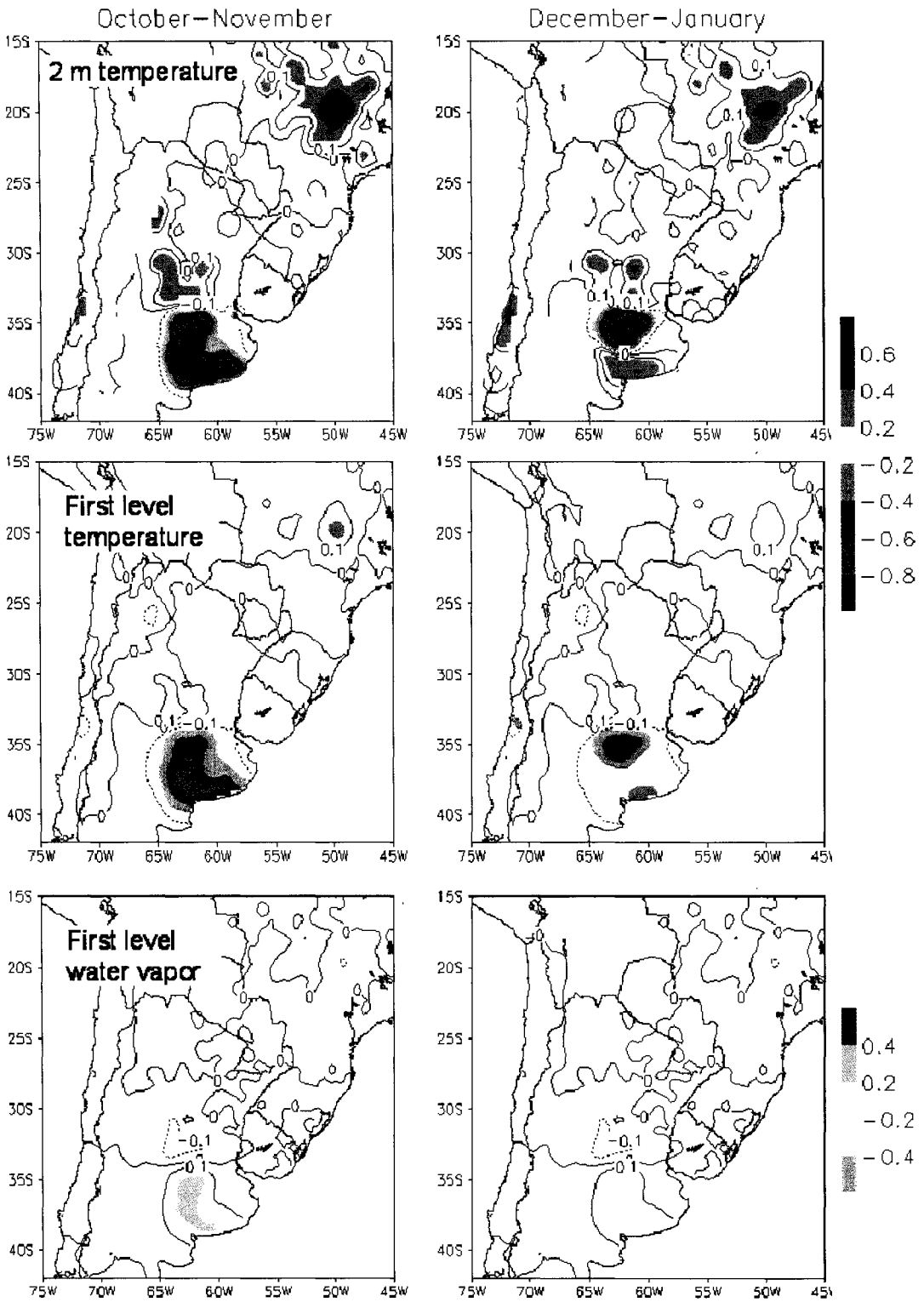

Figure 3.7. Differences between CTRL and NAT experiments for: 2 m temperature (°C) (top); first model level temperature (°C) (middle); water vapor mixing ratio (g kg^{-1}) (bottom).

Reproduced with permission of the copyright owner. Further reproduction prohibited without permission.

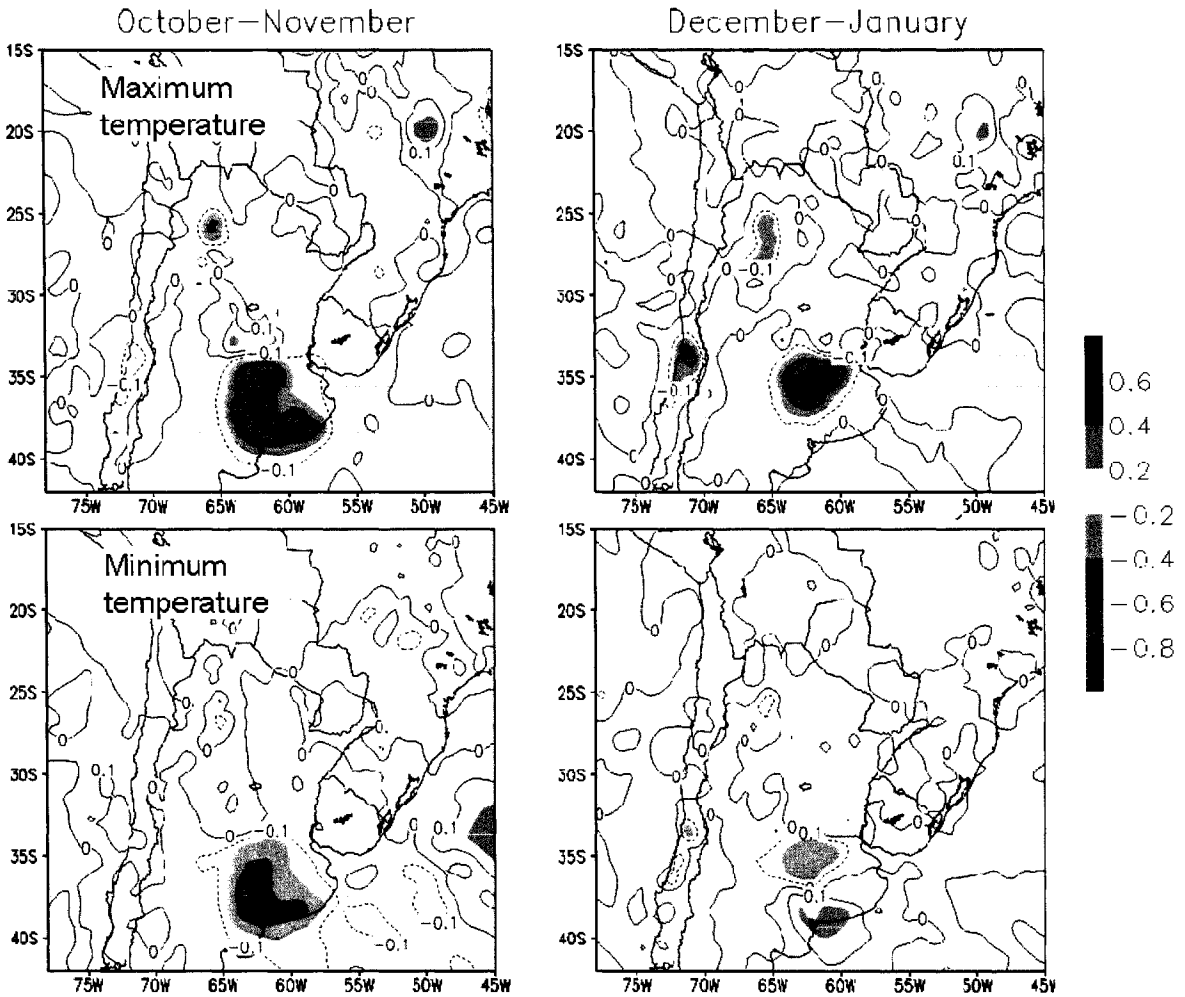

Figure 3.8. Differences between CTRL and NAT experiments for maximum (18Z) and minimum (12Z) temperature (°C).

Reproduced with permission of the copyright owner. Further reproduction prohibited without permission.

A Z-test was performed over each grid cell between the current and natural vegetation. Table 3.3 showed the percentage of grid cells, inside each of the specified areas, in which the mean values were statistically significantly different between the two land-cover scenarios. The test shows that seasonal and spatial differences exist inside each of those areas. For instance, for the Tmax (temperature at 18Z) in the southern Pampas, an 83% of those cells were significantly different in spring compared to only 7% in summer. The percentage for the area in Chile is misleading because of the small area considered

		Region			
Variable	Season	SPA	NW	BRA	CHI
LH	SPR	51	25	16	30
	SUM	39	18	14	27
SH	SPR	64	32	17	37
	SUM	21	22	13	44
T18	SPR	83	35	11	53
	SUM	7	23	5	50
T12	SPR	77	18	5	22
	SUM	35	18	1	27
DELLAI	SPR	44	19	4	79
	SUM	52	16	6	76
GS	SPR	79	48	30	78
	SUM	40	45	42	19
TOTPREC	SPR	33	36	47	32
	SUM	32	40	52	31
LAI	SPR	78	45	49	73
	SUM	54	39	45	84

Table 3.3. Percentage of grid cells significantly different for means, between the control simulation and natural vegetation. Regions are: SPA (south PA, corresponded to wheat); NW (northwest, corresponded to soybean in the Pampas and northwestern Argentina; BRA (Brazil); CHI (Chile). Also, SPR: spring; SUM summer. LH: latent heat; SH: sensible heat; T18: temperature at 18Z (14LST); T12: temperature at 12Z (8LST); DELLAI: daily LAI change; GS: stomatal conductance; TOTPREC: daily accumulated precipitation; LAI; leaf area index.

Reproduced with permission of the copyright owner. Further reproduction prohibited without permission.

3.3.2 Sensitivity to Doubled CO_2 Concentrations

The combined effects of landscape change and doubled CO_2 concentrations are examined in this Section. No interactions between the factors (i.e., radiation and biological doubled CO_2) were explicitly addressed here, as in Eastman et al. (2001a). The total effect of the CO_2 radiative forcing (i.e., the pure CO_2 radiative effect plus the contributions from the interactions between the radiation and biological doubled CO_2 concentration) are given by the differences between the CO2 and CO2bio experiments, both with the same vegetation distribution. No major differences were found between these experiments in this study, indicating that the radiation forcing had a secondary role in these coupled simulations. As previously discussed, these are regional-scale sensitivity experiments, in which the same present-time large-scale forcing is considered. The effects of the long-term increased CO_2 concentration (i.e., a general increase in temperature) were not addressed in these simulations. Therefore, the model sensitivity to the overall CO_2 forcing under current vegetation conditions is addressed by the differences between the CO2 and CTRL experiments.

On a domain-averaged basis, the effect of increasing CO_2 concentration over the near-surface atmospheric and biological variables was almost negligible. Nevertheless, spatial differences were noticeable. As an example, Figure 3.9 shows the differences in LAI, stomatal conductance, SH and LH between the CO2 and CTRL simulations. Higher CO_2 concentrations led to an increase in aboveground biomass (not shown) and LAI.

Areas with the lowest changes in LAI corresponded to C_4 grasses and the highest to broadleaf trees and wooded grasslands over the northern part of the domain. This response is the result of saturated C_4 photosynthesis at current atmospheric CO_2 levels (in

Reproduced with permission of the copyright owner. Further reproduction prohibited without permission.

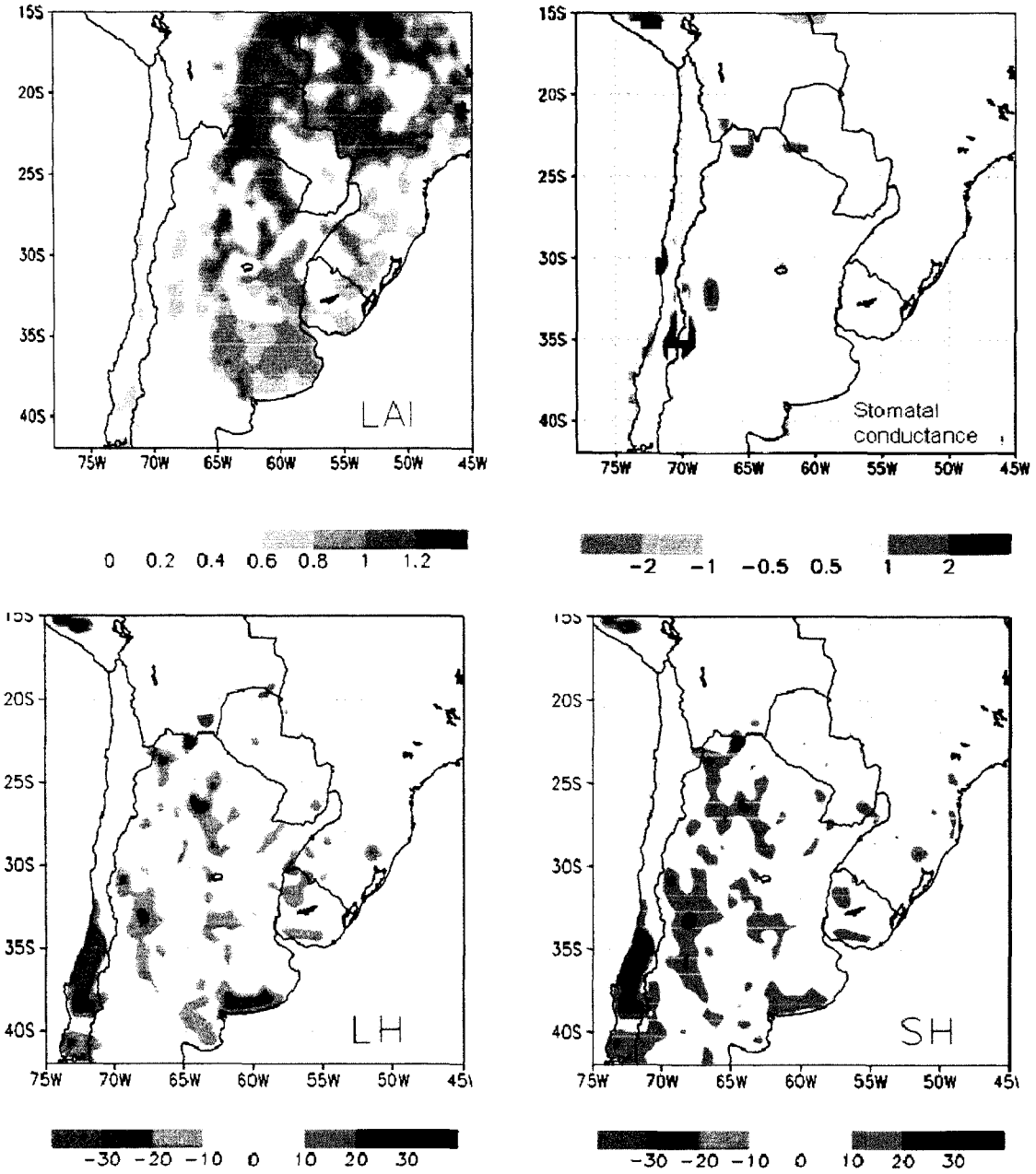

Figure 3.9. Differences in the CO2-CTRL experiments for LAI, stomatal conductance (mm s^{-1}), LH (W m^{-2}), and SH (W m^{-2}).

Reproduced with permission of the copyright owner. Further reproduction prohibited without permission.

the simulations is assumed to be 360 ppm) and higher temperatures in the subtropics. C_3 plants tends to responds more to increasing CO_2 than C_4 species (Poorter 1993), although soil water status may enhanced the response of C_4 plants to CO_2 levels (i.e., Morgan et al. 2001).

Grid cells with different photosynthesis pathways C_3 and C_4 were grouped and aboveground and belowground biomass and transpiration were computed for the spring for CTRL and CO2 experiments (Table 3.4). Aboveground biomass under double CO_2 concentrations increased by 24% and 12% for C_3 and C_4 species with respect to the CTRL simulation. Relative root biomass increases were 22% and 3% for C_3 and C_4 plants, respectively. Water consumption was very similar between C_3 and C_4 plants and experiments. Water use efficiency of productivity (Larcher, 1995) for the whole plant was higher in C_3 than in C_4 plants, and higher in CO2 than in CTRL experiments. C_4 plants had a relative higher response to CO_2 enrichment than C_3 plants: WUE in C_4 plants increased 19% compared to 17% of C_3 plants. Comparisons between C_3 and C_4 species usually suggest a higher WUE in C_4 than in C_3 plants. Aboveground biomass for C_3 plants may be overestimated because of the short period considered here.

	Aboveground		Root		Transpiration		WUE	
Species	CTRL	CO2	CTRL	CO2	CTRL	CO2	CTRL	CO2
C_3	0.55	0.68	0.58	0.71	118	122	4.7	5.6
C_4	0.17	0.19	0.75	0.77	114	100	3.2	3.8

Table 3.4. Mean aboveground and root biomass (kgDM m^{-2}), transpiration (kgH_2Om^{-2}) and whole-plant water use efficiency (WUE, average plant production/water transpired, gDM kg^{-1} H_2O) of C_3 and C_4 grid cells for the CTRL and CO2 simulations for the first 90 days.

Reproduced with permission of the copyright owner. Further reproduction prohibited without permission.

Overall, stomatal conductance tended to be lower in the CO2 experiment (not shown). A general closure of the stomata is the expected response to the CO2 enrichment. The LH and SH spatial pattern between CO2 and CTRL simulations appeared mostly related to the LAI pattern. Areas with lower LAI increase tended to present lower LH (higher SH). Overall, an increase in CO_2 led to higher temperatures, although there are some spatial differences (Figure 3.10). In spring, Tmax was up to 0.6°C warmer in CO2 than in CTRL experiments, but also were up to 0.2°C cooler. The effect of increased CO_2 levels was not noticeable in precipitation.

The difference between CO2 and NAT indicates the total sensitivity to land-cover and CO_2 changes (Figure 3.10). The cooling effect of the vegetation shift has been reduced in most of the domain (e.g., in the southern Pampas) and the warming effect has been enhanced (e.g., in southern Brazil) (compared to Figure 3.8). The 2xCO2 effect operates over the entire domain with different magnitude. Therefore, its signal is also present in areas not associated with vegetation change, like the warmer area west of the domain and a cooler one around 20°S. This indicates that increase in CO_2 levels mitigates the temperature decrease in the southern Pampas and enhances the temperature increase associated with the changes from C_4 grasses, wooded grasslands and trees to crops.

3.3.3 Current vs. "Afforestation" Scenario

Overall, afforestation led to a decrease in albedo, and increases of LAI and roughness length. These are the typical changes in the vegetation characteristics expected when converting from grass or crops to forest (Sellers 1992). Therefore, alterations in

Reproduced with permission of the copyright owner. Further reproduction prohibited without permission.

near-surface fluxes, latent heat and sensible heat, and eventually temperature and humidity, are expected.

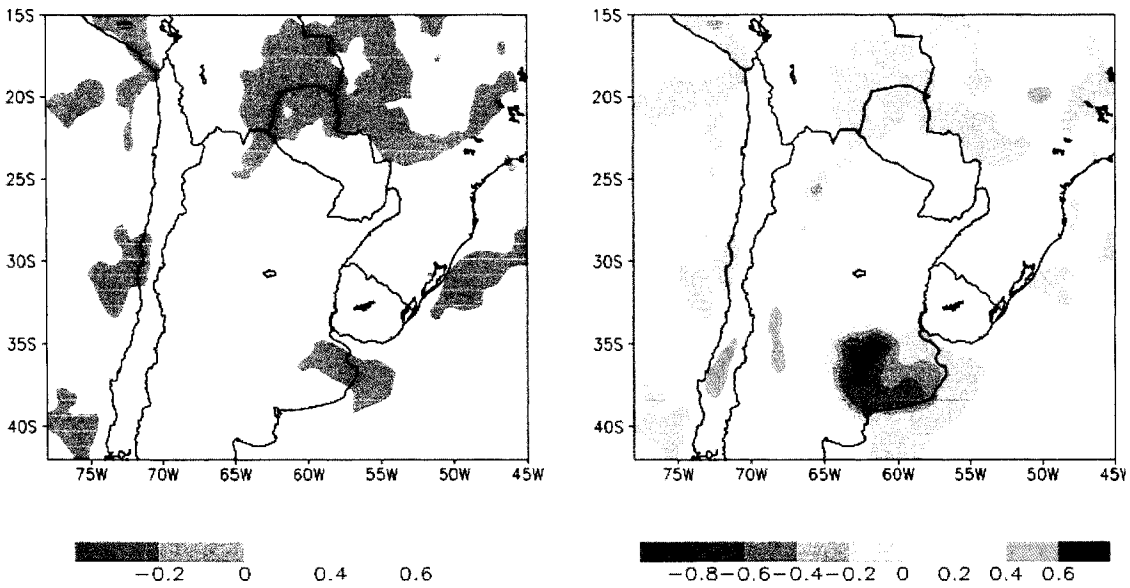

Figure 3.10. Differences between CO2-CTRL (left) and CO2-NAT for spring temperature (°C) at 18Z (1400LST).

Latent and sensible heat were higher and lower respectively in the AFFOR experiment than in the CTRL case, i.e., with current vegetation cover (Figure 3.11). The changes were observed in the grid cells that experience the land-cover modification. Averaging over all those grid cells from October to January, daytime LH flux increased 95 W m^{-2}, and SH decreased 66 W m^{-2} (48 % and 73% respectively relative to LH and SH for current land cover).

Latent heat comprises the heat associated with physical evaporation (i.e., from soil and leaf surfaces) and transpiration through the stoma. Total evaporation decreased

Reproduced with permission of the copyright owner. Further reproduction prohibited without permission.

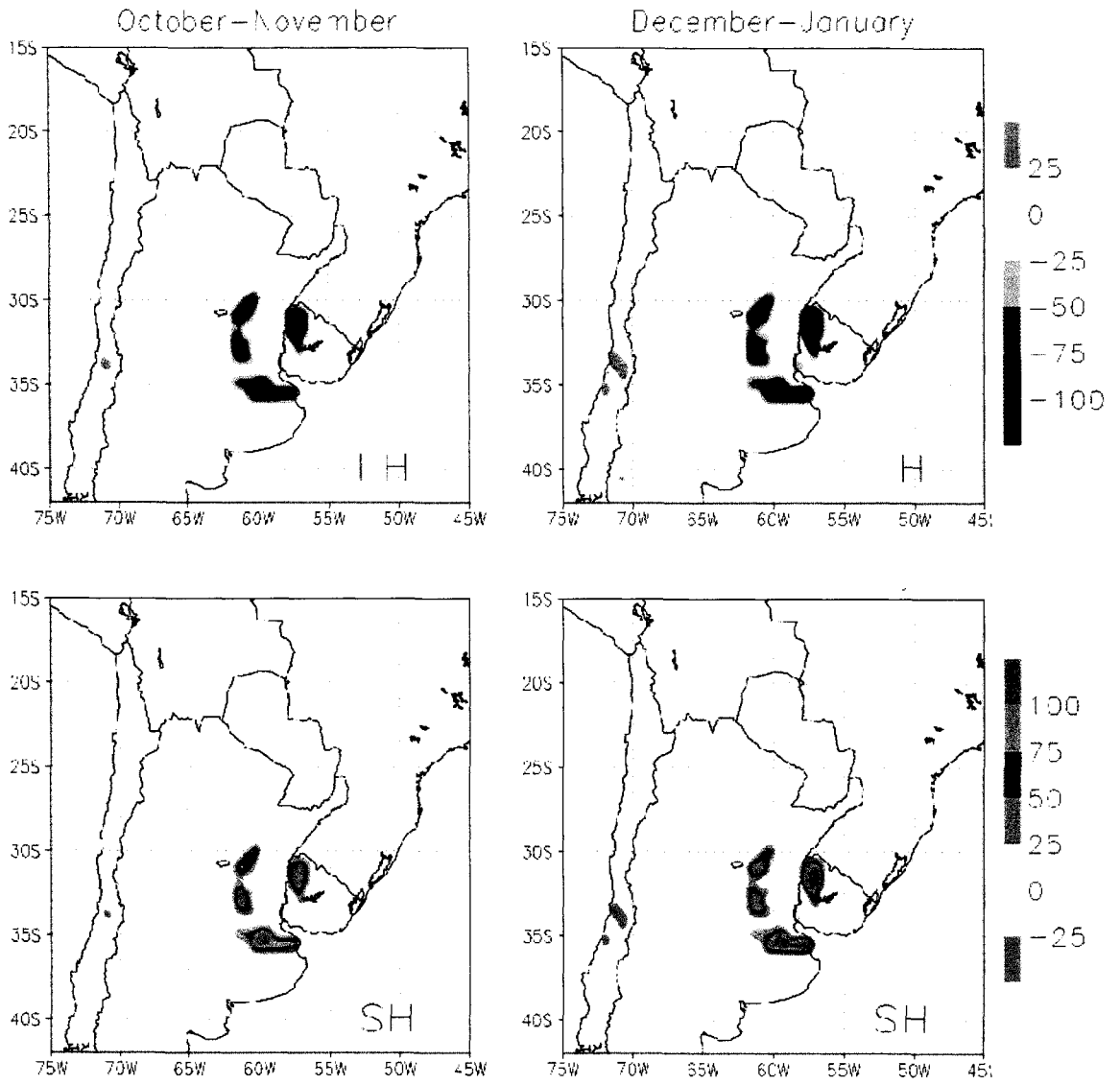

Figure 3.11. Spatial changes in latent heat (LH) and sensible heat (SH) fluxes averaged for spring (October-November) and summer (December-January) between CTRL and AFFOR simulations.

Reproduced with permission of the copyright owner. Further reproduction prohibited without permission.

(7.5 W m^{-2} or 10% with respect to the CTRL) mainly because of the decrease in soil evaporation. The increase in latent heat was mostly due to the transpiration (102.5 W m^{-2}, 85%). More energy was used in transpiration than in heating the atmosphere in the afforested scenario.

Mean Bowen ratio (β=SH/LH) decreased from 0.47 in the CTRL case to 0.08 in the afforested scenario. This indicates a shift in the partition of available energy between LH and SH. This behavior was found in most of the grid cells, except the ones that converted from wooded grasslands. In this case, SH and LH were slightly higher and lower respectively in the afforested case than under current conditions.

As expected, afforestation led to cooler and wetter near-surface atmospheric conditions over most of the afforested grid cells (Figure 3.12). Area-mean temperature differences between current and afforested conditions were 0.6°C and 0.8°C in spring and summer respectively. For water vapor mixing ratio mean values were -0.4 g kg^{-1} and -0.5 g kg^{-1} respectively. Vertically, those changes could be seen up to around 1000 m.

Changes in precipitation were also observed, especially in summer, and tended to coincide with the grid cells that experienced the vegetation changes (Figure 3.13). In some areas, absolute values in the afforested scenario were up to 60 mm (in mm day^{-1}) higher than for the current scenario for the summer of 1996-1997. During the summer of 1999-2000 the absolute differences were smaller than in 1996-1997, but the relative changes were larger. The spatial pattern of the precipitation changes was associated with changes in moisture convergence (due to changes in roughness length and displacement height) and LH (not shown).

Reproduced with permission of the copyright owner. Further reproduction prohibited without permission.

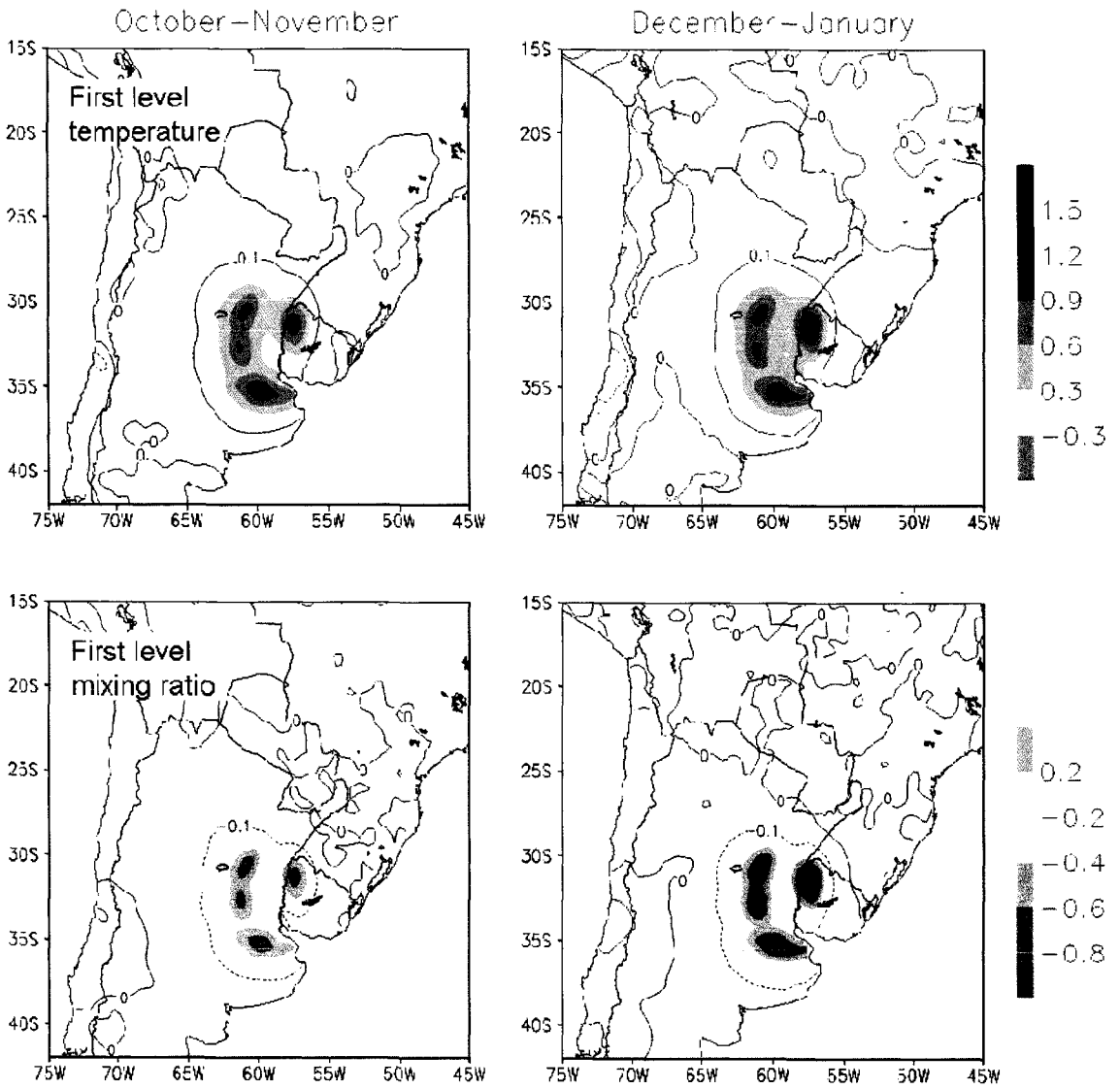

Figure 3.12. Differences between CTRL and AFFOR experiments for first model level temperature (°C) (top) and water vapor mixing ratio (g kg^{-1}) (bottom).

Reproduced with permission of the copyright owner. Further reproduction prohibited without permission.

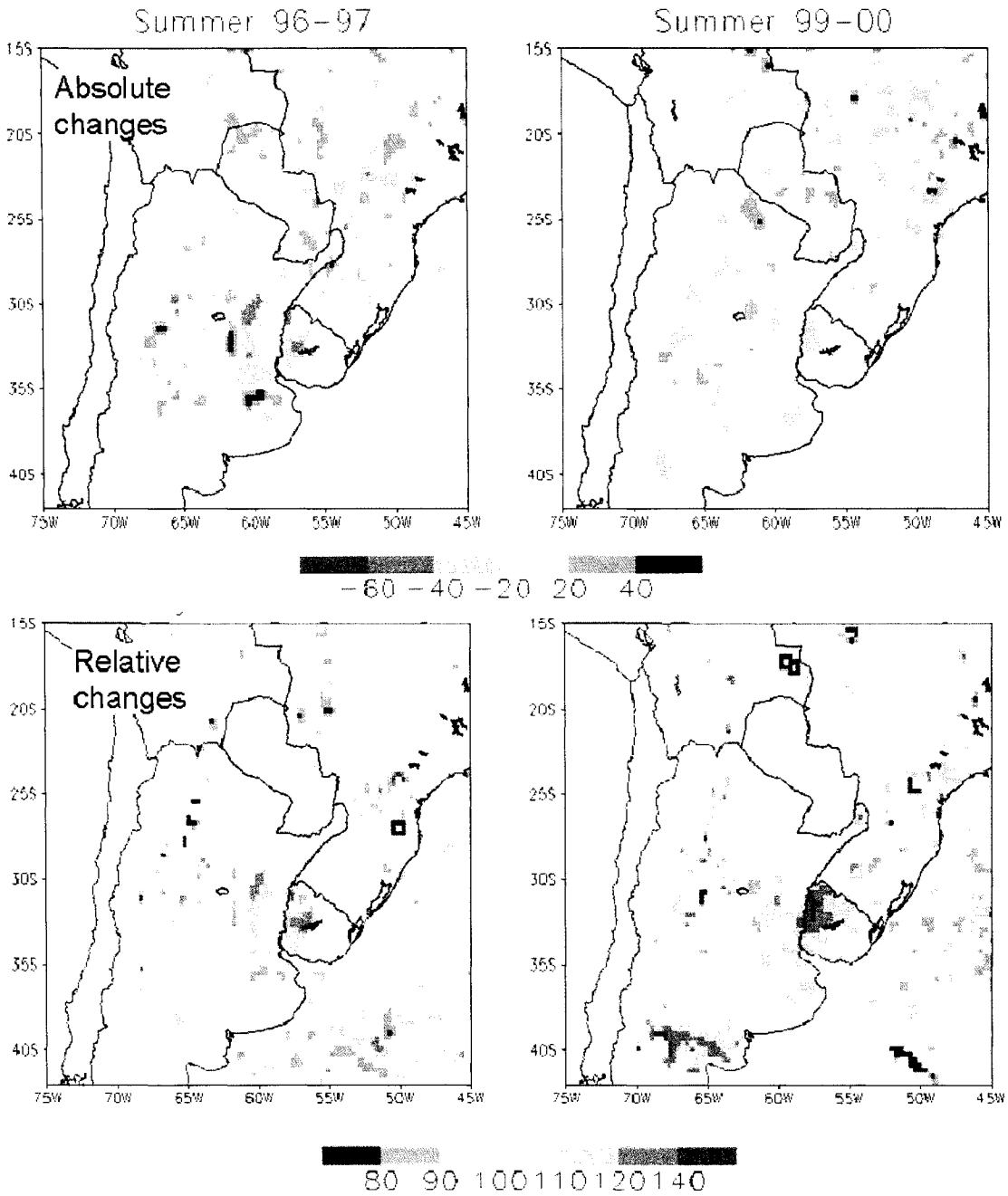

Figure 3.13. Differences between CTRL and AFFOR experiments for precipitation: absolute changes (mm month^{-1}) (top); relative changes (bottom).

Reproduced with permission of the copyright owner. Further reproduction prohibited without permission.

3.4 Discussion and Conclusions

Simulated changes in near-surface fluxes, temperature, and humidity for the different land-cover modifications were the ones expected based on changes in physical and physiological parameters. They also compare well with other studies, carried out for the Northern Hemisphere, mostly over North America (e.g., Bonan 1997; Twine et al. 2004; Bounoua et al. 2002; Narisma and Pitman 2003; Pitman et al. 2004). The type of land-cover changes simulated here, where shifts in vegetation were associated with changes in LAI, albedo, and root depth with a direct effect on LH and SH, might affect mainly maximum temperatures.

The general potential effect of agriculture was cooling, when the shift was from grasses (C_3) to crops; warming when the shift was from grasses (C_4), wooded grasslands or trees to crops. In this experiment, it was evident that spatial and temporal variability are important. After harvest, a drastic change in vegetation takes place that affected LAI and albedo. The results are consistent with the observed trends in temperature over Argentina. For the austral summer (December to February), Rusticucci and Barrucand (2004) found a negative trend in maximum temperatures during the 1959-1998 period, especially in the center of the Pampas region. On the other hand, minimum temperatures increased. A slight increase in the first level 12Z (800 LST) temperature for the entire domain was found in this study, except for a small region in the center of the Pampas.

In these sensitivity experiments, no effects of initial soil moisture content were explicitly addressed. In particular, the Flooding Pampas region may show saturation to flooded soil moisture conditions in low areas during winter in some years that may impact the near-surface weather during the following spring and summer months.

Reproduced with permission of the copyright owner. Further reproduction prohibited without permission.

In this sensitivity experiments, the effect of the doubled CO_2 concentrations was a generalized warming, causing a reduction/enhancement of the cooling/warming effect of the simulated land-cover changes. Regional and global modeling results have shown that the effects of land-cover changes on near-surface temperature and precipitation may be comparable in magnitude to that of increasing CO_2 levels (Pitman and Zhao 2000; Chase et al. 2001; Eastman et al. 2001a). Because all the simulations were performed with present-day large-scale forcing, only the short-term sensitivities to doubled CO_2 were addressed. The effect of a potentially different large-scale weather pattern under increasing CO_2 levels, with associated higher temperatures than present conditions, was not considered. Many uncertainties are associated with the future climate scenarios derived from different GCMs. In the previous Chapter, it was shown that large-scale forcing had a major role in the climate simulated by the regional model. The dynamic downscaling of this GCM forcing with GEMRAMS or RAMS might result in near-surface weather very different to present conditions. In the long-term, large and persistent changes in near-surface temperature would result in changes in vegetation cover, which would be in equilibrium with the "new" climate. No long-term ecosystems processes, like resource competition, population dynamics, and soil organic matter dynamics are addressed with this regional coupled atmospheric-biospheric model.

In this study, a current fixed vegetation type and C_3/C_4 distribution were assumed for all the experiments with double CO_2 concentrations. The long-term effects of CO_2 enrichment include possible shift in species and/or C_3/C_4 composition through the indirect effect of increased WUE (Mooney et al. 1999). In these experiments, WUE for both C_3 and C_4 was higher under doubled CO_2 concentrations than in current CO_2 levels,

Reproduced with permission of the copyright owner. Further reproduction prohibited without permission.

and were relatively similar between C_3 and C_4 grasses. In addition, a slight decrease in transpiration was simulated in C_4 plants under doubled CO_2 conditions. Several environmental conditions, like soil water and nitrogen levels, may also affect the response. A better understanding of this effect is still needed to predict how the possible WUE enhancement may affect the C_3/C_4 distribution in grasslands.

An afforestation scenario also modified near-surface fluxes and temperature. From October to January, afforested grid cells had higher LH (48%) and cooler temperatures (-0.5 °C) than the ones under current vegetation cover (mainly grasslands). Using estimations from seven cloud-free Landsat 7 ETM+ images for a location very close to the area with the land-cover change used in this study, Nosetto et al. (2005) found increases in LH and decreases in temperature of around 80% and 5°C respectively. Higher evaporation and transpiration rates in forest compared to grasslands were also found in other observational studies (e.g., Larcher 1995; Hodnett et al. 1995). Higher values of LAI, higher efficiency in water transfer from the soils, and a deeper root system were the vegetation characteristics associated with those changes. Although only two years were considered with only one afforestation scenario, these results showed that this potential future land-cover change may also influence the lower atmosphere. No analysis was performed in hydrological variables, such as runoff or deep water processes.

Precipitation was also affected by the vegetation changes. Although a general increase was found for the entire simulation domain with an afforested scenario, areas of increase and decrease rainfall were associated with changes in LH, roughness length, and areas of moisture convergence. Some dependency of afforested pattern and moisture flux convergence could also be seen, indicating that interannual variability in the fluxes may

Reproduced with permission of the copyright owner. Further reproduction prohibited without permission.

also affect the simulated patterns and values. Changes in precipitation and wind patterns have also been found to be linked to changes in vegetation cover (Kanae et al. 2001; Marshall et al. 2004; Pitman et al. 2004). Precipitation in this region is highly related to regional (i.e., SACZ position and strength) and large-scale processes (i.e., ENSO events). In the previous chapter, it was shown that large-scale forcing strongly influenced simulated precipitation patterns. Although a weak interior nudging was used in these simulations, this might offset any local contribution to precipitation. Local influences may enhance/decrease precipitation in some areas. Additional simulations are needed to address the degree of influence of local land-cover changes on precipitation in the region.

The impacts were mostly limited to the areas of the land-cover changes, although changes also appeared in locations far from where the change was assumed. The spatial scale of the change is also important. For example, increasing the afforested area would increase the area of cooling and the effect on precipitation may also be more noticeable. However, "realistic" land-cover scenarios were addressed in these simulations. One of the important characteristics of regional atmospheric models is that they can be used to explore processes that occur at spatial scales that cannot be resolved by the global atmospheric models. Lu and Shuttleworth (2002) found that spatial heterogeneity in LAI also affected the near-surface atmosphere.

GEMRAMS was able to capture the physiological differences between vegetation types, which also led to spatial differences in the response. Different crops, with their associated phenology, had a great impact in the simulations. Biomass and LAI, in

Reproduced with permission of the copyright owner. Further reproduction prohibited without permission.

particular for crops, had a very strong seasonality, which needs to be considered if seasonal simulations are being conducted.

Reproduced with permission of the copyright owner. Further reproduction prohibited without permission.

Chapter 4

THE EFFECTS OF HISTORICAL VEGETATION CHANGE ON NEAR-SURFACE CLIMATE IN THE NORTHERN CHIHUAHUAN DESERT

4.1. Background: Landscape Changes in Semiarid Areas

Deforestation, afforestation, desertification, cultivation, and irrigation are landscape modifications that often lead to changes in near-surface fluxes that may affect weather and climate with feedbacks to the vegetation (see Pielke at al. 1998 for a listing of published work related to these research topics). A key example of landscape change involves woody plant invasion into perennial grasslands and has occurred in arid and semiarid regions globally over the past several centuries. In the Chihuahuan Desert of North America, shrub cover has increased dramatically in areas that were predominantly grassland in the mid-1800s (Buffington and Herbel 1965; Gibbens et al. 1992, 2005). Since the early 1900s, C_3 shrubs, mesquite (*Prosopis glandulosa*) and creosotebush (*Larrea tridentata*), have increased in cover at the expense of C_4 grasses, mainly black grama (*Bouteloua eriopoda*) (e.g., Figures 4.1 and 4.2). For example, in 1858, grasses comprised more than 80% of the Jornada Experimental Range in the northern Chihuahuan Desert (Gibbens et al. 2005). By 1998, 59% of the area is now occupied by mesquite and 25% is dominated by creosote with only 7% grass cover. Overgrazing combined with extreme drought are two factors that have contributed to these changes (Buffington and Herbel 1965; Neilson 1986; Grover and Musick 1990; Schlesinger et al. 1990; Peters, 2000).

Reproduced with permission of the copyright owner. Further reproduction prohibited without permission.

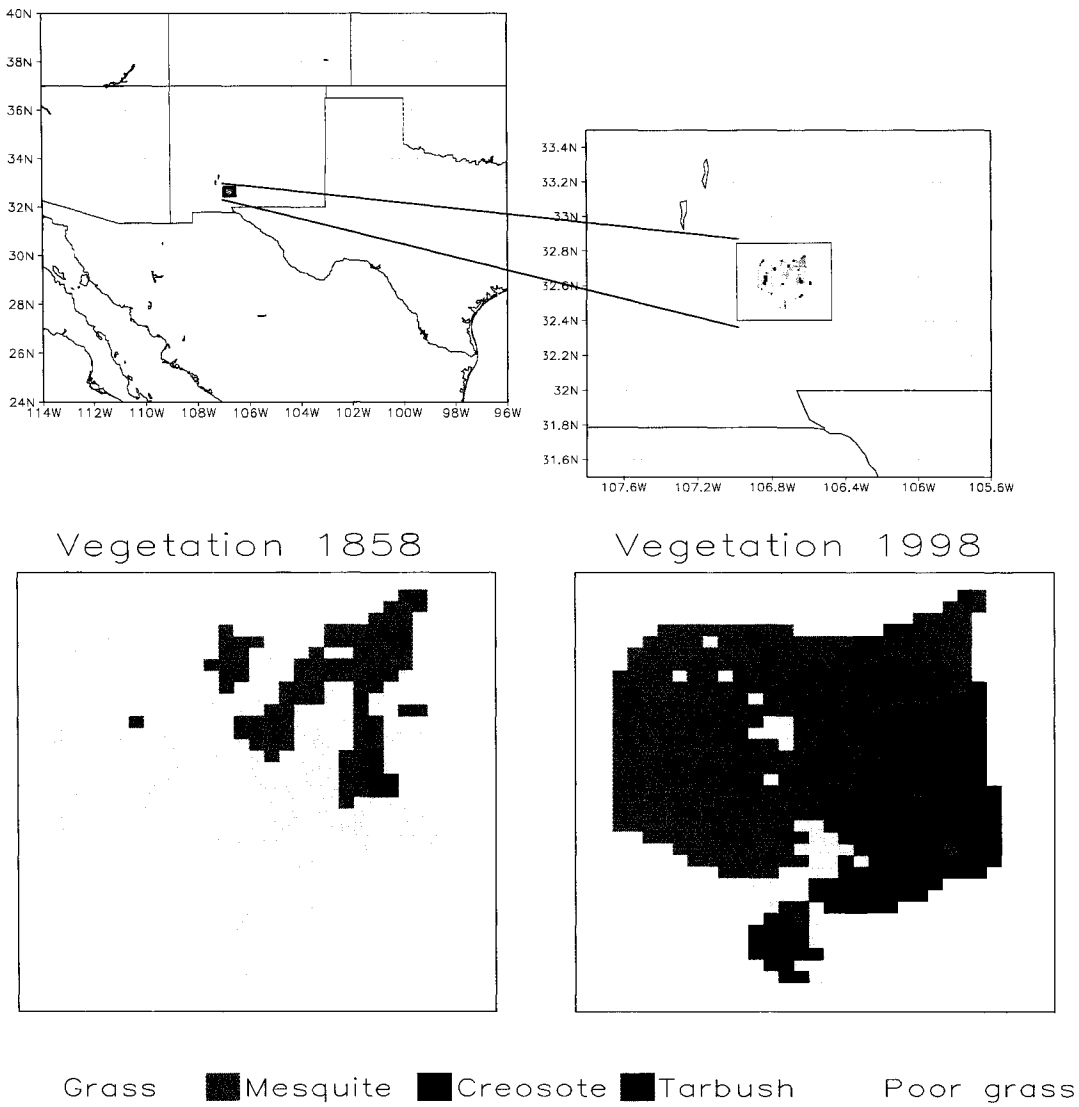

Figure 4.1. Location of the Jornada Long Term Experimental Range site, the GEMRAMS model domain for the simulations (top), and the vegetation distribution in 1858 and 1998 (bottom). Each grid cell is 1 × 1 km.

Reproduced with permission of the copyright owner. Further reproduction prohibited without permission.

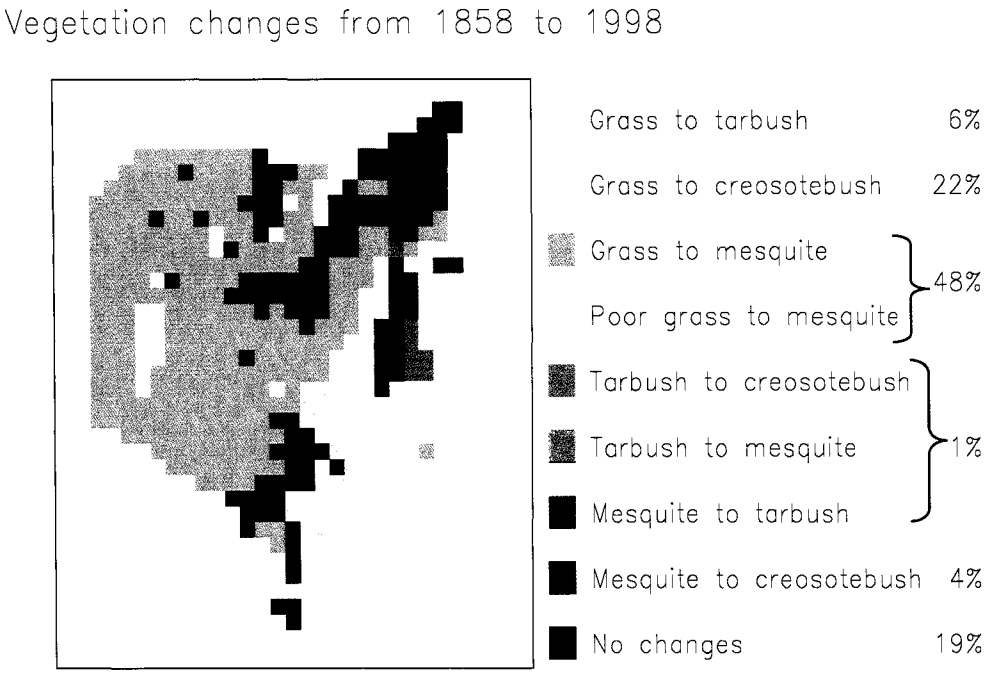

Figure 4.2. Vegetation changes occurred between 1858 and 1998 at the Jornada Long Term Experimental Range. The fraction of grid cells with the corresponding vegetation change is shown on the right.

Structural changes of the land surface have occurred as a result of this shift in plant dominance with potential effects on climate with feedbacks to the vegetation. Surface and vegetation characteristics affected by this shift include albedo, leaf area, roughness length, and root biomass distribution (Gibbens et al. 1996; Asner and Heidebrecht 2005). These changes can potentially alter surface latent and sensible heat fluxes with feedbacks to the biophysical variables (Pitman 2003). A positive feedback is illustrated by the impact of albedo on precipitation. An increase in albedo could decrease precipitation through its effect on the surface fluxes, which leads to declines in soil moisture, therefore eventually increasing the albedo, reducing the net radiation, that could decrease sensible and/or latent heat, leading to a decrease in clouds, with further

Reproduced with permission of the copyright owner. Further reproduction prohibited without permission.

reductions in precipitation. This land-cover/atmospheric feedback is proposed as one of the processes that can explain desertification dynamics (Charney 1975; Schlesinger et al. 1990; Peters et al. 2004).

Several observational and modeling studies have found different effects of grass or herbaceous reduction in cover (i.e., overgrazing, drought) on near-surface fluxes and temperature. One set of studies (e.g., Otterman 1974, 1989; Charney 1975; Charney et al. 1977) showed that higher albedo in response to vegetation removal led to less available energy to heat the atmosphere, thus producing cooler temperatures. Another set of studies, along the Mexico-U.S. border in the Sonoran Desert, also showed a 5% higher albedo on the overgrazed Mexican side relative to the adjacent vegetated area in Arizona (Balling 1988; Bryant et al. 1990). However, the low vegetation cover on the Mexican side, with 29% more bare soil than in Arizona, increased latent heat flux (i.e., soil evaporation and transpiration) for the first few days after a rain event. After a few days, transpiration in the more heavily vegetated area on the U.S. side drew on remaining subsurface infiltrated rainfall, and the vegetated area had a greater latent heat flux. Initially, the less vegetated side had cooler surface temperatures and about the same air temperatures than the more vegetated side. However, after the initial period, the air temperatures on the U.S. side were markedly cooler (Warner 2004). This contrasting behavior in fluxes and temperature with respect to the increase in albedo can be attributed to differences in soil moisture content, vegetation cover, and roughness length between the two studies.

Semiarid areas are characterized by very low soil water conditions, except following precipitation events (Noy-Meir 1973). Those events are usually of short

Reproduced with permission of the copyright owner. Further reproduction prohibited without permission.

duration, and generally only shallow soil layers are affected. An above-average winter precipitation can result in a deep soil wetting scenario. Soil moisture conditions can greatly influence surface fluxes, changing the way available energy (i.e., sensible plus latent heat) is partitioned, potentially affecting near-surface temperature and humidity (Small and Kurc 2003).

Due to the highly complex interactions between plants, soils, and atmosphere, observational studies provide a contemporary and limited view of the myriad of land-atmosphere interactions occurring in these semiarid ecosystems. Fully coupled atmospheric-biospheric models constitute a powerful tool for addressing the effect of historical vegetation changes on the near-surface atmosphere. With these models, plants and atmosphere are nonlinearly interacting with each other.

The objective of this study was to examine the effects of historical vegetation changes that have occurred on the Jornada Experimental Range on surface latent and sensible heat fluxes and the resultant near-surface temperature and humidity using a coupled plant and atmospheric model. A set of experimental simulations with GEMRAMS, referred to as the control runs, were carried out using the 1858 and 1998 vegetation cover with identical initial atmospheric conditions. Additionally, sensitivity tests to soil moisture initial conditions and to mesquite cover were performed to evaluate their effects on the partition of available energy and to test assumptions about the role of albedo on model results.

Reproduced with permission of the copyright owner. Further reproduction prohibited without permission.

4.2. Model Configuration

The experiments were set up with one grid, centered on the Jornada Experimental Range (JER) site (32°37' N, 106°44'W), New Mexico, U.S.A. with 50 × 50 grid points and a horizontal grid increment of 1 km (Figure 4.1). There are 60 vertical levels that extend to about 23 km above the ground, and 12 soil layers, down to a depth of 4 m. The vertical grid spacing varies from 80 m near the surface to 800 m at the top of the domain. The time step for the model integration is 10 seconds. In this case, the simulations are set up with the following options: no precipitation processes are active, only condensation is allowed; Mellor and Yamada (1982) parameterization for vertical diffusion; modified Smagorinsky (1963) scheme for horizontal diffusion; lateral boundary conditions according to Klemp and Wilhelmson (1978); for top boundary conditions, a Raleigh friction layer was specified on the top 20 grid points; radiation scheme according to Chen and Cotton (1983).

Land-cover data for the domain were obtained from vegetation maps for 1858 and 1998 based on Gibbens et al. (2005) for the Jornada Experimental Range (Figure 4.1) (Peters, unpublished data). For the purpose of these simulations, the different species of grass and shrubs were grouped into four vegetation classes based on the dominant species: black grama grass (dominated by *Bouteloua eriopoda*), mesquite (*Prosopis glandulosa*), creosotebush (*Larrea tridentata*), and tarbush (*Fluorensia cernua*) classes. For the 1858 vegetation map, yucca (*Yucca elata*) and other shrub-free cells were grouped into poor grass. Parameters values derived for each vegetation type were assigned to each group based on observed data (Table 4.1). Initial conditions for GEMRAMS also included root distributions for each vegetation type (Figure 4.3), based

Reproduced with permission of the copyright owner. Further reproduction prohibited without permission.

on published and unpublished data (H. Johnson and R.P. Gibbens, personal communication; Moorhead et al. 1989).

Vegetation types	LAI (m^2 m^{-2})		Vegetation cover (%)		Albedo		Roughness length (m)	Displacement height (m)
	May	Aug	May	Aug	May	Aug		
Grass	0.8	0.8	25.1	41.8	0.25	0.21	0.018	0.120
Poor grass	0.3	0.3	15.0	15.0	0.27	0.27	0.018	0.120
Mesquite	1.1	0.9	16.8	22.5	0.34	0.35	0.060	0.467
Creosotebush	1.6	0.9	36.5	37.5	0.24	0.28	0.060	0.760
Tarbush	1.4	0.8	28.7	32.4	0.22	0.24	0.050	0.433

Table 4.1. Parameter values for the vegetation types.

The USDA soil texture class was assigned to each grid cell according to vegetation-soil texture associations: grass and mesquite were associated with loamy sand and tarbush, and creosotebush with silt loam and sandy loam, respectively. Values from Cosby et al. (1984) were used for the soil thermal and hydrological parameters.

Initial atmospheric conditions are given by horizontally homogeneous vertical profiles of temperature, relative humidity and wind speed, derived from NCEP reanalysis (Kalnay et al. 1996), for two days (May 23rd and August 25th, 2002). These two days were considered as typical mid-spring and late-fall clear and sunny days. The initial time is 12 UTC and the simulation lasted 20 hours.

4.3. Experimental Design

In order to examine the effects of vegetation change on near-surface atmospheric conditions, and the sensitivity of model results to soil moisture and mesquite cover, pairs

Reproduced with permission of the copyright owner. Further reproduction prohibited without permission.

of simulations were performed using the two dates as initial atmospheric conditions. Within a given pair, one run used 1858 vegetation distribution and the other used 1998 vegetation. The "control" experiments (CTRL) used average initial soil moisture conditions based on neutron probe measurements of volumetric soil moisture content (Snyder et al. 2005) (Figure 4.3).

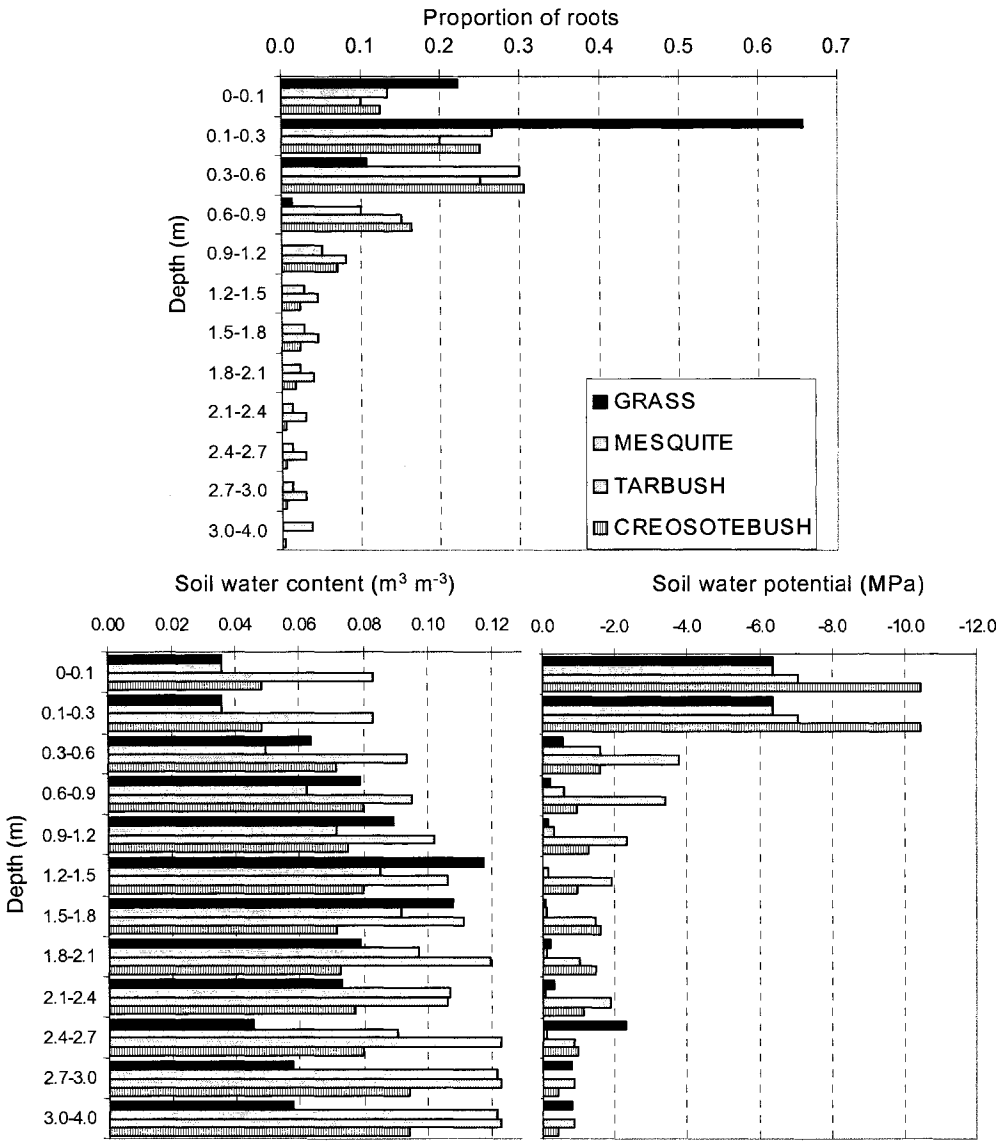

Figure 4.3. Top: root profile for the vegetation types considered in this study. Bottom: initial soil water content (m^3 m^{-3}) (left) and soil water potential (MPa) (right)

Reproduced with permission of the copyright owner. Further reproduction prohibited without permission.

Sensitivity tests to initial soil moisture initial conditions were conducted using four different soil moisture profiles. A "dry" condition (DRY) used an initial soil moisture profile that was 20% drier than the control run conditions throughout the whole profile. The DRY sensitivity experiments could represent the system several days after a precipitation event. For the "wet" condition (WET), the top 90 cm was 20% wetter than the control run, and the rest of the layers had the same soil moisture values as the control run. Two additional "wet" numerical experiments were performed. In a "wetter" simulation, the top 90 cm initial soil moisture conditions were increased by 50% with respect to the control run (WETT_sfc). In a second "wetter" simulation, soil water content of the entire profile (4 m) was increased by 50% with respect to the control run (WETT_all). A typical summertime precipitation event would be the situation associated with the WET and WETT_sfc experiments. These summertime events are usually of short duration and generally wet only the top-most soil layers. A wet winter condition is represented by the WETT_all experiments where wetting occurs in deep soil layers during longer duration winter precipitation events.

Additionally, a set of sensitivity experiments explored the mesquite cover within grid cells. For these simulations, the mesquite cover was 25%, 50%, 75%, 125%, and 150% of the cover (25cov, 50cov, 75cov, 125cov and 150cov in Figure 4.11) assumed in the CTRL simulations (Table 4.1).

4.4. Results from Control Simulation

Overall, lower values of latent heat (LH) than sensible heat (SH) were the result of the combined effect of low soil moisture content, low leaf area index (LAI) and low

Reproduced with permission of the copyright owner. Further reproduction prohibited without permission.

vegetation cover (Tables 4.1 and 4.2). LH is composed of the heat required by physical evaporation (e.g., from soils and from leaf surfaces) and transpiration through the stoma of leaves, while SH is the transfer of heat directly by temperature. LH and SH are expressed in units of Watts per meter squared. Evaporation and transpiration rates in mm day^{-1} can be obtained as the ratio between LH and the latent heat of vaporization of water (λ = 2.454 MJ kg^{-1} at 20°C). Bowen ratio values (β=SH/LH), computed from the diurnal area averages, ranged from 3.0 to 4.3 (Table 4.2). These values are within the typical Bowen ratio range of 3 to 6 for a semiarid area (Oke 1993). In our control simulations, more than 65% of the LH flux corresponded to soil evaporation. This value is higher than those observed by Dugas et al. (1996) and Schlesinger et al. (1987), which ranged between 30% and 60%. However, Reynolds et al. (2000), in a modeling study, found that evaporation from soil represented 66% of the annual LH flux, which ranged between 40% and 99% over their 100 yr simulation.

		Diurnal Average		1300 LST	
	Year	May 3rd	Aug 25th	May 3rd	Aug 25th
SH		194	158	333	300
LH	1858	48	37	70	50
β		4.0	4.3		
SH		201	153	342	292
LH	1998	54	51	78	69
β		3.7	3.0		

Table 4.2. Diurnal and 1300 LST area-averaged values of sensible (SH) and latent (LH) heat (W m^{-2}) for the CTRL case for August 25th and May 3rd experiments. The Bowen ratio (β) was computed based on the diurnal area-averaged values of SH and LH.

Reproduced with permission of the copyright owner. Further reproduction prohibited without permission.

The diurnal area-averaged SH and LH were slightly higher in May than in August (Table 4.2), but their spatial patterns were similar in both runs (Figures 4.4 and 4.5). SH flux was greatest in creosotebush and lowest in mesquite mainly due to differences in albedo. The lowest values of LH corresponded to grass and creosotebush, depending on the day, and the highest value was found in tarbush. Higher values of soil moisture in tarbush may be responsible for the differences in LH. Variability in LH was higher than in SH among vegetation types. Figures 4.4 and 4.5 also show the averaged SH and LH values at 1300 LST. Our simulated values of SH and LH are within the range of measured values reported by Dugas et al. (1996), Rango et al. (1998) and Prueger et al. (2004) for a variety of JER sites, and smaller than the SH+LH values observed by Small and Kurc (2003) for the Sevilleta National Wildlife Refuge in central New Mexico.

The shift between the two different 1858 and 1998 vegetation scenarios, with their associated soils and distinctive structural and physiological vegetation characteristics, resulted in changes in near-surface fluxes, temperature and humidity. When averaged over the grid cells in the JER domain, LH increased from 1858 to 1998 for both days (Table 4.2). This means that more water is being added to the atmosphere through evaporation and transpiration processes. However, the area-averaged SH slightly increased in May and decreased in August. Relative to 1858, changes in LH were more important than changes in SH. The diurnal area-averaged LH flux increased 13% and 38% for May and August, respectively. Conversely, the relative changes in SH were -4% and 3% for May and August, respectively. This led to an overall change in how the energy is partitioned between LH and SH in the area, as it is evident in the decrease of Bowen ratio from 1858 to 1998 (Table 4.2). The decrease in Bowen ratio indicates that,

Reproduced with permission of the copyright owner. Further reproduction prohibited without permission.

over the domain, relatively more heat is now being used in transpiration and evaporation than in heating the atmosphere, with a cooling effect associated with both processes. This suggests that, as a result of the vegetation change, the near-surface atmosphere of the area would be cooler and wetter in 1998 than in 1858.

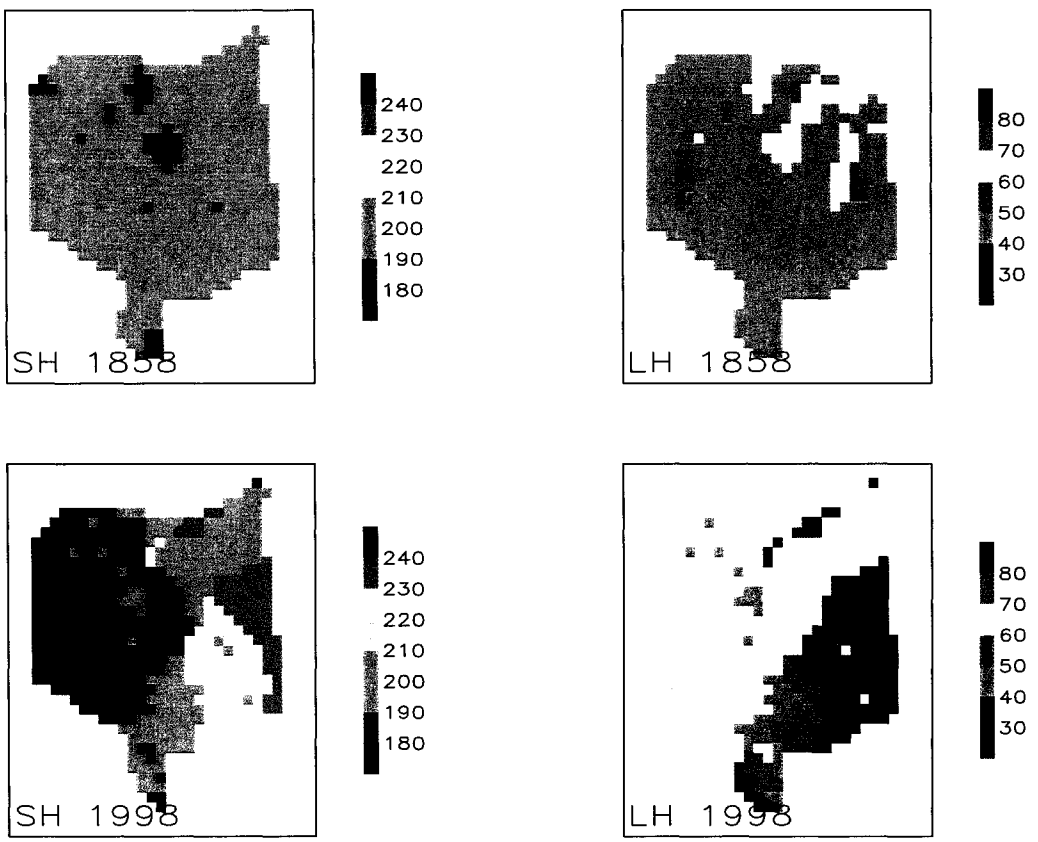

	SH	LH
Grass	331	62
Mesquite	324	90
Cresosotebush	387	45
Tarbush	331	111

Figure 4.4. Diurnal mean of sensible (SH) and latent (LH) heat fluxes for 1858 (top) and 1998 (bottom) conditions for the CTRL May experiment. Values at the bottom are the average for each group of vegetation at 1300 LST. Values are in W m^{-2}.

Reproduced with permission of the copyright owner. Further reproduction prohibited without permission.

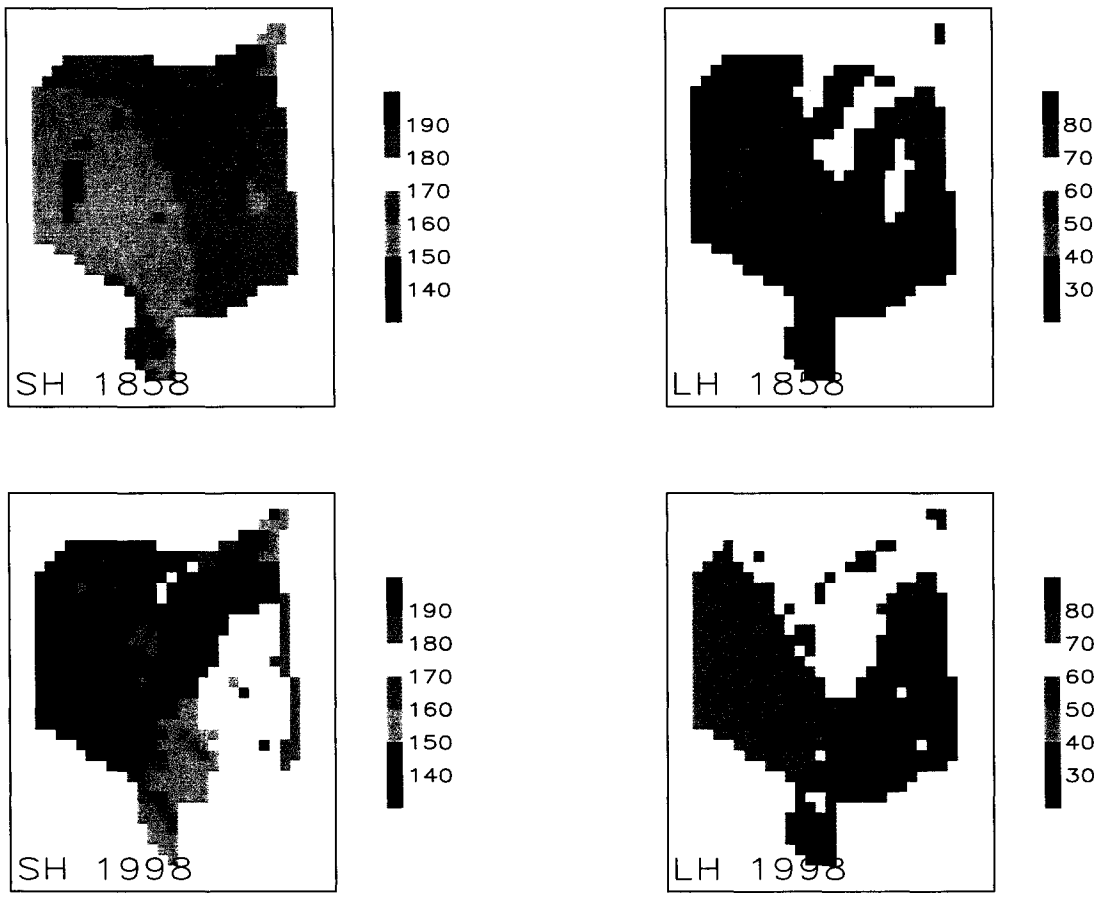

	SH	LH
Grass	303	42
Mesquite	271	75
Cresosotebush	333	47

Figure 4.5. Diurnal mean of sensible (SH) and latent (LH) heat fluxes for 1858 (top) and 1998 (bottom) conditions for the CTRL August experiment. Values at the bottom are the average for each group of vegetation at 1300 LST. Values are in W m^{-2}.

Reproduced with permission of the copyright owner. Further reproduction prohibited without permission.

Examination only of area-averaged values of changes in the fluxes could be misleading because spatial differences in surface fluxes between 1858 and 1998 are noticeable. This spatial variation can be visually assessed comparing the maps in Figures 4.4 and 4.5, but more pronounced differences appear at approximately 1300 LST (Figure 4.6). The spatial variability is explained by different biophysical and physiological characteristics of the vegetation. Grid cells exhibiting similar vegetation changes (Figure 4.2) were grouped and differences in the average fluxes between 1858 and 1998 were calculated (Table 4.3).

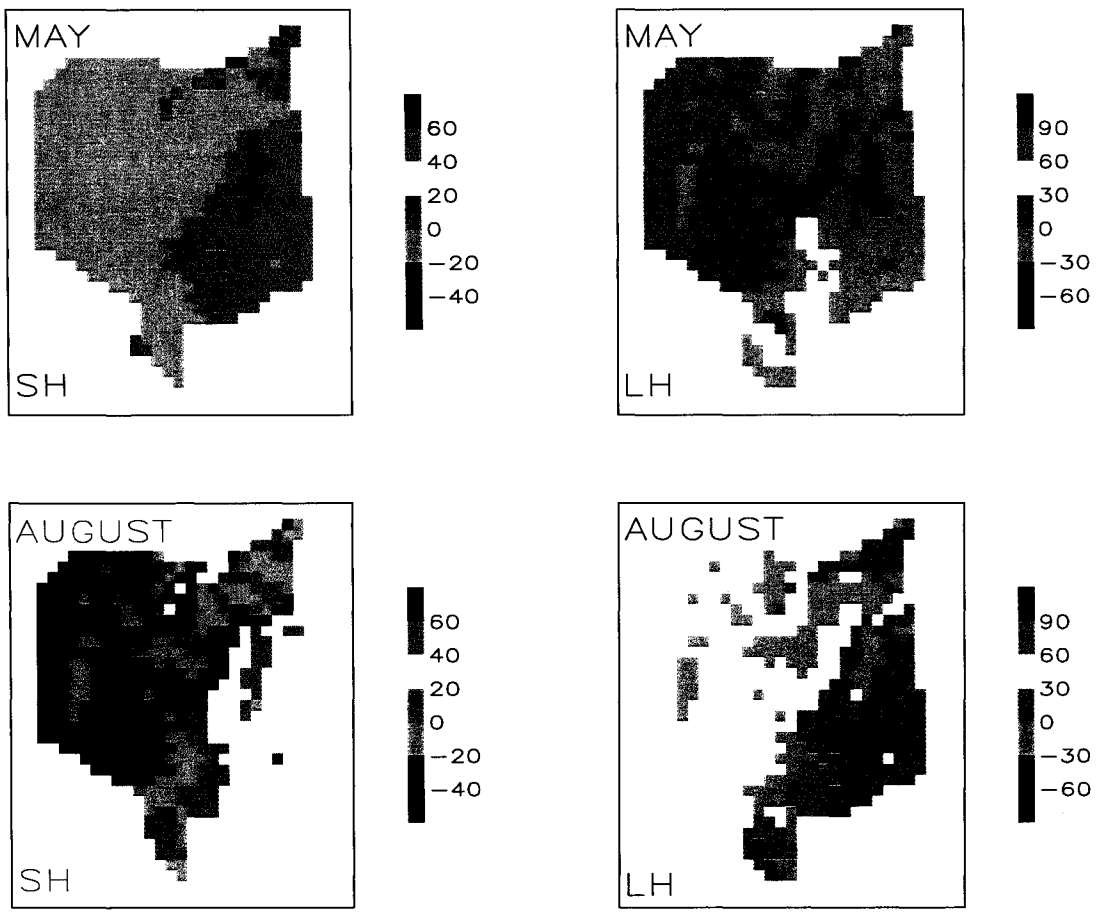

Figure 4.6. Differences in sensible (SH) and latent (LH) heat fluxes between 1998 and 1858 at 1300 LST for CTRL May (top) and August (bottom) runs. Values are in W m^{-2}.

Reproduced with permission of the copyright owner. Further reproduction prohibited without permission.

Two main patterns can be recognized (Figure 4.6). First, SH decreased and LH increased (Table 4.3) on the west side of the domain, where a conversion from grass to mesquite occurred. The higher average albedo of the mesquite area relative to grasses reduced the available energy. The simulated increase in LH flux was mainly due to an increase in transpiration (not shown) associated with the deeper root profile in mesquite than in the grasses; the available energy is being dissipated mainly as LH, so sensible heat flux decreased. Second, on the east side of the domain, SH clearly increased and LH decreased or increased depending on the type of the vegetation conversion and the simulated day. LH decreased in the areas that converted from mesquite to creosotebush, mainly due to a decrease in transpiration (not shown). Volumetric soil moisture contents were slightly higher in creosotebush, but due to the sandy-loam soil texture, the corresponding soil water potentials of creosotebush were much lower than mesquite (Figure 4.3) and transpiration was limited in creosotebush. Increase in SH may be attributed to a decrease in albedo.

Changes in the latent heat flux were subtle in the grass to creosotebush conversion area on the east side. Furthermore, the direction of change differed between May and August (Table 4.3 and Figure 4.6). The very small decrease in LH in both months was due to a decrease in evaporation (not shown), that may be associated with the combined effects of increased vegetation cover and soil texture change, similar to the mesquite to creosotebush conversion (Figure 4.3). Higher SH may be associated with an increase in the roughness length (from 0.018 to 0.060 m) and displacement height (0.12 to 0.76 m) because changes in albedo were not so noticeable (Pitman 2003).

Reproduced with permission of the copyright owner. Further reproduction prohibited without permission.

In the small area that changed from grass to tarbush, there was a slight variation in SH, but the increase in LH was the largest among all the vegetation conversions (Table 4.3). In this case, physical evaporation increased more than transpiration, due to higher soil water content.

Changes in near-surface fluxes modified near-surface air temperature and humidity (Figure 4.7). The near-surface atmosphere tended to be cooler and more humid with shrub-dominated vegetation than with the historic grass-dominated vegetation. The diurnal average (right) are shown in each figure. Area-averaged differences are small (Figure 4.7) but, like the modeled changes in surface fluxes, they are spatially heterogeneous. The analysis of the 2 m temperature at 1300 LST (computed using similarity theory) showed warmer temperatures (up to 0.8°C) on the east side of the domain and cooler temperatures (up to -0.6°C) on the west side of the domain (Figure 4.7), consistent with an increase and decrease respectively of sensible heat flux (see Figure 4.6 and Table 4.3). Temperatures decreased when grasses were converted to mesquite or tarbush. Conversely, temperatures increased when either grass or mesquite was replaced with creosotebush (see also Figure 4.10). At the first model vertical level (approximately 40 m) differences become smaller and influenced by the background flow, but the spatial pattern remains. Changes in vapor mixing ratio and relative humidity are less noticeable. Nevertheless, an increase and decrease in humidity are found on the west and east side of the domain, respectively associated with the corresponding changes in the latent heat flux (Figures 4.6 and 4.7).

Reproduced with permission of the copyright owner. Further reproduction prohibited without permission.

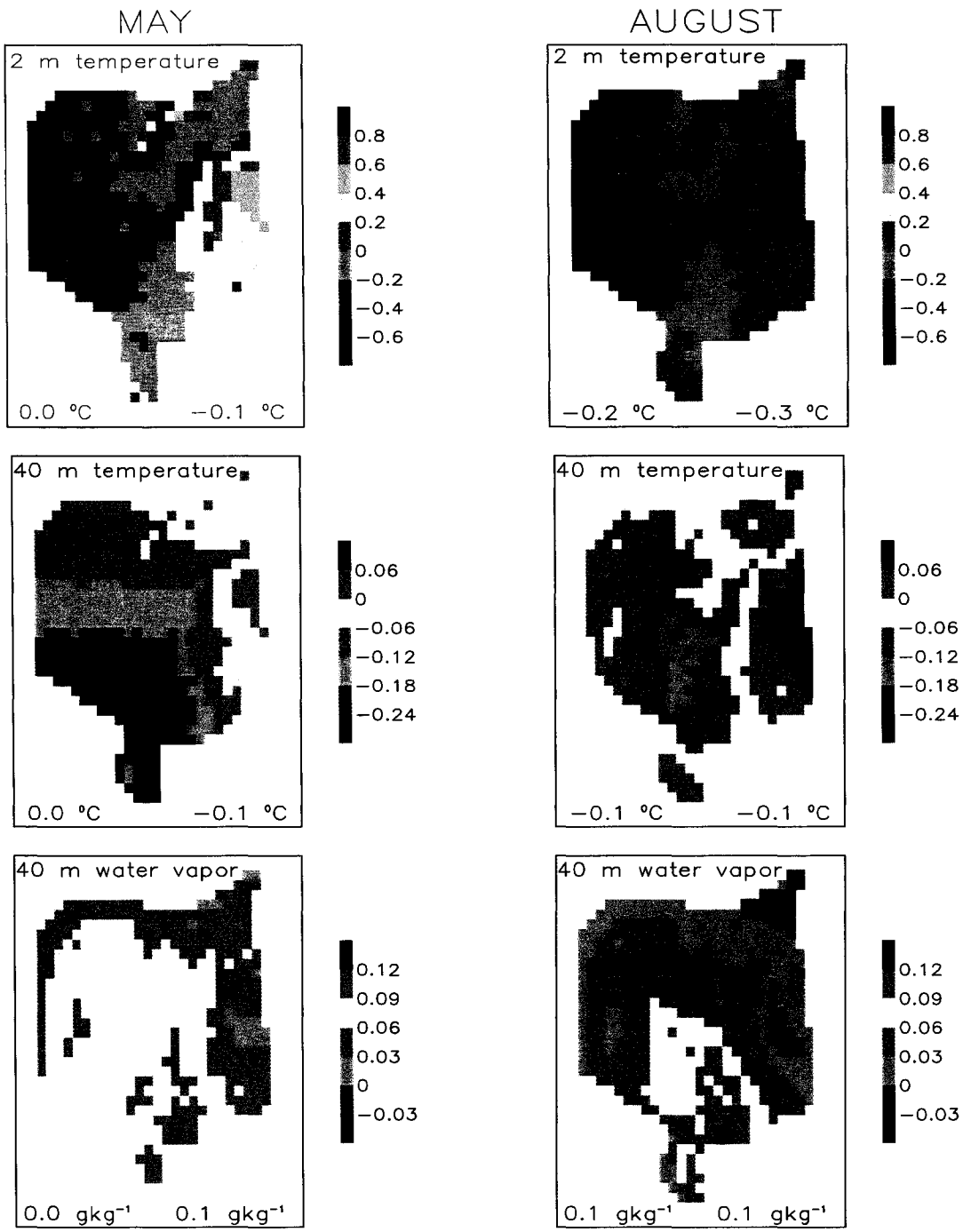

Figure 4.7. Differences between 1858 and 1998 at 1300 LST for: 2 m temperature (°C) (top); first model level temperature (°C) (middle); water vapor mixing ratio (g kg^{-1}) (bottom). The area-averaged differences at 1300 LST (left) and the diurnal-averaged (right) are shown in each figure.

Reproduced with permission of the copyright owner. Further reproduction prohibited without permission.

	SH		LH	
	May	Aug	May	Aug
Grass to mesquite	↓ -10 (-3)	↓ -33 (-11)	↑ 26 (40)	↑ 32 (77)
Grass to creosotebush	↑ 50 (15)	↑ 23 (8)	↓ -18 (29)	↑ 3 (7)
Grass to tarbush	≈ 0 (0)	↑ ≈ 1 (0)	↑ 47 (73)	↑ 87 (200)
Mesquite to creosotebush	↑ 61 (19)	↑ 58 (21)	↓ -47 (-51)	↓ -29 (-38)

Table 4.3. Changes (1998-1858) in sensible heat (SH) and latent heat (LH) at 1300 LST for the CTRL case for August 25th and May 3rd experiments for the main vegetation changes (values are in W m^{-2}). The changes in sensible and latent fluxes (%) between 1998 and 1858, relative to1858 are shown in parentheses.

In our simulations, conversion of grasses to shrubs produced a heterogeneous response in fluxes and temperature. Changes in sensible heat fluxes from 1858 to 1998 are largely due to changes in albedo: increases in albedo led to a decrease in SH. Our results agree with the findings of Otterman (1974). Roughness length and displacement height are additional factors that may explain the increase in SH in the cells that converted from grass to creosotebush, where changes in albedo were not large. Isolating the factors affecting the changes in LH can be more complex because of the two different processes involved, transpiration and evaporation. In our simulations, changes in LH from 1858 to 1998 can be attributed to changes in rooting depth, different physiological response to soil water content, changes in soil texture, and changes in soil moisture. Nevertheless, the changes in LH were relatively higher than in SH. Changes in sensible and latent heat fluxes acted in the same direction to affect the near-surface temperature: lower (higher) SH and higher (lower) LH produced cooler (warmer) temperatures.

Reproduced with permission of the copyright owner. Further reproduction prohibited without permission.

4.5. Sensitivity to Soil Moisture Initial Conditions

In semiarid areas, soil moisture content can have a strong effect on the surface fluxes, and in available energy partitioning (Small and Kurc 2003). Initial soil moisture conditions strongly affected the surface fluxes, temperature, and humidity. Sensitivity to soil water content simulations showed that SH and LH were respectively higher and lower than the CTRL case in the DRY experiment, not only on an area-averaged basis (Table 4.4) but also for each of the vegetation conversions (Figure 4.8). Increasing initial soil moisture (WET and WETT experiments) decreased SH and increased LH with respect to the control run. In all experiments, relative changes in latent heat were higher than in sensible heat. A 50% increase in initial soil moisture conditions in the first 90 cm (WETT_sfc) led to a maximum 104% change in LH but only a 16% change in SH, with respect to the CTRL run (Table 4.4). When more water was also available in the deeper soil layers (below 90 cm, WETT_all experiments) LH increased up to 135%.

	MAY				AUGUST			
	SH		LH		SH		LH	
	58	98	58	98	58	98	58	98
DRY	7	18	-5	-20	11	9	-1	-18
CTRL	**333**	**342**	**70**	**78**	**300**	**292**	**50**	**69**
WET	-11	-12	0	16	-12	-12	1	16
WETT_sfc	-20	-55	13	75	-18	-41	15	72
WETT_all	-20	-56	14	81	-18	-42	21	93

Table 4.4. Differences in sensible heat (SH) and latent heat (LH) between the soil moisture sensitivity experiments (WETT_all, WETT_sfc, WET and DRY) and the CTRL run. The values in bold, for the CTRL run, are the actual area-averaged values at 1300 LST of SH and LH. All values are in W m^{-2}.

Reproduced with permission of the copyright owner. Further reproduction prohibited without permission.

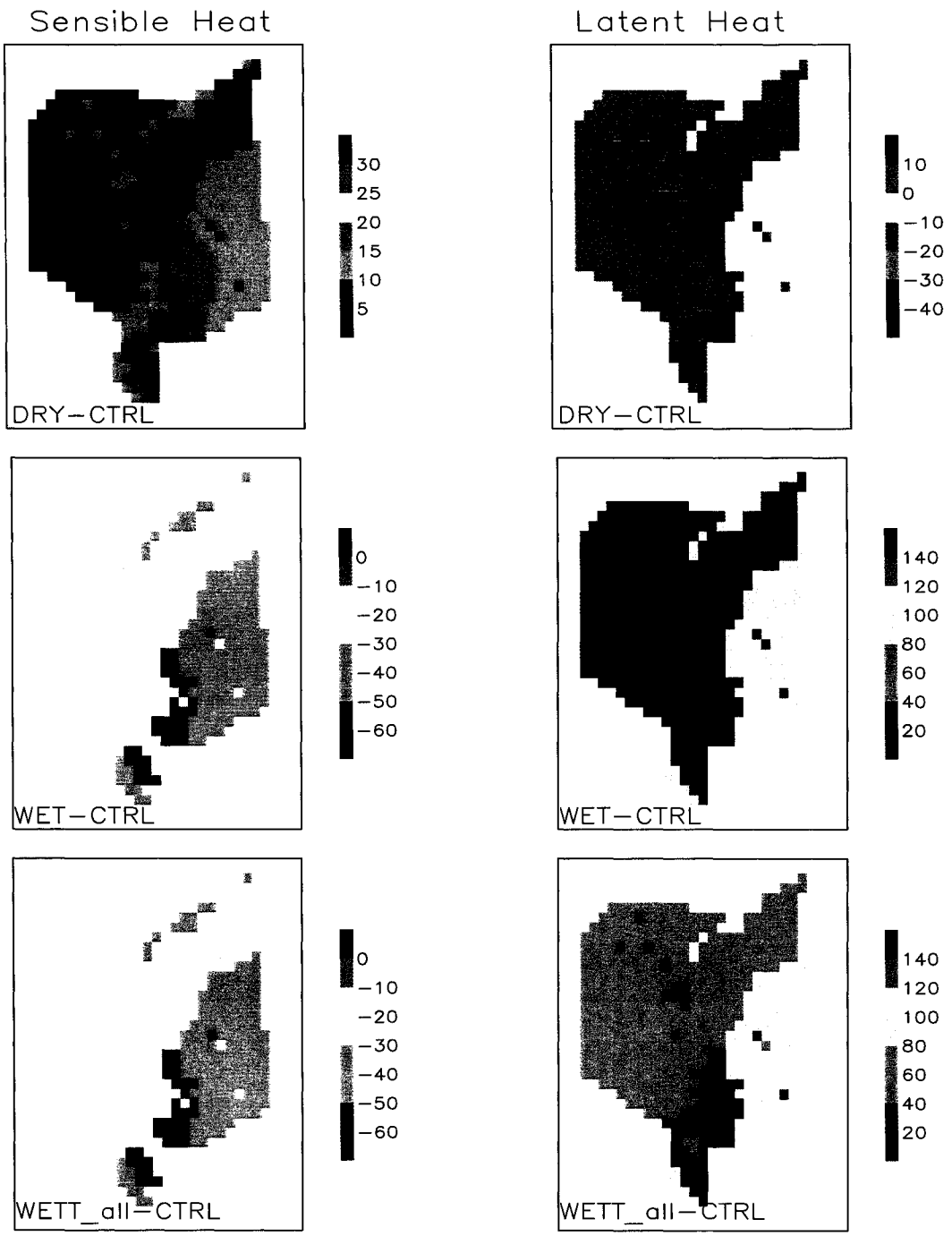

Figure 4.8. Differences of the diurnal-averaged sensible and latent heat for August run, between each sensitivity experiment and the 1998 control run (CTRL) for DRY (top); WET (middle), and WETT_all (bottom), for sensible heat (left) and latent heat (right). Values are in W m^{-2}.

Reproduced with permission of the copyright owner. Further reproduction prohibited without permission.

Changes in LH were mostly a consequence of changes in soil evaporation (not shown), but the contribution of transpiration to LH increased with the initial water content. Although in the WETT_sfc experiment LH increase for grasses was lower than for mesquite (not shown), transpiration for grasses was more responsive than transpiration for mesquite. Increasing deep soil water content slightly increased transpiration and LH (Figure 4.8) in all shrubs.

The differential behavior of grasses and shrubs in response to changes in soil moisture had an effect on the differences in sensible and latent heat fluxes between 1858 and 1998 (Figure 4.9). Dry conditions tended to enhance the differences in SH flux: the area-average differences increase and decrease more than the CTRL run in May and August, respectively (Table 4.5 and Figure 4.9). On the other hand, differences in LH changed sign or were attenuated: latent heat decreased between 1858 and 1998 in the May run, and only increased by 2 W m^{-2} in the August run. The opposite behavior was true as the initial soil moisture conditions increased: LH increased and SH decreased mostly over the entire study area (Figure 4.9 and Table 4.5). In particular, for all the cells converted from grass to shrubs, both transpiration and evaporation contributed to the increase in LH.

Reproduced with permission of the copyright owner. Further reproduction prohibited without permission.

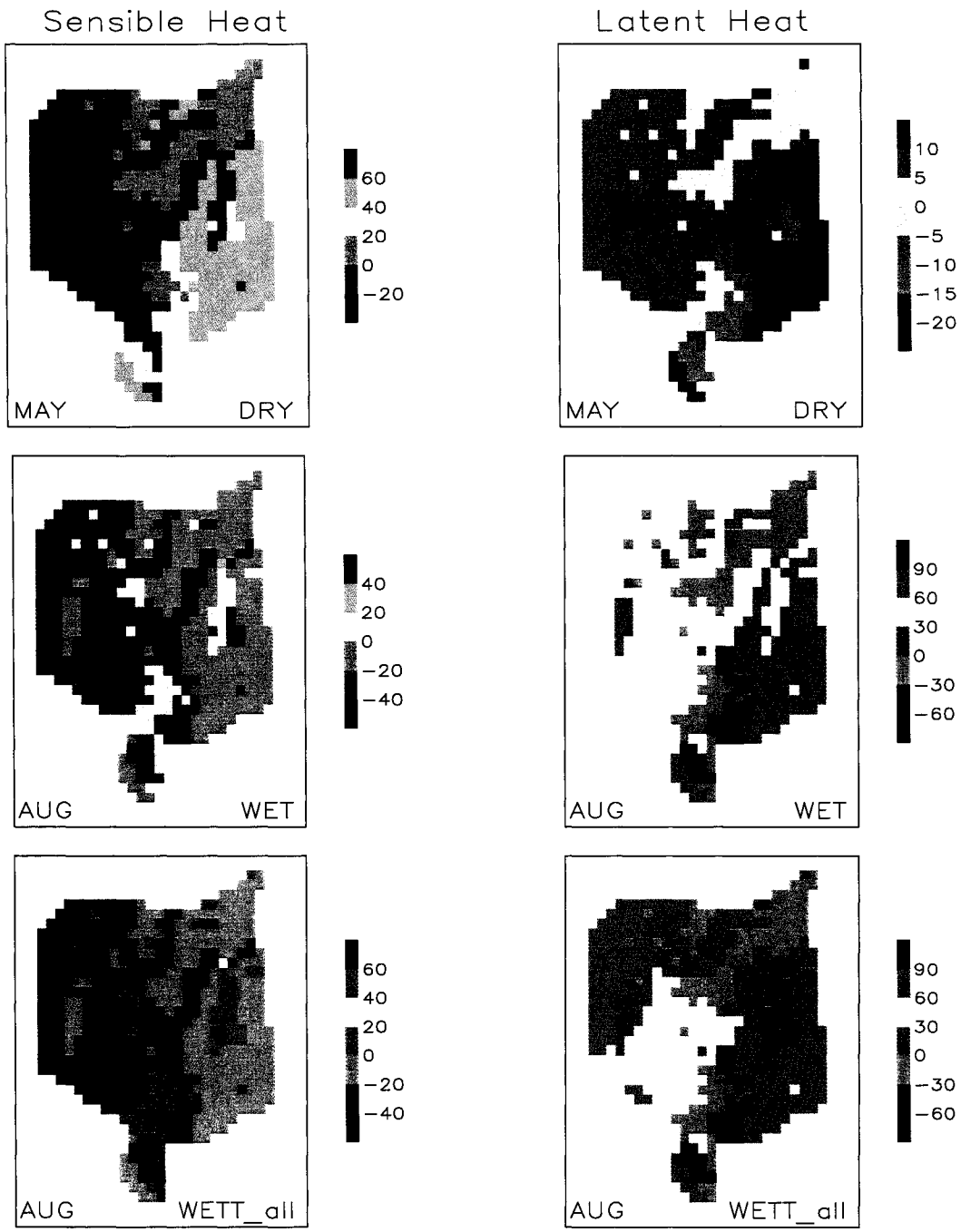

Figure 4.9. Differences in diurnal-averaged sensible heat (left) and latent heat (right) between 1998 and 1858 for the sensitivity experiments: May DRY (top), August WET (middle), and August WETT_all (bottom). Values are in W m^{-2}.

Reproduced with permission of the copyright owner. Further reproduction prohibited without permission.

	MAY		AUG	
	SH	LH	SH	LH
DRY	20 (3)	-7 (-11)	-10 (-3)	2 (4)
CTRL	9 (6)	8 (11)	-8 (-3)	19 (38)
WET	8 (3)	24 (34)	-8 (-3)	34 (67)
WETT_sfc	-26 (-8)	70 (84)	-31 (-11)	76 (117)
WETT_all	-27 (-9)	75 (89)	-32 (-11)	91 (128)

Table 4.5. Differences between 1998 and 1858 area-averaged sensible heat (SH) and latent heat (LH) at 1300 LST for the soil moisture sensitivity experiments, WETT_all, WETT_sfc, WET and DRY, and the CTRL run (values are in Wm^{-2}). The changes in sensible and latent fluxes (%) between 1998 and 1858, relative to 1858 are shown in parenthesis.

The effect of these changes in the 2 m temperatures is shown in Figure 4.10 for the main vegetation conversion. Consistent with the flux trends, as the soil becomes wetter, the differences become larger, i.e., more negative, for the areas converted from grass to shrubs. On the other hand, differences in temperature become smaller, or less positive, for the area converted from mesquite to creosotebush. The response is non-linear in the case of grass to mesquite conversion. As the initial soil water conditions decrease, the temperature differences in this case are similar or become more negative depending on the day.

Reproduced with permission of the copyright owner. Further reproduction prohibited without permission.

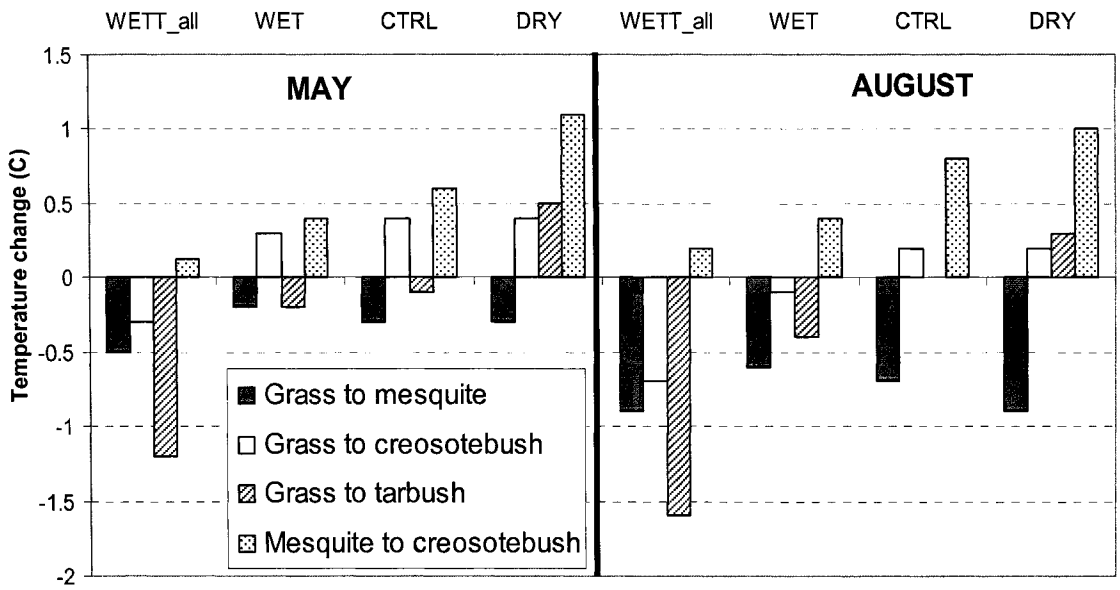

Figure 4.10. Differences in 2 m temperature between 1998 and 1858 at 1300 LST averaged for the main four vegetation conversion types for the soil moisture sensitivity experiments (WETT_all, WET, and DRY) and the control run (CTRL), for May and August.

4.6. Sensitivity to Changes in Mesquite Cover

One of the proposed mechanisms of increased temperature in overgrazed areas is that the low vegetation cover reduces the latent heat, and as a result, ground and air temperature increase. We found that varying the amount of ground cover by mesquite mainly affected albedo. As the percentage of soil covered by mesquite decreased (e.g., more bare soil) the absolute changes in albedo between 1858 and 1998 became larger. Then, in the areas that changed from grass to mesquite, where albedo increased from 1858 to 1998, the albedo increased more, up to 50% in the August run, leading to an enhanced reduction in SH and in temperature (Figure 4.11). On the other hand, in the few

Reproduced with permission of the copyright owner. Further reproduction prohibited without permission.

grid cells that changed from mesquite to creosotebush (where albedo decreased) SH and temperature increased. From 1858 to 1998, cooling in the grid cells that changed from grass to mesquite became larger, while the opposite in the mesquite to creosotebush conversion (Figure 4.11). The differences in temperature between 1858 and 1998 decreased as the percentage of area covered by mesquite increased.

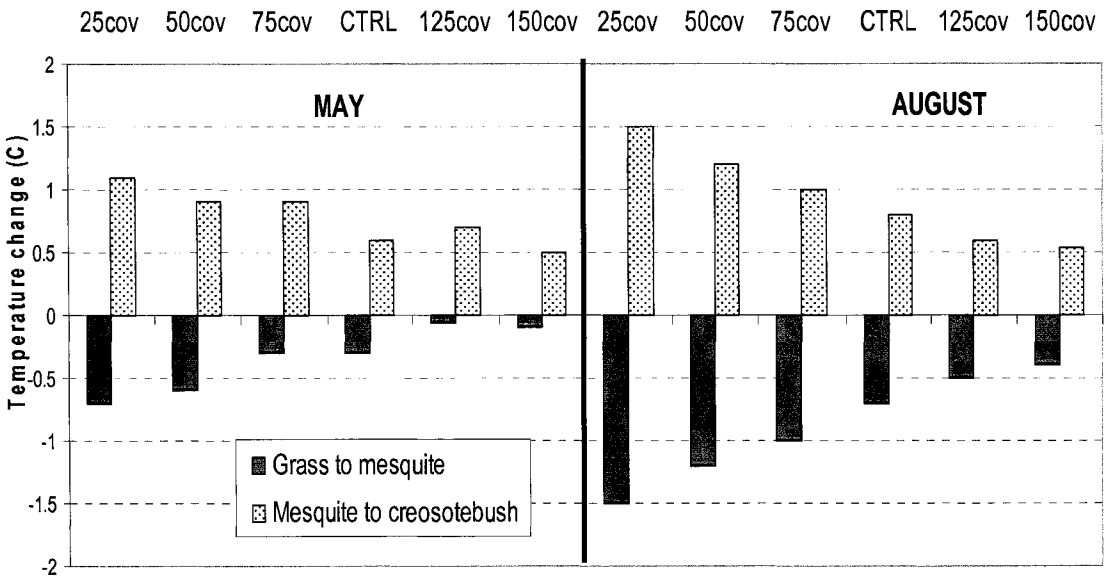

Figure 4.11. Differences in 2 m temperature between 1998 and 1858 at 1300 LST averaged for the main four vegetation conversion types for the mesquite vegetation cover (25cov, 50cov, 75cov, 125cov, 150cov) sensitivity experiments and the control run (CTRL) for May and August.

Reproduced with permission of the copyright owner. Further reproduction prohibited without permission.

In several studies of desertification effects (e.g., Charney et al. 1977; Otterman 1989), a complete removal of the vegetation, with bare soil or desert-like landcover is assumed. Shrub encroachment increased the percentage of bare soil, but the soil was still covered by some percentage of vegetation (Table 4.1). In these one-day simulations, increased albedo as a result of changes in vegetation cover was the dominant factor controlling fluxes and temperature. Drier conditions in the soil than the one assumed here, where evaporation was suppressed, could possibly reverse the effect, although we found a dissimilar response to the decrease in soil moisture.

Reproduced with permission of the copyright owner. Further reproduction prohibited without permission.

Chapter 5

SUMMARY, CONCLUSIONS, AND SUGGESTIONS FOR FUTURE WORK

5.1. Summary and Conclusions

A coupled atmospheric-vegetation model, GEMRAMS, is used to examine how the observed changes in vegetation could potentially affect the near-surface energy balance, temperature, and humidity. At a regional and seasonal scale, several spring-early summer simulations were carried out on a southern South America domain. Land-cover scenarios representing current, natural, and afforestation conditions were implemented for this region and used to simulate the impacts of the land-cover changes on the near-surface atmosphere. At a local and diurnal scale, GEMRAMS was used to evaluate the effects of an observed change in vegetation in the northern Chihuahuan Desert from grasslands in the mid-1800s to shrublands in the late 1900's. Main conclusions drawn from this work are as follows:

- RAMS was able to simulate well the observed monthly temperature and precipitation over southern South America. Sensitivity to lateral boundary conditions was explored for RAMS using NCEP and ECMWF reanalysis (ERA-40) as atmospheric forcing. A cold bias was observed with ERA-40 and a warm bias with NCEP reanalysis. In both cases, precipitation tended to match the precipitation from each of the reanalysis. A weak internal nudging was needed to be applied, forcing the simulation to the corresponding reanalysis at the large

Reproduced with permission of the copyright owner. Further reproduction prohibited without permission.

scale. For the configuration used in these simulations, ERA-40 gave a better performance, in particular for precipitation.

- Results for GEMRAMS simulations of precipitation and temperature were very similar to those of RAMS. LAI, the additional variable prognosed by GEMRAMS, also compared fairly well with some ground-based observations and NDVI-derived LAI. Temporal evolution was also well represented.
- Changes in near-surface fluxes and temperature due to land-cover changes depended on the type of vegetation conversion and the season. Warmer temperatures were found in the conversion from wooded grasslands or forest to agriculture. Afforestation and conversion from grass to agriculture led to a cooler and wetter near-surface atmosphere. Afforestation also led to changes in precipitation, of up to 40% from the control experiment. LAI and albedo were the major players in these sensitivity experiments.
- Additional simulations with a double CO_2 concentration (i.e., 720 ppm) were also performed to assess the relative contributions of the land-cover and doubled CO_2 forcing to meteorological and biological variables. An increase of CO_2 levels might mitigate or enhance the temperature changes between "natural" and current vegetation, depending on the type of vegetation involved in the changes. The impacts were mostly limited to the areas of the land-cover changes, although some remote areas were also affected.
- RAMS and GEMRAMS resulted in a useful tool in the study of the climate in the southern South America region. Although the Kain-Fritsch scheme improved the convective precipitation, there is still work to be done to better represent

Reproduced with permission of the copyright owner. Further reproduction prohibited without permission.

precipitation process for seasonal long simulations, especially in regions with steep topography.

- For the Jornada Experimental Range experiment, the simulations showed that the change from an 1858 environment, dominated by grasses, to a 1998 area mostly covered by shrubs, led to an overall decrease of sensible heat and a pronounced increase of latent heat. Overall, this simulated shift in the energy partition resulted in a cooler and moister lower atmosphere, which would be expected to alter vegetation species competition over a longer time period.
- Through all the experiments performed for this semiarid area, the impacts of shrub encroachment on surface fluxes and temperature was spatially heterogeneous and associated with physical and physiological characteristics of the soils and vegetation: conversion from grass to mesquite cools the near-surface atmosphere and conversion from grass to creosotebush warms it. Albedo changes induced by land-cover modifications played a major role in near-surface atmospheric processes.
- Sensitivity simulations to initial soil moisture conditions showed that latent heat fluxes responded more than sensible heat fluxes to an increase in soil moisture content. Under wet conditions, cooler temperatures were found in the 1998 shrub-dominated area than in the 1858 grass-dominated area. Under initially dry conditions, a warmer eastern domain was simulated, except for the grid cells converted from grass to mesquite, where temperatures were still cooler over grass.

Reproduced with permission of the copyright owner. Further reproduction prohibited without permission.

- Sensitivity experiments to percentage of mesquite cover showed that albedo was the parameter mostly affected. The net effect was an enhancement in the differences in temperature between 1858 and 1998 with respect to the ones found in the control run.

The shift from grasslands to shrublands, increased in agricultural practices and potential afforestation led to complex interactions between biophysical and physiological characteristics of the land and surface fluxes. These results clearly demonstrate that vegetation itself is a weather and climate variable as it significantly influences temperature and humidity, which then feedbacks and affects the vegetation. This view supports the broader view of climate that is reported in the National Academy of Sciences report (NRC, 2005).

5.2 Suggestions for Future Work

In order to asses how the land atmosphere feedbacks behaves in a seasonal timeframe for these semiarid areas, the next step is to extend these one-day long simulations to the whole growing season (i.e. March to October) and also to different years.

Specification of soil moisture conditions may have a significant impact on convective precipitation in regional climate modeling simulations (e.g., Fennessey and Shukla 1999; Pielke et al. 1999; Dirmeyer 2000). An anomalously dry/wet area may persist for several weeks affecting the atmosphere during that period. Additional simulations need to be performed to address the model sensitivity to initial soil moisture conditions

Reproduced with permission of the copyright owner. Further reproduction prohibited without permission.

To better assess potential afforestation effects on hydrological variables, for instance precipitation, a better description of the water table or deep water processes is needed. Then, incorporation of a more complete ground water model would be beneficial (Maxwell and Miller 2005).

Some questions still remain. Are land-use changes that have occurred in the Pampas a potential factor influencing the observed trends in temperature in central Argentina? Multiyear simulations, with a set of "historical" land-cover datasets and a smaller grid size might be needed to study the impacts of anthropogenic land-cover change on observed trends of atmospheric variables.

How much are these simulations affected by the land-surface LEAF2-GEMTM? A variety of regional atmospheric models coupled with different land-surface schemes could be applied to the southern South America domain. For example, RAMS-Sib2, coupled with the plant growth submodel of GEMTM, could be used.

What about other semiarid areas, with observed LULC changes? The same modeling approach carried out in Jornada will be used in the SGS LTER site, which includes a detailed vegetation and soils maps and parameters associated to each vegetation type, like albedo, and soil characteristics. Some of those data will be measured in the fields while others will be put together from different sources and earlier measurements of CO_2 and water and energy fluxes carried out at the SGS.

Reproduced with permission of the copyright owner. Further reproduction prohibited without permission.

REFERENCES

Aceituno, P., 1988: On the functioning of the Southern Oscillation in South America, Part I: Surface Climate. *Mon. Wea. Rev.*, **116**, 505-524.

Amthor, J. S., 1989: *Respiration and crop productivity*. Springer-Verlag, 215 pp.

Arora, V.K., 2002: Modeling vegetation as a dynamic component in soil-vegetation-atmosphere-transfer schemes and hydrological models. *Rev. Geophys.*, **40,** 1006, doi:10.1029/2001RG000103.

Asner, G.P., and K.B. Heidebrecht, 2005: Desertification alters regional ecosystem-climate interactions. *Global Change Bio.,* **11**, 182-194.

Asner, G.P., C.E. Borghi, and R. Ojeda, 2003: Desertification in central Argentina: Changes in ecosystem carbon and nitrogen from imaging spectroscopy. *Ecol. Appl.,* **13**, 629 648.

Baidya Roy, S., and R. Avissar, 2002: Impact of land use/land cover change on regional hydrometeorology in Amazonia. *J. Geophys. Res.*, **107**, doi:10.1029/ 2000JD000266.

Ball, J.T., I.E. Woodrow, and J.A. Berry, 1987: A model predicting stomatal conductance and its contribution to the control of photosynthesis under different environmental conditions. *Progress in Photosynthesis Research,* J. Biggins, Ed., Martinus Nijhof Publishers, IV, 221-224.

Reproduced with permission of the copyright owner. Further reproduction prohibited without permission.

Balling, J.R, 1988: The climatic impact of a Sonoran vegetation discontinuity. *Clim. Change,* **13**, 99-109.

Barros, V.R., M.E. Castañeda, and M.E. Doyle, 2000: Recent precipitation trends in southern South America east of the Andes: An indication of climatic variability. *Southern Hemisphere Paleo- and Neoclimates,* P.P. Smolka and W. Volkheimer, Eds., Springer-Verlag, 187-206.

Bazzaz, F.A., 1990: The response of natural ecosystems to the rising global CO_2 levels. *Annu. Rev. Ecol. Sys.*, **21**, 167-196.

Berbery, E.H., and E.A. Collini, 2000: Springtime precipitation and water vapor flux over southeastern South America. *Mon. Wea. Rev.*, **128**, 1328-1346.

Betts, R.A., P.M. Cox, S.E. Lee, and F.I. Woodward, 1997: Contrasting physiological and structural vegetation feedbacks in climate change simulations. *Nature*, **387**, 796-799.

Bonan, G.B., 1997: Effects of land use on the climate of the United States. *Clim. Change*, **37,** 449-486.

Boote, K.J. and R.S. Loomis, 1991: *Modelling photosynthesis - from biochemistry to canopy*. Crop Science Society of America, Inc., American Society of Agronomy, Inc., 140 pp.

Reproduced with permission of the copyright owner. Further reproduction prohibited without permission.

Bounoua, L., G.J. Collatz, P.J. Sellers, D.A. Randall, D.A. Dazlich, S.O. Los, J. Berry, I. Fung, C.J. Tucker, C. Field, and T. Jensen, 1999: Interactions between vegetation and climate: Radiative and physiological effects of doubled atmospheric CO_2. *J. Climate*, **12**, 309-324.

Bounoua, L., G.J. Collatz, S.O. Los, P.J. Sellers, D.A. Dazlich, C.J. Tucker, and D.A. Randall, 2000: Sensitivity of climate to changes in NDVI. *J. Climate*, **13**, 2278-2292.

Bounoua, L., R.S. DeFries, and G.J. Collatz, 2002: Effects of land cover conversion on surface climate. *Clim. Change*, **52,** 29-64.

Brakenridge, G.R., E. Anderson, and S. Caquard, 2003: Flood Inundation Map DFO 2003-282, Dartmouth Flood Observatory, Hanover, USA. [Available online at: http://www.dartmouth.edu/~floods/2003282.html.]

Bryant, N.A., L.F. Johnson, A.J. Brazel, R.C. Balling, C.F. Hutchinson, and L.R. Beck, 1990: Measuring the effect of overgrazing in the Sonoran Desert. *Clim. Change*, **17**, 243-264.

Buermann, W., J. Dong, X. Zeng, R.B. Myneni, and R.E. Dickinson, 2001: Evaluation of the utility of satellite-based vegetation leaf area index data for climate simulations. *J. Climate*, **14**, 3536-3550.

Buermann, W., Y. Wang, J. Dong, L. Zhou, X. Zeng, R.E. Dickinson, C.S. Potter, and R.B. Myneni, 2002: Analysis of a multiyear global vegetation leaf area index data set. *J. Geophys. Res.*, **107,** 4646, doi:10.1029/2001JD000975.

Buffington, L.C., and C.H. Herbel, 1965: Vegetational changes on a semidesert grassland range from 1853 to 1963. *Ecol. Monographs*, **35**, 139-164.

Reproduced with permission of the copyright owner. Further reproduction prohibited without permission.

Cabrera, A.L., and A. Willink, 1980: *Biogeografía de América Latina.* 2nd ed. Secretaría General de la Organización de los Estados Americanos, Programa Regional de Desarrollo Científico y Tecnológico, 122 pp.

Calderini, D.F., M.F. Dreccer, and G.A. Slafer, 1997: Consequences of plant breeding on biomass growth, radiation interception and radiation use efficiency in wheat. *Field Crops Res.,* **52,** 271–281.

Camillioni, I., and V. Barros, 2000: The Paraná River response to El Niño 1982 – 83 and 1997 – 98 Events. *J. Hydrometeor.,* **1,** 412–430.

Cárcova, J., G.A. Maddonni, and C.M. Ghersa, 2000: Long-term cropping effects on maize: Crop evapotranspiration and grain yield. *Agron. J.,* **92,** 1256-1265.

Castañeda, E., and V. Barros, 1994: Las tendencias de la precipitatión en el cono Sur de America al este de los Andes. *Meteorologica,* **19,** 23-32.

Castro, C.L., W.Y.Y. Cheng, A.B. Beltrán, R.A. Pielke Sr., and W.R. Cotton, 2002: The incorporation of the Kain-Fritsch cumulus parameterization scheme in RAMS with a terrain-adjusted trigger function. *Fifth RAMS users and related applications workshop*. Santorini, Greece. ATMET Inc.

Castro, C.L., R.A. Pielke Sr., and G. Leoncini, 2005: Dynamical downscaling: assessment of value retained and added using the Regional Atmospheric Modeling System (RAMS). *J. Geophys. Res.,* **110**, D05108, doi:10.1029/2004JDD004721.

Ceballos, A., K. Scipal, W. Wagner, and J. Martinez-Fernandez, 2005: Validation and downscaling of ERS Scatterometer derived soil moisture data over the central part of the Duero Basin, Spain. *Hydrol. Processes*, **19**, 1549-1566.

Reproduced with permission of the copyright owner. Further reproduction prohibited without permission.

Charney, J.G., 1975. Dynamics of deserts and droughts in the Sahel. *Quart. J. Roy. Meteor. Soc.*, **101**, 193-202.

Charney, J.G, W.J. Quirk, S. Chow, and J. Kornfield, 1977: A comparative study of the effects of albedo change on drought in semi-arid regions. *J. Atmos. Sci.,* **34**, 1366-1385.

Chase, T.N., R.A. Pielke, Sr., T.G.F. Kittel, M. Zhao, A.J. Pitman, S.W. Running, and R.R. Nemani, 2001: The relative climatic effects of landcover change and elevated carbon dioxide combined with aerosols: A comparison of model results and observations. *J. Geophys. Res.*, **106**, 31,685 -31,691.

Chen, C., and W.R. Cotton, 1983: A one-dimensional simulation of the stratocumuluscapped mixed layer. *Bound.- Layer Meteor.*, **25**, 298-321.

Chen, D-X., and M.B. Coughenour, 1994: GEMTM: A general model for energy and mass transfer of land surfaces and its application at the FIFE sites. *Agric. Forest Meteorol.*, **68**, 145-171.

_____, 2004: Photosynthesis, transpiration, and primary productivity: scaling up from leaves to canopies and regions using process models and remotely sensed data. *Global Biogeochem. Cycles*, **18**, GB4033, doi:10.1029/2002GB001979.

Chen, D-X., M.B. Coughenour, A.K. Knapp, and C.E. Owensby, 1994: Mathematical simulation of C_4 grass photosynthesis in ambient and elevated CO_2. *Ecol. Modelling,* **73**, 63-80.

Chen, D-X., H.W. Hunt, and J.A. Morgan, 1996: Responses of a C_3 and C_4 perennial grass to CO_2 enrichment and climate change: comparison between model predictions and experimental data. *Ecol. Modelling*, **87**, 11-27.

Reproduced with permission of the copyright owner. Further reproduction prohibited without permission.

Chen, M., P. Xie, J.E. Janowiak, and P.A. Arkin, 2002: Global land precipitation: A 50-yr monthly analysis based on gauge observations. *J. Hydrometeor.*, **3**, 249-266.

Chou, S.C., A.M.B. Nunes, and I.F.A. Cavalcanti, 2000: Extended range forecasts over South America using the regional Eta model. *J. Geophys. Res.*, **105,** 10147-10160.

Chou, S.C., C.A.S. Tanajura, Y. Xue, and C.A. Nobre, 2002: Validation of the coupled Eta/SSiB model over South America. *J. Geophys. Res.*, **107,** 8088, doi:10.1029/2000JD000270.

Collison, P., and R.C. Tabony, 1984: The estimation of mean temperatures from daily maxima and minima. *Meteor. Magazine*, **113**, 329-337.

Cosby, B.J., G.M. Hornberger, R.B. Clapp, and T.R. Ginn, 1984: A statistical exploration of the relationships of soil moisture characteristics to the physical properties of soils. *Water Resour. Res.*, **20**, 682-690.

Cotton, W.R., J.F. Weaver, and B.A. Beitler, 1995: An unusual summertime downslope wind event in Fort Collins, Colorado on 3 July 1993. *Wea. Forecasting*, **10**, 786-797.

Cotton, W.R., R.A. Pielke Sr., R.L. Walko, G.E. Liston, C. Tremback, H. Jiang, R.L. McAnelly, J.Y. Harrington, M.E. Nicholls, G.G. Carrio, and J.P. McFadden, 2003: RAMS 2001: current status and future directions. *Meteor. Atmos. Phys.*, 82, 5-29.

Coughenour, M.B., 1984: A mechanistic simulation analysis of water use, leaf angles and grazing in East African graminoids. *Ecol. Modelling.,* **26**, 203-230.

Curtis, P.S., and X. Wang, 1998: A meta-analysis of elevated CO_2 effects on woody plant mass, form, and physiology. *Oecologia*, **113**, 299-313.

Reproduced with permission of the copyright owner. Further reproduction prohibited without permission.

De Pury, D.G.G., and G.D. Farquhar, 1997: Simple scaling of photosynthesis from leaves to canopies without the errors of big-leaf models. *Plant Cell Environ.*, **20**, 537-557.

Dickinson, R.E., A. Henderson-Sellers, and P. Kennedy, 1993: Biosphere-atmosphere transfer scheme (BATS) version 1e as coupled to the NCAR community climate model. Technical Report NCAR/TN-387+STR, NCAR Boulder, Colorado, 99 pp.

Dickinson. R.E., M. Shaikh, R. Bryant, and L. Graumlich, 1998: Interactive canopies for a climate model. *J. Climate*, **11**, 2823-2836.

Dirmeyer, P.A., 2000: Using a global soil wetness data set to improve seasonal climate simulation. *J. Climate*, **13**, 2900-2922.

Drake, B.G., M.A. Gonzales-Meler, and S.P. Long, 1997: More efficient plants: A consequence of rising atmospheric CO_2? *Ann. Rev. Plant Physiol. Plant Molec. Biol.*, **48**, 607-637.

Dugas, W.A., R.A. Hicks, and R.P. Gibbens, 1996: Structure and function of C_3 and C_4 Chihuahuan Desert plant communities. Energy balance components. *J. Arid Environ.*, **34**, 63-79.

Eastman, J.L., 1999: Analysis of the effects of CO_2 and landscape change using a coupled plant and meteorological model. Ph.D. Dissertation, Department of Atmospheric Science, Colorado State University, 148 pp.

Eastman, J.L., M.B. Coughenour, and R.A. Pielke Sr., 2001a: The regional effects of CO_2 and landscape change using a coupled plant and meteorological model. *Global Change Biol.*, **7**, 797-815.

Eastman, J.L., M.B. Coughenour, and R.A. Pielke Sr., 2001b: Does grazing affect

Reproduced with permission of the copyright owner. Further reproduction prohibited without permission.

climate? *J. Hydrometeor.*, **2**, 243-253.

Engel, V., E.G. Jobbágy, M. Stieglitz, M. Williams, and R.B. Jackson, 2005: The hydrological consequences of Eucalyptus afforestation in the Argentine Pampas. *Water Resour. Res.*, **41**, W10409, doi:10.1029/2004WR003761.

FAO, 1998: FAO yearbook production. FAO Statistics. Rome. Series N° 148. 142 pp.

FAO, 2001a: Global Forest Resources Assessment 2000. FAO Forestry Paper 140. Rome, Food and Agriculture Organization. [Available online at: http://www.fao.org/forestry/fo/fra/].

FAO, 2001b: State of the World's Forests 2001. Rome, Food and Agriculture Organization. [Available online at: http://www.fao.org/forestry/FO/SOFO/SOFO2001/publ-e.stm.]

Farley, K.A., E.G. Jobbágy, and R.B. Jackson, 2005: Effects of afforestation on water yield: a global synthesis with implications for policy. *Global Change Biol.*, **11,** 1565-1576.

Farquhar, G.D., S. von Caemmerer, and J.A. Berry, 1980: A biochemical model of photosynthetic CO_2 assimilation in leaves of C_3 species. *Planta,* **149**, 78-90.

Fennessy, M.J., and J. Shukla, 1999: Impact of initial soil wetness on seasonal atmospheric prediction. *J. Climate*, **12**, 3167-3180.

Field, C.B., R.B. Jackson, and H.A. Mooney, 1995: Stomatal responses to increased CO_2: implications from the plant to the global scale. *Plant Cell Environ.,* **18,** 1214-1225.

Figueroa, N., P. Satyamurty, and P.L. Silva Dias, 1995: Simulations of the summer circulation over the South American region using an Eta coordinate model. *J.*

Reproduced with permission of the copyright owner. Further reproduction prohibited without permission.

Atmos. Sci., **52,** 1573-1584.

Foley, J.A., R. DeFries, G.P. Asner, C. Barford, G. Bonan, S.R. Carpenter, F.S. Chapin, M.T. Coe, G.C. Daily, H.K. Gibbs, J.H. Helkowski, T. Holloway, E.A. Howard, C.J. Kucharik, C. Monfreda, J.A. Patz, I.C. Prentice, N. Ramankutty, and P.K. Snyder, 2005: Global Consequences of land use. *Science*, **309,** 570-574.

Frechilla S., L.D. Talbott, and E. Zeiger, 2002: The CO_2 response of *Vicia* cells acclimates to growth environment. *J. Exp. Bot.,* **53,** 1-6.

Gardiol, J.M, L.A. Serio, and A.I. Della Maggiora, 2003: Modelling evapotranspiration of corn (*Zea mays*) under different plant densities. *J. Hydrol.*, **271**, 188-196.

Gibbens, R.P., R.F. Beck, R.P. McNeely, and C.H. Herbel, 1992: Recent rates of mesquite establishment in the northern Chihuahuan Desert. *J. Range Mgt.*, **45**, 585-588.

Gibbens, R.P, R.A. Hicks, and W.A. Dugas, 1996: Structure and function of C_3 and C_4 Chihuahuan Desert plant communities. Standing crop and leaf area index. *J. Arid Environ.*, **34**, 47-62.

Gibbens, R.P, R.P. McNeely, K.M. Havstad, R.F. Beck, and B. Nolen, 2005: Vegetation changes in the Jornada Basin from 1858 to 1998. *J. Arid Environ.*, **61**, 651-668.

Gomez, S.E., and N.I. Toresani, 2001: Las Pampas. *Wetlands of South America. An agenda for Biodiversity Conservation and Policies Development.* P. Canevari, I. Davidson, D. E. Blanco, G. Castro, and E.H. Bucher, Eds., Wetlands International, Annex II, Chapter 12,. [Available online at: http://www.wetlands.org/inventory&/SAA/Intro/_INDEX@.htm.]

Goudriaan, J., 1977: *Crop micrometeorology: A simulation study.* Pudoc, 249 pp.

Reproduced with permission of the copyright owner. Further reproduction prohibited without permission.

Grimm, A., V. Barros, and M. Doyle, 2000: Climate variability in southern South America associated with El Niño and La Niña events. *J. Climate*, **13,** 35-58.

Grossi Gallegos, H., 1998: Distribución de la radiación solar global en la República Argentina. II. Cartas de radiación. *Energías Renovables y Medio Ambiente*, **5,** 33-42.

Grossi Gallegos, H., G. Atienza, and M. García, 1987: Cartas de radiación solar global para la región meridional de América del Sur. *Anales del II Congreso Interamericano de Meteorología*, Buenos Aires, Argentina, 16.3.1-16.3.10.

Grover, H.D., and H.B. Musick, 1990: Shrubland encroachment in Southern New Mexico, U.S.A.: An analysis of desertification processes in the American Southwest. *Clim. Change*, **17**, 305-330.

Guerschman, J.P., and J.M. Paruelo, 2005: Agricultural impacts on ecosystem functioning in temperate areas of North and South America. *Global Planetary Change*, **47,** 170-180.

Guerschman, J.P, J.M. Paruelo, and I.C. Burke, 2003: Land use impacts on the normalized difference vegetation index in temperate Argentina. *Ecol. Applications*, **13**, 616-628.

Gunderson, C.A., and S.D. Wullschleger, 1994: Photosynthetic acclimation of forest trees to a doubling of atmospheric CO_2: A broader perspective. *Photosynth. Res.*, **39**, 369-388.

Hall, A.J., C.M. Rebella, C.M. Ghersa, and J. Ph. Culot, 1992: Field-crop systems of the pampas. *Field Crop Ecosystems*. C.J. Pearson, Ed., Ecosystems of the World, Vol. 19. Elsevier, 413-450.

Reproduced with permission of the copyright owner. Further reproduction prohibited without permission.

Hahmann, A.N., and R.E. Dickinson, 1997: RCCM2-BATS Model over Tropical South America: Applications to Tropical Deforestation. *J. Climate*, **10,** 1944-1964.

Herrick, J., and R. Thomas, 2001: No photosynthetic acclimation in sweetgum trees (*Liquidambar styraciflua* L.) after three years of CO_2 enrichment at the Duke Forest FACE experiment. *Plant Cell Environ.,* **24,** 53-64.

Herzer, H., M.G. Caputo, and A. Celis, 2004: Gestión de riesgo de desastre ENSO en América Latina: una propuesta para la consolidación de una red regional de investigación comparativa, información y capacitación desde una perspectiva social. Informe final. Argentina. CENTRO Estudios Sociales y Ambientales. [Available at: http://www.cambioglobal.org/enso/informes/anho4/Argentina/index.html].

Hodnett, M.G., L. Pimentel da Silva, H.R. da Rocha, and R. Cruz Senna, 1995: Seasonal soil water storage changes beneath central Amazonian rainforest and pasture. *J. Hydrol.,* **170**, 233–254.

Hoffmann, J.A.J., S.E. Nuñez, and W.M. Vargas, 1997: Temperature, humidity and precipitation variations in Argentina and the adjacent sub-Antarctic region during the present century. *Meteorologische Zeitschrift*, **6,** 3-11.

Hoffmann, W.A., and R.B. Jackson, 2000: Vegetation-climate feedbacks in the conversion of Tropical Savanna to Grassland. *J. Climate*, **13,** 1593-1602.

Horel, J.D., J.B. Pechman, A.N. Hahman, and J.E. Geisler, 1994: Simulation of the Amazon basin circulation with a regional model. *J. Climate*, **7,** 56-71.

Houghton, J.T., Y. Ding, D.J. Griggs, M. Noguer, P.J. Van Der Linden, X. Dai, K. Maskell, and C.A. Johnson, 2001: *Climate change 2001: The scientific basis.*

Reproduced with permission of the copyright owner. Further reproduction prohibited without permission.

Contribution of Working Group I to the Third Assessment Report of the Intergovernmental Panel on Climate Change. Cambridge University Press, 881 pp.

Huffman, G.J., R.F. Adler, M.M. Morrissey, D.T. Bolvin, S. Curtis, R. Joyce, B. McGavock, and J. Susskind, 2001: Global precipitation at One-degree daily resolution from Multisatellite Observations. *J. Hydrometeor.*, **2**, 36-50.

Hurtado, R., I. Barnatán, C. Mesina, A. Beltrán, and L. Spescha, 1996: Corrimiento de las Isoyetas Trimestrales Medias en la Región Pampeana Argentina, 1940-1990. *IV Congreso Colombiano de Meteorología*, Santa Fe de Bogotá, Colombia, Sociedad Colombiana de Meteorología, 141-146.

Huxman, T. E., E.P. Hamerlynck, B.D. Moore, S.D. Smith, D.N. Jordan, S.F. Zitzer, R.S. Nowak, J.S. Coleman, and J.R. Seemann, 1998: Photosynthetic down-regulation in Larrea tridentata exposed to elevated atmospheric CO_2: Interaction with drought under glasshouse and field (FACE) exposure. *Plant Cell Environ.,* **21**, 1153-1161.

Hymus, G.J., T.G. Snead, D.P. Johnson, B.A. Hungate, and B.G. Drake, 2002: Acclimation of photosynthesis and respiration to elevated atmospheric CO2 in two Scrub Oaks. *Global Change Biol.*, **8**, 317-328.

Inzunza, B.J., and G. Berri, 1990: Comportamiento del viento y transporte del vapor de agua en la baja troposfera en el norte de Argentina. *Meteorologica*, **17**, 17-25.

Jones, H.G., 1994: *Plants and microclimate.* 2nd ed. Cambridge University Press. 428 pp.

Kain, J.S., 2004: The Kain-Fritsch convective parameterization: an update. *J. Appl. Meteor.*, **43**, 170-181.

Reproduced with permission of the copyright owner. Further reproduction prohibited without permission.

Kalnay, E. M. Kanamitsu, R. Kistler, W. Collins, D. Deaven, L. Gandin, M. Iredell, S. Saha, G. White, J. Woolen, Y. Zhu, M. Chelliah, W. Ebisuzaki, W. Higgins, J. Janowiak, K. C. Mo, C. Ropelewski, J. Wang, A. Leetma, R. Reynolds, R. Jenne, and D. Joseph, 1996: The NCEP/NCAR 40-Year reanalysis project. *Bull. Amer. Meteor. Soc.*, **77**, 437-471.

Kanae, S., T. Oki, and K. Musiake, 2001: Impact of deforestation on regional precipitation over the Indochina Peninsula. *J. Hydrometeor.*, **2**, 51-70.

Kiladis, G.N., and H.F. Diaz, 1989: Global climatic anomalies associated with extremes in the Southern Oscillation. *J. Climate*, **2,** 1069-1090.

Klemp, J.B., and R.B. Wilhelmson, 1978: The simulation of three-dimensional convective storm dynamics. *J. Atmos. Sci.*, **35,** 1070-1096.

Kogan, F.N., 2000: Satellite-observed sensitivity of world land ecosystems to El Niño/La Niña. *Remote Sen. Environ.,* **74**, 445-462.

Küchler, A.W., 2000: World map of natural vegetation. *Goode's World Atlas.* 20th ed. Rand McNally, 24-25.

Larcher, W., 1995: *Physiological Plant Ecology.* 3rd ed. Springer-Verlag, 506 pp.

Lenters, J.D., and K.H. Cook, 1997: On the origin of the Bolivian High and related circulation features of the South American precipitation climatology. *J. Atmos. Sci.*, **54,** 656-677.

León, R.J.C., and M.R. Aguiar, 1985: El deterioro por uso pasturil en estepas herbáceas patagónicas. *Phytocoenologia*, **13**, 181-196.

Los, S.O., G.J. Collatz, P.J. Sellers, C.M. Malmstroem, N.H. Pollack, R.S. DeFries, L. Bounoua, M.T. Parris, C.J. Tucker, and D.A. Dazlich, 2000: A Global 9-yr

Reproduced with permission of the copyright owner. Further reproduction prohibited without permission.

Biophysical Land Surface Dataset from NOAA AVHRR Data. *J. Hydrometeor.*, **1,** 183-199.

Lu, L., and W.J. Shuttleworth, 2002: Incorporating NDVI-Derived LAI into the climate version of RAMS and its impact on regional climate. *J. Hydrometeor.*, **3**, 347-362.

Lu, L., R.A. Pielke, G.E. Liston, W.J. Parton, D. Ojima, and M. Hartman, 2001: Implementation of a two-way interactive atmospheric and ecological model and its application to the central United States. *J. Climate*, **14,** 900-919.

Madonni, G.A., and M.E Otegui, 1996: Leaf area, light interception and crop development in maize. *Field Crops Res.*, **48**, 81-87.

Marshall, C.H. Jr., R.A. Pielke Sr., L.T. Steyaert, and D.A. Willard, 2004: The impact of anthropogenic land-cover change on the Florida peninsula sea breezes and warm season sensible weather. *Mon. Wea. Rev.*, 132, 28-52.

Matthews, E., 1983: Global vegetation and land use: New high-resolution data bases for climate studies. *J. Clim. Appl. Meteorol.*, **22,** 474-487.

Maxwell, R.M., and N.L. Miller, 2005: Development of a Coupled Land Surface and Groundwater Model. *J. Hydrometeor.*, **6**, 233-247.

Mellor, G.L., and T. Yamada, 1982: Development of a turbulence closure model for geophysical fluid problems. *Rev. Geophys. and Space Phys.*, **20**, 851-875.

Messina, C.D., A. Beltrán, and A. Ravelo, 1996a: El fenómeno ENSO:Su relación con la productividad de maíz en la región pampeana argentina (The ENSO phenomenon: Its relationship with maize productivity in the Argentine Pampas). *IV Congreso Colombiano de Meteorología*, Santa Fe de Bogotá, Colombia, Sociedad

Reproduced with permission of the copyright owner. Further reproduction prohibited without permission.

Colombiana de Meteorología, 236-241.

——, 1996b: La variabilidad interanual de los rendimientos de trigo en la región pampeana y su relación con el fenómeno ENSO (El Niño/Southern Oscillation) (Interannual variability of wheat yields in the Pampas, and their association with the ENSO phenomenon). *Actas del VII Congreso Argentino y VII Congreso Latinoamericano e Ibérico de Meteorología*, Buenos Aires, Argentina, Centro Argentino de Meteorólogos and Federación Latinoamericana e Ibérica de Sociedades de Meteorología, 55-56.

Messina, C.D., J.W. Hansen, and A.J. Hall, 1999: Land allocation conditioned on ENSO phases in the Pampas of Argentina. *Agric. Systems*, **60,** 197-212.

Miguez-Macho, G., and J. Paegle, 2000: Sensitivity of a Global Forecast Model to Initializations with Reanalysis Datasets. *Mon. Wea. Rev.*, **128,** 3879-3889.

Min, W., and S. Schubert, 1997: The climate signal in regional moisture fluxes: A comparison of three global data assimilation products. *J. Climate*, **10,** 2623-2642.

Miralles, D.J., and G.A. Slafer, 1997: Radiation interception and radiation use efficiency of near isogenic wheat lines with different height. *Euphytica*, **97,** 201-208.

Misra, V., P.A. Dirmeyer, and B.P. Kirtman, 2002a: A comparative study of two land surface schemes in regional climate integrations over South America. *J. Geophys. Res.*, **107,** LBA 48.1-48.9.

Misra, V., P.A. Dirmeyer, B.P. Kirtman, H.-M. Juang, and M. Kanamitsu, 2002b: Regional simulation of interannual variability over South America. *J. Geophys. Res.*, **107,** LBA 3.1-3.16.

Misra, V., P.A. Dirmeyer, and B.P. Kirtman, 2003: Dynamic Downscaling of Seasonal

Reproduced with permission of the copyright owner. Further reproduction prohibited without permission.

Simulations over South America. *J. Climate*, **16**, 103-117.

Moeremans, B., and S. Dautrebande, 2000: Soil moisture evaluation by means of multi-temporal ERS SAR PRI images and interferometric coherence. *J. Hydrol.*, **234**, 162-169.

Mooney, H.A., J. Canadell, F.S. Chapin III, J.R. Ehleringer, Ch. Körner, R.E. McMurtrie, W.J. Parton, L.F. Pitelka, and E.D. Schulze, 1999: Ecosystem physiology responses to global change. *Implications of Global Change for Natural and Managed Ecosystems. A Synthesis of GCTE and Related Research.* B.H. Walker, W.L. Steffen, J. Canadell, and J.S.I. Ingram, Eds., IGBP Book Series No. 4, Cambridge University Press, 141-189.

Moorhead, D.L., J.F. Reynolds, and P.J. Fonteyn, 1989: Patterns of stratified soil water loss in a Chihuahuan Desert community. *Soil Sci.*, **148**, 244-249.

Moran, M.S., D.C. Hymer, J. Qi, and E. Sano, 2000: Soil moisture evaluation using multi-temporal synthetic aperture radar (SAR) in semiarid rangeland. *Agric. For. Meteorol.*, **105**, 69–80.

Morgan, J.A., D.R. LeCain, A.R. Mosier, and D.G. Milchunas, 2001: Elevated CO_2 enhances water relations and productivity and affects gas exchange in C_3 and C_4 grasses of the Colorado shortgrass steppe. *Global Change Biol.*, **7**, 451-466.

Morison, J.I.L., 1987: Intercellular CO_2 concentration and stomatal response to CO_2. *Stomatal function.* E. Zeiger, G.D. Farquhar, and I.R. Cowan, Eds., Stanford University Press, 229-252.

Morison, J.I.L., 2001: Increasing atmospheric CO_2 and stomata, Commentary. *New Phytol.*, **149**, 154-158.

Reproduced with permission of the copyright owner. Further reproduction prohibited without permission.

Myneni, R.B, R.R. Nemani, and S.W. Running, 1997: Estimation of global leaf area index and absorbed PAR using radiative transfer models. *IEEE Trans. Geosci. Remote Sens.*, **36**, 1380-1393.

Narisma, G. T. and A. J. Pitman, 2003: The impact of 200 years of land cover change on the Australian near-surface climate. *J. Hydrometeor.*, **4,** 424-436.

Narisma, G.T., and A.J. Pitman, 2004: The effect of including biospheric responses to CO2 on the impact of land-cover change over Australia. *Earth Interactions,* **8**, 8-005.

Narisma, G.T., A.J. Pitman, J.L. Eastman, I.G. Watterson, R.A. Pielke Sr., and A. Beltrán-Przekurat, 2003: The role of biospheric feedbacks in the simulation of the impact of historical land cover change on the Australian January climate. *Geophys. Res. Lett.*, **30**, 2168, doi:10.1029/2003GL018261.

Neilson, R.P., 1986: High resolution climatic analysis and Southwest biography. *Science,* **232**, 27-34.

Nicolini, M., P. Salio, J.J. Katzfey, J.L. McGregor, and A.C. Saulo, 2002a: January and July regional climate simulation over South America. *J. Geophys. Res.,* **107**, 637, doi:10.1029/2001JD000736.

Nicolini, M., A.C. Saulo, J.C. Torres, and P. Salio, 2002b: Enhanced precipitation over southeastern South America related to strong low-level jet events during austral warm season. *Meteorologica*, **27**, 59-69

Nicolini, M., Y.G. Skabar, A.G. Ulke, and A.C. Saulo, 2002c: RAMS model performance in simulating precipitation during strong poleward low level jet events over northeastern Argentina. *Meteorologica*, **27**, 1-18.

Reproduced with permission of the copyright owner. Further reproduction prohibited without permission.

Nikolov, N., W. Massman, and A. Schoettle, 1995: Coupling biochemical and biophysical processes at the leaf level: An equilibrium photosynthesis model for leaves of C_3 plants. *Ecol. Modelling*, **80,** 205-235.

Nobre, C.A., P.J. Sellers, and J. Shukla, 1991: Amazonian deforestation and regional climate change. *J. Climate*, **4**, 957-988.

Nogues-Paegle J., C. Mechoso, R. Fu, H. Berbery, C. Winston, T. Chao, K. Cook, A. Diaz, D. Enfield, R. Ferreira, A. Grimm, V. Kousky, B. Liebmann, J. Marengo, K. Mo, D. Neelin, J. Paegle, A. Robertson, A. Seth, C. Vera, and J. Zhou, 2002: Progress in Pan American CLIVAR Research: Understanding the South American Monsoon. *Meteorologica*, **27**, 3-32.

Norby, R. J., J.S. Hartz-Rubin, and M.J. Verbrugge, 2003: Phenological responses in maple to experimental atmospheric warming and CO_2 enrichment. *Global Change Biol.*, **9**, 1792 1801.

Nosetto, M.D, E.G. Jobbagy, and J.M. Paruelo, 2005: Land-use change and water losses: The case of grassland afforestation across a soil textural gradient in central Argentina. *Global Change Biol.*, **11**, 1101-1117.

Noy-Meir, I., 1973: Desert ecosystems: Environment and producers. *Ann. Rev. Ecol. Syst.*, **4,** 25-41.

NRC, (National Research Council): 2005, *Radiative forcing of climate change: Expanding the concept and addressing uncertainties.* Committee on Radiative Forcing Effects on Climate Change, Climate Research Committee, Board on Atmospheric Sciences and Climate, Division on Earth and Life Studies, The National Academies Press, Washington, D.C.. [Available online at:

Reproduced with permission of the copyright owner. Further reproduction prohibited without permission.

http://www.nap.edu/openbook/0309095069/html/]

Oesterheld, M., J. Loreti, M. Senmartin, and J.M. Paruelo, 1999: Grazing, fire and climate effects on primary productivity of grasslands and savannas. *Ecosystems of Disturbed Ground.* L.R. Walker, Ed., Ecosystems of the World, Vol. 16, Elsevier, 287-306.

Oke, T.R., 1993: *Boundary layer climates.* 2nd Ed. Routledge, 435 pp.

Olson, J.S., 1994: *Global ecosystem framework-definitions.* USGS EROS Data Center Internal Report, Sioux Falls, SD, 37 pp.

Otterman, J., 1974: Baring high-albedo soils by overgrazing: A hypothesized desertification mechanism. *Science*, 531-533.

Otterman, J., 1989: Enhancement of surface-atmosphere fluxes by desert fringe vegetation through reduction of surface albedo and of soil heat flux. *Theor. Appl. Climatol.*, **40**, 67-79.

Owensby, C.E., J.M. Ham, A.K. Knapp, D.J. Bremer, and L.M. Auen, 1997: Water vapour fluxes and their impact under elevated carbon dioxide in a C_4-tallgrass prairie. *Global Change Biol.*, **3**, 189-195.

Owensby, C.E., J.M. Ham, A.K. Knapp, and L.M. Auen, 1999: Biomass production and species composition change in a tallgrass prairie ecosystem after long-term exposure to elevated atmospheric CO_2. *Global Change Biol.*, **5**, 497–506.

Oyama, M.D., and C.A. Nobre, 2004: Climatic consequences of a large-scale desertification in northeast Brazil: A GCM simulation study. *J. Climate*, **17**, 3203–3213.

Reproduced with permission of the copyright owner. Further reproduction prohibited without permission.

Paegle, J., 1998: A comparative review of South American low-level jets. *Meteorologica*, **23**, 73-81.

Paruelo, J.M., and O. E. Sala, 1990: Caracterización de las inundaciones en la Depresión del Salado: dinámica de la capa freática. *Turrialba*, **40**, 5-11.

Paruelo J.M., E.G. Jobbagy, O.E. Sala, W.K. Lauenroth, and I.C. Burke, 1998: Functional and structural convergence of temperate grassland and shrubland ecosystems. *Ecol. Applications*, **8**, 194-206.

Paruelo, J.M., O.E. Sala, and A. Beltrán, 2000: Long-term dynamics of water and carbon in semiarid ecosystems: a gradient analysis in the Patagonian steppe. *Plant Ecol.*, **150**, 133-143.

Paruelo, J.M., E.G. Jobbágy, and O.E. Sala, 2001: Current distribution of ecosystem functional types in temperate South America. *Ecosystems*, **4**, 683-698.

Paruelo, J.M., M.F. Garbulsky, J.P. Guerschman, and E.G. Jobbágy, 2004: Two decades of Normalized Difference Vegetation Index changes in South America: Identifying the imprint of global change. *Int. J. Remote Sens.*, **25,** 2793-2806.

Penalba, O., A. Beltrán, and C.D. Messina, 2005: Monthly rainfall in Central-Eastern Argentina and ENSO. *Revista Brasileira de Agrometeorologia.* Accepted.

Pereyra, C.A., 1988: Evaluación del balance de energía en un cultivo de soja bajo condiciones hídricas extremas. *Rev. Fac. Agronomía*, **9**, 1-8.

Peters, D.P.C., 2000: Climatic variation and simulated patterns in seedling establishment of two dominant grasses at a semi-arid–arid grassland ecotone. *J. Veg. Sci.*, **11**, 493-504.

Peters, D.P.C., R.A. Pielke Sr., B.T. Bestelmeyer, C.D. Allen, S. Munson-McGee, and

Reproduced with permission of the copyright owner. Further reproduction prohibited without permission.

K.M. Havstad, 2004: Cross-scale interactions, nonlinearities, and forecasting catastrophic events. *Proc. Natl. Acad. Sci.*, **101**, 15130-15135.

Pielke, R.A. Sr., 2001: Influence of the spatial distribution of vegetation and soils on the prediction of cumulus convective rainfall. *Rev. Geophys.*, **39**, 151-177.

Pielke, R.A. Sr., W.R. Cotton, R.L. Walko, C.J. Tremback, W.A. Lyons, L.D. Grasso, M.E. Nicholls, M.D. Moran, D.A. Wesley, T.J. Lee, and J.H. Copeland, 1992: A comprehensive meteorological modeling system–RAMS. *Meteor. Atmos. Phys.*, **49**, 69-91.

Pielke, R.A. Sr., R. Avissar, M. Raupach, H. Dolman, X. Zeng, and S. Denning, 1998: Interactions between the atmosphere and terrestrial ecosystems: Influence on weather and climate. *Global Change Biol.*, **4**, 461-475.

Pielke, R.A. Sr., G.E. Liston, J.L. Eastman, L. Lu, and M. Coughenour, 1999: Seasonal weather prediction as an initial value problem. *J. Geophys. Res.*, **104**, 19463-19479.

Pinzon, J.E., 2002: Using HHT to successfully uncouple seasonal and interannual components in remotely sensed data. *SCI 2002*, Conference Proceedings, Orlando, Florida.

Pinzon, J.M., M. Brown, and C.J. Tucker, 2004: Satellite time series correction of orbital drift artifacts using empirical mode decomposition. *Hilbert-Huang Transform: Introduction and Applications*, N. Huang, Ed. Chapter 10, Part II. Applications. To appear.

Pitman, A.J., 2003: The evolution of, and revolution in, land surface schemes designed for climate models. *Int. J. Climatol.*, **23**, 479-510.

Reproduced with permission of the copyright owner. Further reproduction prohibited without permission.

Pitman, A.J., and M. Zhao, 2000: The relative impact of observed change in land cover and carbon dioxide as simulated by a climate model. *Geophys. Res. Lett.*, **27**, 1267-1270.

Pitman, A.J., G.T. Narisma, R.A. Pielke Sr., and N.J. Holbrook, 2004: The impact of land cover change on the climate of southwest Western Australia. *J. Geophys. Res.*, **109,** D18109, doi:10.1029/2003JD004347.

Podestá, G.P., C.D. Messina, M.O. Grondona, and G.O. Magrin, 1999: Associations between grain crop yields in Central-Eastern Argentina and El Niño-Southern Oscillation. *J. Appl. Meteorol.*, **38**, 1488–1498.

Poorter, H., 1993: Interspecific variation in the growth response of plants to an elevated and ambient CO_2 concentration. *Vegetatio*, **104/105**, 77-97.

Prueger, J.J, W.P. Kustas, L.E. Hipps, and J.L. Hatfield, 2004: Aerodynamic parameters and sensible heat flux estimates for a semi-arid ecosystem. *J. Arid Environ.*, **57**, 87-100.

Qian, J.-H., A. Seth, and S. Zebiak, 2003: Reinitialized versus continuous simulations for regional climate downscaling. *Mon. Wea. Rev.*, **131,** 2857-2874.

Raddatz, R.L., 2005: Evidence for the influence of agriculture on weather and climate through the transformation and management of vegetation: Illustrated by examples from the Canadian Prairies. *Agric. For. Meteorol.*, submitted.

Raich, J.W., and W.H. Schlesinger, 1992: The global carbon dioxide flux in soil respiration and its relationship to vegetation and climate. *Tellus*, **44 B**, 81-99.

Ramankutty, N., and J.A. Foley, 1998: Characterizing patterns of global land use: an analysis of global croplands data. *Global Biogeochem. Cycles*, **12**, 667-685.

Reproduced with permission of the copyright owner. Further reproduction prohibited without permission.

Randall, D.A., P.J. Sellers, D.A. Dazlich, C. Zhang, G.J. Collatz, A.S. Denning, S.O. Los, C.B. Field, and I. Fung, 1996: A revised land-surface parameterization (SiB2) for GCMs. Part III: The greening of the Colorado State University general circulation model. *J. Climate*, **9,** 738-763.

Rango, A., J.C. Ritchie, W.P. Kustas, T.J. Schmugge, and K.M. Havstad, 1998: JORNEX: Remote sensing to quantify long-term vegetation change and hydrological fluxes in an arid rangeland environment. *Hydrology in a changing environment.* H. Wheater, and C. Kirby, Eds., John Wiley, 585-590.

Ravelo, A., and R. Zanvettor, 2000: Using the SPI to monitor the 1999-2000 drought in northeastern Argentina. *Drought network news*, **12**, 3-4.

Reynolds, R.W., and T.M. Smith, 1994: Improved global sea surface temperature analyses using optimum interpolation. *J. Climate*, **7**, 929-948.

Reynolds, J.F., P.R. Kemp, and J.D. Tenhunen, 2000: Effects of long-term rainfall variability on evapotranspiration and soil water distribution in the Chihuahuan Desert: a modeling analysis. *Plant Ecol.*, **150**, 145-159.

Roads, J., S. Chen, S. Cocke, L. Druyan, M. Fulakeza, T. LaRow, P. Lonergan, J.-H. Qian, and S. Zebiak, 2003: International Research Institute/Applied Research Centers (IRI/ARCs) regional model intercomparison over South America. *J. Geophys. Res.*, **108**, 4425, doi:10.1029/2002JD003201.

Rojas, M., and A. Seth, 2003: Simulation and sensitivity in a nested modeling system for South America. Part II: GCM boundary forcing. *J. Climate*, **16,** 2454-2471.

Ropelewski, C.F., and H.S. Halpert, 1987: Global and regional scale precipitation patterns associated with the El Niño/Southern Oscillation. *Mon. Wea. Rev.*, **115**,

Reproduced with permission of the copyright owner. Further reproduction prohibited without permission.

1606-1626.

_____, 1989: Precipitation patterns associated with high index phase of Southern Oscillation. *J. Climate*, **2**, 268-284.

Rosenblüth, B., H.A. Fuenzalida, and P. Aceituno, 1997: Recent temperature variations in southern South America. *Int. J. Climatol.*, **17**, 67-85.

Rusticucci, M., and O. Penalba, 2000: Interdecadal changes in the precipitation seasonal cycle over southern South America: Relationship with surface temperature. *Climate Res.*, **16,** 1-15.

Rusticucci, M., and M. Barrucand, 2004: Observed trends and changes in temperature extremes over Argentina. *J. Climate*, **17,** 4099-4107.SAGPYA, 2000: Estimaciones Agrícolas. Buenos Aires, Argentina: Secretaría de Agricultura, Ganadería, Pesca y Alimentación. [Available online at: http//:www.sagpya.mecon.gov.ar].

Sala, O.E., M. Oesterheld, R.J.C. León, and A. Soriano, 1986: Grazing effects upon plant community structure in subhumid grasslands of Argentina. *Vegetatio*, **67**, 27-32.

Salio, P., M. Nicolini, and A.C. Saulo, 2002: Chaco low-level jet events characterization during the austral summer season. *J. Geophys. Res.*, **107,** 4816.

Santrucek J., and R.F. Sage, 1996: Acclimation of stomatal conductance to a CO_2-enriched atmosphere and elevated temperature in *Chenopodium album. Aust. J. Plant Physiol.,* **23,** 467–478.

Saulo, A.C., M. Nicolini, and S.C. Chou, 2000: Model characterization of the South American low-level flow during the 1997-1998 spring-summer season. *Climate Dyn.*, **16**, 867-881.

Reproduced with permission of the copyright owner. Further reproduction prohibited without permission.

Schenk, H.J., and R.B. Jackson, 2002: The global biogeography of roots. *Ecol. Monographs,* **72**, 311-328.

Schlesinger, W.H., P.J. Fonteyn, and G.M. Marion, 1987: Soil moisture content and plant transpiration in the Chihuahuan Desert of New Mexico. *J. Arid Environ.*, **12**, 119-126.

Schlesinger, W.H., J.F. Reynolds, G.L Cunningham, L.F. Huenneke, W.M. Jarrel, R.A. Virginia, and W.G. Whitford, 1990: Biological feedbacks in global desertification. *Science*, **247**, 1043-1048.

Schulze, E.-D., F.M. Kelliher, C. Koerner, J. Lloyd, and R. Leuning, 1994: Relationships among maximal stomatal conductance, carbon assimilation rate, and plant nitrogen nutrition. *Annu. Rev. Ecol. System.*, **25**, 629-660.

Schwerdtfeger, W., 1976: *Climates of Central and South America.* Vol. 12, *World Survey of Climatology*, Elsevier, 532 pp.

Scurlock, J.M.O., G.P. Asner, and S.T. Gower. 2001. Global Leaf Area Index Data from field measurements, 1932-2000. Oak Ridge National Laboratory, Oak Ridge, TN. [Available online at: http://daac.ornl.gov/daacpages/vegetation_collections.html].

Sellers, P.J., 1992: Biophysical models of land surface processes. *Climate System Modeling*, K.E. Trenberth, Ed., Cambridge University Press, 451-490.

Sellers, P.J., S.O. Los, C.J. Tucker, C.O. Justice, D.A. Dazlich, G.J. Collatz, and D.A. Randall, 1996: A revised land surface parameterization (SiB2) for atmospheric GCMs. Part II: the generation of global fields of terrestrial biophysical parameters from satellite data. *J. Climate*, **9**, 706-737.

Seth, A., and M. Rojas, 2003: Simulation and sensitivity in a nested modeling system for

Reproduced with permission of the copyright owner. Further reproduction prohibited without permission.

South America. Part I: Reanalyses boundary forcing. *J. Climate*, **16,** 2437-2453.

Seth, A., M. Rojas, B. Liebmann, and J.-H. Qian, 2004: Daily rainfall analysis for South America from a regional climate model and station observations. *Geophys. Res. Lett.*, **31,** L07213, 10.1029/2003GL019220.

Sierra, E.M., M. Conde Prat, and S. Perez, 1995: La migración de cultivos de granos como indicador del cambio climatico 1941-1993 en la region pampeana argentina. *Rev. Fac. Agronomía,* **15**, 171-176.

Sitch, S., B. Smith, I. C. Prentice, A. Arneth, A. Bondeau, W. Cramer, J. O. Kaplan, S. Levis, W. Lucht, M. T. Sykes, K. Thonicke, and S. Venevsky, 2003: Evaluation of ecosystem dynamics, plant geography and terrestrial carbon cycling in the LPJ dynamic global vegetation model. *Global Change Biol.*, **9,** 161-185.

Smagorinsky, J., 1963: General circulation experiments with the primitive equations. Part I: the basic experiment. *Mon. Wea. Rev.*, **91,** 99-164.

Small, E.E., and S.A. Kurc, 2003: Tight coupling between soil moisture and the surface radiation budget in semiarid environments: implications for land-atmosphere interactions. *Water Resour. Res.*, **39**, 1278, doi:10.1029/2002WR001297.

Snyder, K.A., K.A. Mitchell, and J.E. Herrick, 2005: Patterns and controls of soil water in the Jornada Basin. *Structure and function of a Chihuahuan Desert ecosystem: the Jornada Basin LTER*, K.M. Havstad, K.M., L.F. Huenneke, and W. H. Schlesinger, Eds., Oxford University Press, In press.

Soriano, A., 1991: Rio de la Plata grasslands. *Natural grasslands. Introduction and Western Hemisphere,* R.T. Coupland, Ed., Ecosystems of the World, Vol. 8A, Elsevier, 367-408.

Reproduced with permission of the copyright owner. Further reproduction prohibited without permission.

Soriano, A., C.P. Movia, and R.J.C. León, 1983: Deserts and semi-deserts of Patagonia. *Temperate deserts and semi-deserts of the world,* N.E. West, Ed., Ecosystems of the World, Vol. 5, Elsevier, 440-454.

SOTER, 1998: Soil and terrain database for Latin America and the Caribbean. FAO, CD-ROM. FAO Land and water digital media series. No. 5.

Still, C.J., J.A. Berry, G.J. Collatz, and R.S. DeFries, 2003: Global distribution of C_3 and C_4 vegetation: carbon cycle implications. *Global Biogeochem. Cycles*, **17**, 1006, doi:10.1029/2001GB001807.

Sud, Y.C., and M.J. Fennessy, 1982: A study of the influence of surface albedo on July circulation in semi-arid regions using the GLAS GCM. *J. Climatology*, **2**, 105-125.

Sun, L., D.F. Moncunill, H. Li, A.D. Moura, and F.d.A. de Souza Filho, 2005: Climate downscaling over Nordeste, Brazil, using the NCEP RSM97. *J. Climate*, **18,** 551-567.

Trápani, N., A.J. Hall, V.O. Sadras, and F. Vilella, 1992: Ontogenic changes in radiation use efficiency of sunflower (*Helianthus annuus* L.) crops. *Field Crops Res.*, **29**, 301-316.

Trewin, B.C., 2004: Effects of changes in algorithms used for the calculation of Australian mean temperature. *Australian Meteorol. Mag.*, **53**, 1-11.

Tsvetsinskaya, E., L.O. Mearns, and W.E. Easterling, 2001a: Investigating the effect of seasonal plant growth and development in 3-Dimensional atmospheric simulations. Part I: Simulation of surface fluxes over the growing season. *J. Climate,* **14,** 692-709.

Reproduced with permission of the copyright owner. Further reproduction prohibited without permission.

Tsvetsinskaya, E., L.O. Mearns, and W.E. Easterling, 2001b: Investigating the effect of seasonal plant growth and development in 3-Dimensional atmospheric simulations. Part II: Atmospheric response to crop growth and development. *J. Climate,* **14**, 711-729.

Tucker, C.J., J.E. Pinzon, M.E. Brown, D. Slayback, E.W.W. Pak, R. Mahoney, E. Vermote, and N. El Saleous, 2005: An extended AVHRR 8-km NDVI data set compatible with MODIS and SPOT vegetation NDVI Data. *Int. J. Remote Sens,*. In press.

Twine, T.E., C.J. Kucharik, and J.A. Foley, 2004: Effects of land cover change on the energy and water balance of the Mississippi River Basin. *J. Hydrometeor.*, **5,** 640-655.

USDA, 1987: *Major World Crop Areas and Climatic Profiles*. USDA Agricultural Handbook No. 664. World Agricultural Outlook Board, U.S. Department of Agriculture, 159 pp.

Viglizzo, E.F., Z. Roberto, F. Lertora, G. Lopez, and J. Bernardos, 1997: Climate and land use change in field-crop ecosystems of Argentina. *Agric. Ecosys. Environ.*, **66**, 61-70.

Viglizzo, E.F., F. Lertora, A.J. Pordomingo, J.N. Bernardos, Z.E. Roberto, and H. Del Valle, 2001: Ecological lessons and applications from one century of low external-input farming in the pampas of Argentina. *Agric. Ecosys. Environ.,* **83**, 65-81.

Villalba, R., and T. Veblen, 1997: Regional patterns of tree population age structures in northern Patagonia: Climatic and disturbance influences. *J. Ecol.*, **85**, 113-124.

Reproduced with permission of the copyright owner. Further reproduction prohibited without permission.

Villamil, M.B., N.M. Amiotti, and N. Peinemann, 2001: Soil degradation related to overgrazing in the semi-arid Southern Caldenal area of Argentina. *Soil Sci.*, **166,** 441-452.

Wagner, W., J. Noll, M. Borgeaud, and H. Rott, 1999a: Monitoring soil moisture over the Canadian Prairies with the ERS scatterometer. *IEEE Trans. Geosci. Remote Sens.*, **37**, 206-216.

Wagner, W., G. Lemoine, M. Borgeaud, and H. Rott, 1999b: A study of vegetation cover effects on ERS scatterometer data. *IEEE Trans. Geosci. Remote Sens.*, **37**, 938-948.

Wagner, W., G. Lemoine, H. Rott, 1999c: A method for estimating soil moisture from ERS Scatterometer and soil data. *Remote Sens. Environ.*, **70**, 191-207.

Wagner, W., K. Scipal, C. Pathe, D. Gerten, W. Lucht, and B. Rudolf, 2003: Evaluation of the agreement between the first global remotely sensed soil moisture data with model and precipitation data. *J. Geophys. Res.*, **108**, 4611, doi:10.1029/ 2003JD003663.

Walko, R.L. L.E. Band, J. Baron, T.G.F. Kittel, R. Lammers, T.J. Lee, D.S. Ojima, R.A. Pielke, C. Taylor, C. Tague, C.J. Tremback, and P.L. Vidale, 2000: Coupled atmosphere-biophysics-hydrology models for environmental modeling. *J. Appl. Meteor.*, **39**, 931-944.

Wang, M., and J. Paegle, 1996: Impact of analysis uncertainty upon regional atmospheric moisture flux. *J. Geophys. Res.*, **101**, 7291-7303.

Warner, T.T., 2004: *Desert Meteorology*, Cambridge University Press, 620 pp.

Weaver, C.P., S. Baidya Roy, and R. Avissar, 2002: Sensitivity of simulated mesoscale

Reproduced with permission of the copyright owner. Further reproduction prohibited without permission.

atmospheric circulations resulting from landscape heterogeneity to aspects of model configuration. *J. Geophys. Res.*, **107,** 8041, doi:10.1029/2001JD000376.

Weber, R.O., 1993: Influence of different daily mean formulas on monthly and annual averages of temperature. *Theor. Appl. Climatol.*, **47**, 205-213.

White, M.A, P.E. Thornton, S.W. Running, and R.R. Nemani, 2000: Parameterization and sensitivity analysis of the BIOME-BGC terrestrial ecosystem model: net primary production controls. *Earth Interactions,* **4**, 1-85.

Wilks, D.S., 1995: *Statistical methods in the atmospheric sciences: An introduction*, International Geophysics Series, Vol. 59, Academic Press, 464 pp.

Willmott, C. J., and K. Matsuura, 1995: Smart interpolation of annually averaged air temperature in the United States. *J. App. Meteor.,* 34, 2577-2586.

Willmott, C.J., and S.M. Robeson, 1995: Climatologically Aided Interpolation (CAI) of terrestrial air temperature. *Int. J. Climatol.*, **15**, 221-229.

Woodrow, I.E., and J.A. Berry, 1988: Enzymatic regulation of photosynthetic CO_2 fixation in C_3 plants. *Annu. Rev. Plant Physiol. Plant Mol. Biol.*, **39,** 533-594.

Woodward, F.I., 1987: Stomatal numbers are sensitive to CO_2 increases from pre-industrial levels. *Nature,* **327**, 617-618.

World Bank, 2000: Argentina Water Resources Management: Policy Elements for Sustainable Development in the XXI Century. Sector Report. 83 pp. [Available online at: http://www-wds.worldbank.org/]

Reproduced with permission of the copyright owner. Further reproduction prohibited without permission.

Wu, W., A.H. Lynch, and A. Rivers, 2005: Estimating the uncertainty in a regional climate model related to initial and lateral boundary conditions. *J. Climate*, **18**, 917–933.

Wullschleger, S.D., C.A. Gunderson, P.J. Hanson, K.B. Wilson, and R.J. Norby, 2002: Sensitivity of stomatal and canopy conductance to elevated CO_2 concentration - interacting variables and perspectives of scale. *New Phytol.*, **153**, 485-496.

Zeng, X., 2001: Global vegetation root distribution for land modeling. *J. Hydrometeor.*, **2**, 525-530.

Reproduced with permission of the copyright owner. Further reproduction prohibited without permission.

Zhou, J., and K.-M. Lau, 2002: Intercomparison of model simulations of the impact of 1997/98 El Niño on South American summer monsoon. *Meteorologica*, **27**, 99-116.

Reproduced with permission of the copyright owner. Further reproduction prohibited without permission.